EQUALIZATION FOR ENERGY EFFICIENT MODULATION

A Dissertation

Presented to the Faculty of the Graduate School

of Cornell University

in Partial Fulfillment of the Requirements for the Degree of

Doctor of Philosophy

by

Andrew G. Klein

January 2006

EQUALIZATION FOR ENERGY EFFICIENT MODULATION

Andrew G. Klein, Ph.D.

Cornell University 2006

To help meet the demand for ubiquitous wireless data services, national regulatory agencies worldwide have recently made available several gigahertz of contiguous spectrum for unlicensed indoor use, notably the ultra-wideband and 60 GHz bands. This is causing a paradigm shift in the design of wireless networks, as energy efficiency supplants spectral efficiency as the primary design concern. Energy efficient modulations have existed for decades, but have only recently been considered for use in high-speed wireless networks where dispersive channels hinder performance through multipath and intersymbol interference.

This dissertation presents the first investigation of equalization for a class of energy efficient modulations that comprises orthogonal, biorthogonal, and transorthogonal modulation. We consider the use of a (possibly fractionally-spaced[1]) finite-length decision-feedback equalizer (DFE), and begin by presenting a generalized multirate system model that encapsulates all of these energy efficient modulations, as well as some classical modulations such as pulse amplitude modulation. The DFE structures we propose assume two forms: a chip-rate DFE very similar to the classical DFE, and a block DFE implemented as a multirate filter bank that operates symbol-by-symbol. We derive the minimum mean-squared error DFE tap values for these two structures, which follow from straightforward application of

[1] A "fractionally-spaced DFE" has a fractionally-spaced forward filter, but a chip-spaced feedback filter.

Wiener filter theory. However, we show that several modifications to the equalizer enable us to exploit inherent signal properties of some of the modulation schemes; these changes have the effect of permitting perfect equalization with a finite-length equalizer in situations where perfect equalization would otherwise not have been possible, and also permit a reduction in equalizer complexity.

Adaptive equalization of these modulations is the focus of the second half of the dissertation. We briefly discuss the trained least mean square algorithm, and demonstrate that its decision-directed counterpart is unsuitable for cold startup of equalizers for these modulations. This leads us to consider the use of the two most popular classical blind equalization algorithms – the Constant Modulus Algorithm (CMA) and the Shalvi-Weinstein Algorithm (SWA) – both of which we show to be similarly unsuitable in their pure form largely due to their reliance on i.i.d. source statistics. With the lack of a suitable blind algorithm, we proceed with a general discussion of blind algorithm development, including the desired properties of blind algorithm cost functions, a methodology for algorithm assessment, and guidelines for selecting cost functions. Finally, we present the first two blind algorithms beyond decision direction for biorthogonal modulation, including a discussion of their characteristics and convergence. The first algorithm, called LTBOMB, is CMA-like in spirit, and we show that the zero-forcing solutions are locally stable under ideal conditions. The second algorithm, called TROMBONE, was designed with a SWA-like philosophy in mind, and thus relies on a spectral prewhitener before equalization. We show that the ZF solutions are stationary points of TROMBONE, and include simulations demonstrating the performance of the two blind algorithms. We conclude with a summary of results and a listing of some immediate open issues revealed by this dissertation.

BIOGRAPHICAL SKETCH

Andrew G. Klein was born near Cleveland, Ohio. He received the B.S. degree in electrical engineering from Cornell University, and the M.S. degree in electrical engineering from the University of California, Berkeley. He then worked for awhile at some Bay Area startup companies before returning to Cornell to pursue a Ph.D. in electrical engineering. His areas of interest are statistical signal processing and adaptive parameter estimation for wireless communication systems.

ACKNOWLEDGEMENTS

I extend my sincere gratitude and appreciation to the many people who helped keep me on course toward the completion of this thesis. By far the biggest thanks goes to my advisor, Prof. C. Richard Johnson, Jr. Mentor, sage, and one of my closest friends over the past four years, Rick has made graduate school far too enjoyable. Had he not been so good at guiding and motivating me to the end, I might have happily stayed forever. His patience, advice, and the opportunities he has provided have made this the most enriching experience of my life.

Next, I would like to thank the financial support of the National Science Foundation (grants CCF-0310023 and INT-0233127), Applied Signal Technology, Texas Instruments, and the Lockheed Martin Fellowship. Many thanks to my committee members, Prof. Lang Tong and Prof. Anna Scaglione, for their advice, guidance, and ideas throughout the past four years. I would also like to thank Dr. John Treichler for his friendship, support, and the practical perspective he provided. Prof. Pierre Duhamel has been a great help – for providing many new research directions to explore, and for taking me under his wing at Supélec in Paris, France.

I owe a huge thanks to many (current and former) members of the CU-BERG: Rick Brown, Phil Schniter, Raul Casas, Tom Endres, Jai Balakrishnan, Wonzoo Chung, Rick Martin, Anand Shah, and John Walsh. I have learned so much from this eclectic group of trouble-makers, and they have all helped me through in one way or another... that first wild van ride, trips to crazy places, antics at the Triumph, wow... I am not sure how I was so lucky to be able to interact with such an entertaining group of colleagues.

Next, a big thanks to the many people in Ithaca who have made life interesting outside of school, including Ruby Beil, Betty & Sam, Andy Browder, Doug Chan,

the Chanti crowd, Frank Ciaramello, Park Doing, Ted Feldpausch, Matt Gaubatz, Joanne Giggey, Yann Guillo, Jessica May, Dan Pendleton, and Christina Peraki.

Of course, my immediate family deserves an enormous thanks. I am most grateful for their love, support, encouragement, laughter, wisdom, food fights, and willingness to lend an ear at all hours. Finally, I would like to thank the adorable Isabelle Moy for the radiance and joy she has brought to my time in Ithaca and Paris.

TABLE OF CONTENTS

LIST OF TABLES

LIST OF FIGURES

LIST OF ABBREVIATIONS

Abbreviation	Meaning
AWGN	Additive White Gaussian Noise
BER	Bit Error Rate
BPSK	Binary Phase Shift Keying
CMA	Constant Modulus Algorithm
DD	Decision Directed
DFE	Decision Feedback Equalizer
DFT	Discrete Fourier Transform
FIR	Finite Impulse Response
FM	Frequency Modulation
FSK	Frequency Shift Keying
i.i.d.	Independent and Identically Distributed
IIR	Infinite Impulse Response
ISI	Intersymbol Interference
LMS	Least Mean Square
MBOK	M-ary Biorthogonal Keying
MIMO	Multiple-Input Multiple-Output
ML	Maximum Likelihood
MMSE	Minimum Mean-Squared Error
MSE	Mean-Squared Error
OFDM	Orthogonal Frequency Division Modulation
PAM	Pulse Amplitude Modulation
PPM	Pulse Position Modulation
PSK	Phase Shift Keying
QAM	Quadrature Amplitude Modulation
SNR	Signal-to-Noise Ratio
SWA	Shalvi-Weinstein Algorithm
VSB	Vestigal Sideband Modulation
WLAN	Wireless Local Area Network
WPAN	Wireless Personal Area Network
ZF	Zero Forcing

LIST OF SYMBOLS

Symbol	Meaning
$\boldsymbol{e}_i$	Unit canonical vector
$\mathbf{0}_{m\times n}$	$m \times n$ matrix of all 0's
$\mathbf{1}_{m\times n}$	$m \times n$ matrix of all 1's
$\boldsymbol{I}_n$	$n \times n$ identity matrix
$\boldsymbol{J}_n$	$\boldsymbol{I}_n - \mathbf{1}_{n\times n}/n$
$\otimes$	Kronecker product (i.e. matrix direct product)
$\times_n$	n-mode tensor/matrix product
$(\cdot)^\top$	matrix transpose
$(\cdot)^H$	matrix conjugate transpose
$[\boldsymbol{S}]_i$	ith column of matrix $\boldsymbol{S}$
$[\boldsymbol{S}]_{i,j}$	i,jth entry of matrix $\boldsymbol{S}$
$\text{sgn}(\cdot)$	signum function
$\text{diag}(\boldsymbol{x})$	Square diagonal matrix with vector $\boldsymbol{x}$ along diagonal
$\text{diag}(\boldsymbol{A})$	Vector resulting from extraction of diagonal elements of $\boldsymbol{A}$
$\lceil\cdot\rceil, \lfloor\cdot\rfloor$	round up, down to nearest integer
$\text{tr}(\cdot)$	matrix trace
$\Re\{\cdot\}$	Extraction of real-valued component
$\nabla_{\boldsymbol{f}}$	Gradient with respect to $\boldsymbol{f}$
$\|\|\boldsymbol{x}\|\|_p$	ℓ_p norm
$E[\cdot]$	Expectation
$\mathcal{C}_n(\cdot)$	nth order cumulant
$\delta[\cdot]$	Discrete Kronecker delta function

Chapter 1

Introduction

Increasing demand for ubiquitous wireless data services combined with recent legislation in the way radio-frequency spectrum is allocated is causing a paradigm shift in the design of wireless networks. Historically, available spectrum has been scarce and wireless system designers have had to focus their efforts on designing bandwidth efficient systems, with energy efficiency generally considered as an afterthought. To help meet the demand for ubiquitous wireless data services, national regulatory agencies worldwide have recently opened up several gigahertz of contiguous spectrum for unlicensed indoor use, notably the ultra-wideband (UWB) and 60 GHz bands. The amount of available spectrum in these bands is enormous, and short range systems expected to operate in these bands have the additional benefit of large frequency reuse due to the low transmit power (in the case of UWB) and oxygen absorption (in the 60 GHz band). The anticipated users of these bands are expected to be consumer electronics devices, many of which may be handheld and battery powered. Thus, wireless systems designers will increasingly be required to focus their efforts on designing *energy* efficient systems, while high *spectral* efficiency may receive less attention due to the relative abundance of available bandwidth.

While energy efficient modulation schemes have existed for more than half a century and have been used in countless applications, their use has tradition-

ally been restricted to channels well-approximated by the additive white Gaussian noise (AWGN) model. Energy efficient modulations have only recently garnered attention for use in high data-rate applications with indoor communication channels that are expected to be non-line-of-sight (NLOS), and have been considered for use in several consumer wireless standards, including the IEEE 802.11 WLAN standard [46] and the ultra wideband IEEE 802.15.3a WPAN standard [9]. In such dispersive environments, multipath and intersymbol interference (ISI) are known to be major impairments to acceptable performance, and ISI compensation for energy efficient modulation schemes has received little attention until now.

1.1 Motivation

The design of energy efficient modulations for transmission over AWGN channels has been an active area of research for decades. We define energy efficient modulations as those which, regardless of bandwidth or data rate, minimize the bit error rate under an average power constraint. Surprisingly, the optimal selection of M signal vectors corrupted by only AWGN is not known in general [37]. Historically, a standard design criterion for constructing energy efficient modulations has been to design waveforms such that their minimum Euclidean distance is maximized. Indeed, this leads to the optimal signal set on the Gaussian channel when the SNR is sufficiently high, though not when the SNR is very low [37]. Nevertheless, this design criterion is often employed, for lack of a better approach, both on AWGN channels and on channels that deviate little from the Gaussian model, e.g. those with only a moderate amount of ISI.

Perhaps the three most popular energy efficient modulation schemes, originating from this design criterion, are orthogonal modulation, biorthogonal modula-

tion, and transorthogonal modulation. These modulations all fall into a class that is sometimes referred to as *multipulse* modulation or *nonlinear* modulation, since the modulator output cannot be expressed as a simple scalar symbol multiplying a single band-limited pulse shape. All of these modulations appeared in communications textbooks as early as the 1960's [45], and persist in modern communication texts [1][29].

Because traditional uses of energy efficient modulations have been in situations with little or no ISI, up to now there has been little motivation to explore ISI compensation of such signals to the extent that ISI compensation has been explored for linearly modulated signals. The optimum detector in ISI is the so-called maximum-likelihood detector, but its complexity is usually far too high for practical implementation, and thus practical suboptimal schemes are necessary. One suboptimal scheme — the one most widely used in practice — is the channel equalizer [25], which is the focus of this dissertation. In Table 1.1 we provide a comprehensive list of the classical modulation techniques found in standard communication textbooks [29]. In spite of the fact that such modulations are fairly classical, there is a lack of practical techniques for ISI compensation for energy efficient modulations. Market forces are causing system designers to give energy efficient modulation schemes a fresh look for use in environments where the AWGN channel assumption no longer holds. For their deployment in frequency selective environments, some form of practical ISI compensation will be necessary.

While equalizers assume many forms, we will propose the first constrained length linear and decision-feedback equalizers (DFE) suitable for use with energy efficient modulations, and we will give particular attention to those that are adaptive and do not have knowledge of the channel (though, in practice, some knowledge

Table 1.1: Adaptive Equalizers for Classical Modulation Schemes

	Signaling	Adaptive Equalizer Exists?
bandwidth efficient	FM	✓[42]
	VSB	✓[32]
	M-PAM	✓[13][42]
	M-QAM, M-PSK	✓[13][42]
	OFDM	✓[28]
energy efficient	orthogonal modulation	×
	biorthogonal modulation	×
	transorthogonal modulation	×

of channel delay spread is helpful in choosing the required equalizer lengths). We will focus on the minimum mean-squared error (MMSE) criterion, and stochastic gradient-descent based algorithms that converge to (or near) the MMSE solution. In addition, we will devote considerable attention to several novel blind equalization algorithms which are useful when training data is unavailable or is insufficient.

1.2 Previous and Related Work

The first work to address (non-adaptive) equalization of orthogonal signals was [2], wherein the author focused on the particular class of orthogonal modulation called pulse position modulation (PPM). The zero-forcing (ZF) DFE was derived under the following restrictive assumptions: the channel is known, the channel is monic and minimum phase, the additive noise is ignored (i.e. since it is a ZF equalizer), and the feedback portion of the equalizer is as long as the channel (and possibly

infinite). In [44], the equalization of general orthogonal modulation was addressed, wherein the author proposed a ZF DFE that employs an infinite impulse response (IIR) feedforward filter under the assumption of a known channel. Equalization of biorthogonal systems was considered in [39], wherein the authors conducted a simulation study of a reduced state Viterbi equalizer. Again, however, the equalizer used in [39] requires perfect channel knowledge, and is quite complex since it requires sequence estimation. To our knowledge, the equalization of systems employing transorthogonal modulation has never been studied. Nevertheless, we see there have been a handful of previous investigations of equalization for orthogonal and biorthogonal signaling, though they all suffer from shortcomings which raise doubts about their use in practical systems:

- Non-adaptive equalizers that require perfect channel knowledge [2][39][44]
- Restrictive assumptions on channel (monic, minimum phase) [2]
- Inferior performance in noisy environments (due to ZF criterion) [2][44]
- No length constraint on equalizer [2][39][44]
- High complexity [39][44]

Because energy efficient modulations are non-i.i.d. at the chip level, the adaptive equalization of non-i.i.d. sources is a related area of research. However, the majority of work on adaptive filtering of non-i.i.d. sources has been in the context of blind source separation of convolutive mixtures [3][35]. In that application, the mixing matrix is prescribed to be tall, and the goal is to adapt a multichannel filter to recover the source data. The problem of interest here is fundamentally different since the channel matrix may not be tall, and may be constrained to be Tœplitz.

Lastly, we note that another related work is [23], where the effect of source statistics on an adaptive algorithm is analyzed; however, the focus there is on correlated sources rather than non-i.i.d. sources.

1.3 Description of Energy Efficient Modulations

An M-ary modulator in a digital communication system maps a sequence of bits into a set of corresponding signal waveforms. The mapping is performed by taking blocks of $\log_2 M$ bits at a time and selecting one of M deterministic, finite energy waveforms for transmission over the channel. In general, these waveform can differ in amplitude, phase, frequency, or in some combination of these. In orthogonal modulation, the M waveforms are chosen to be orthonormal. Biorthogonal modulation uses $M/2$ orthonormal waveforms, and modulates them antipodally to make M total waveforms. Transorthogonal modulation uses M equal energy waveforms with power $1 - 1/M$, and the waveforms have mutual correlation $-1/M$.

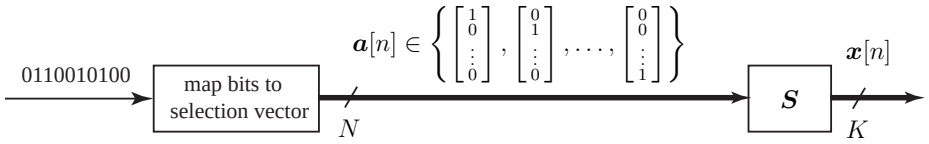

Figure 1.1: Modulator Block Diagram

To more easily accommodate all these classes of signal sets in the most generality, we break the modulator into two steps: the mapping of bits into a *selection vector* which we call $\boldsymbol{a}[n]$, and the selection of the corresponding waveform in the signal set matrix $\boldsymbol{S}$. Below, we will specify $\boldsymbol{a}[n]$ and $\boldsymbol{S}$ explicitly for each modulation. The selection vector $\boldsymbol{a}[n]$ will be a (possibly antipodally modulated) unit canonical vector, and the columns of $\boldsymbol{S}$ will represent the chosen signal waveforms.

The modulator is shown pictorially in Fig. 1.1 and allows us to write the symbol at time n as

$$\boldsymbol{x}[n] = \boldsymbol{S}\boldsymbol{a}[n]. \tag{1.1}$$

Note that we have assumed a digital baseband model, where we assume that each symbol waveform consists of K samples or *chips*. We will specify the minimum value of K necessary for representation of symbols from each M-ary modulation. Because fractionally-sampled receivers can be modelled by zero-padding the source sequence [18], our model is general enough to include fractional-sampling simply by increasing the number of samples K per waveform and zero-padding rows of $\boldsymbol{S}$. We assume throughout the dissertation that all signals are real[1], though the extension to complex signals is fairly straightforward.

We now consider each of the three modulation scheme in turn, specifying explicitly the allowable choices of $\boldsymbol{S}$ and $\boldsymbol{a}[n]$ for each modulation scheme. To indicate the modulation type, a signal with subscript o indicates orthogonal modulation, b indicates biorthogonal modulation, and t indicates transorthogonal modulation. If an equation applies to all modulation schemes, we omit the subscript.

1.3.1 Orthogonal Modulation

Orthogonal modulation, and its many variants including frequency shift keying (FSK) and pulse position modulation (PPM), has been used in countless applications over many decades. However, its use has typically been restricted to line-of-sight communication or low-data rate narrowband systems which are well modelled by AWGN channels. This modulation scheme is often used with receivers

[1] with the exception of Appendix F, which demonstrates a complex implementation of a blind algorithm

employing non-coherent detection, which results in an SNR penalty but permits the receiver to be implemented very simply. In fact, it has been conjectured that orthogonal modulation is the globally optimal modulation scheme for the AWGN channel with noncoherent reception, and this has been shown to be the case at high SNR [38]. The focus here, however, is on on high performance, high data-rate systems, and so we only consider coherent detection.

A signal set for orthogonal modulation is constructed by selecting M equal energy orthogonal waveforms. We let $\boldsymbol{S}_o \in \mathbb{R}^{K \times M}$ be the matrix of symbol waveforms, where K is the number of chips per symbol. The orthogonality of the signal waveforms requires that $\boldsymbol{S}_o$ be chosen to satisfy

$$\boldsymbol{S}_o^\top \boldsymbol{S}_o = \boldsymbol{I}_M.$$

This condition implies that $K \geq M$. We let the selection vector $\boldsymbol{a}_o[n] \in \mathbb{R}^M$ be a unit canonical vector, where the position of the 1 in $\boldsymbol{a}_o[n]$ indicates which column of $\boldsymbol{S}_o$ will be selected, and so a symbol originating from a system employing orthogonal modulation can be expressed as in (1.1).

1.3.2 Biorthogonal Modulation

Biorthogonal modulation, sometimes called M-ary biorthogonal keying (MBOK), combines orthogonal modulation with antipodal modulation, giving up some of the energy efficiency of orthogonal modulation in exchange for spectral efficiency. This modulation has recently been considered for use in several consumer wireless standards, including the IEEE 802.11 WLAN standard [46] and the ultra wideband IEEE 802.15.3a WPAN standard [9]. In biorthogonal modulation, the M waveforms comprise $M/2$ orthonormal waveforms along with their antipodal

counterparts. We let $\boldsymbol{S}_b \in \mathbb{R}^{K \times M/2}$ represent the matrix of chosen orthonormal waveforms, but now the selection vector $\boldsymbol{a}_b[n] \in \mathbb{R}^{M/2}$ is an antipodally modulated unit canonical vector, where the position of the ± 1 in $\boldsymbol{a}_b[n]$ indicates which column of $\boldsymbol{S}_b$ is selected, as well as its sign. For orthonormality of the waveforms, we again require

$$\boldsymbol{S}_b^\top \boldsymbol{S}_b = \boldsymbol{I}_{M/2}.$$

which in this case implies $K \geq M/2$.

1.3.3 Transorthogonal Modulation

Transorthogonal modulation, also called simplex modulation, is one of the most energy efficient modulation known for the AWGN channel. For decades it was thought to be the optimal modulation for the AWGN channel with coherent reception [37], but this was recently discovered not to be the case in general, particularly at low SNR.

Transorthogonal modulation improves upon the energy efficiency of orthogonal modulation. Signals in systems employing orthogonal modulation are not zero-mean, since it is impossible for M orthogonal vectors to sum to zero — and this is wasteful of energy. By simple coordinate translation of an orthogonal signal set (i.e. subtracting the DC component or mean of all M waveforms from each waveform), we arrive at a new signal set with the same Euclidean distance properties as the orthogonal signal set, but requires less transmission power to maintain the same Euclidean distance. The resulting signals are equally correlated with the most negative correlation that can be achieved with M equal energy signals [36].

The waveforms in the translated signal set correspond to the vertices of a regular M-simplex, explaining why this modulation is sometimes called simplex

modulation. Thus, given any M-ary orthogonal signal set $\boldsymbol{S}_o$, we can construct a transorthogonal signal set by subtracting the mean of its columns via

$$\begin{aligned} \boldsymbol{S}_t &= \boldsymbol{S}_o - \frac{1}{M}\boldsymbol{S}_o \mathbf{1}_{M\times M} \\ &= \boldsymbol{S}_o \underbrace{\left(\boldsymbol{I}_M - \frac{1}{M}\mathbf{1}_{M\times M}\right)}_{\triangleq \boldsymbol{J}_M} \end{aligned} \tag{1.2}$$

Lemma 1.1. *Properties of* $\boldsymbol{J}_M$

The matrix $\boldsymbol{J}_M \triangleq \boldsymbol{I}_M - \frac{1}{M}\mathbf{1}_{M\times M}$ *is idempotent, symmetric, semi-positive definite, and has rank* $M-1$.

Proof. To see that $\boldsymbol{J}_M$ is idempotent,

$$\begin{aligned} \boldsymbol{J}_M^2 &= \left(\boldsymbol{I}_M - \frac{1}{M}\mathbf{1}_{M\times M}\right)^2 \\ &= \boldsymbol{I}_M - \frac{2}{M}\mathbf{1}_{M\times M} + \frac{1}{M^2}\mathbf{1}_{M\times M}^2 \\ &= \boldsymbol{I}_M - \frac{1}{M}\mathbf{1}_{M\times M} \\ &= \boldsymbol{J}_M \end{aligned}$$

As for symmetry, it is easy to see that $\boldsymbol{J} = \boldsymbol{J}^\top$. It is well known that the eigenvalues of an idempotent matrix can only assume values zero or one [17], thus the matrix is semi-positive definite. The trace of a matrix equals the sum of its eigenvalues, so the trace of $\boldsymbol{J}$ is $M-1$. Thus, the matrix $\boldsymbol{J}$ has $M-1$ eigenvalues that are 1, one eigenvalue that is 0, and hence has rank $M-1$. ∎

From (1.2), the matrix of transorthogonal signal waveforms $\boldsymbol{S}_t \in \mathbb{R}^{K\times M}$ satisfies

$$\boldsymbol{S}_t^\top \boldsymbol{S}_t = \boldsymbol{I}_M - \frac{1}{M}\mathbf{1}_{M\times M}, \tag{1.3}$$

and we see that the transorthogonal waveforms are equally correlated with correlation $-1/M$. Furthermore, the transorthogonal signals require less energy, by

Table 1.2: Conditions on $\boldsymbol{S} \in \mathbb{R}^{K \times N}$ for each M-ary modulation

modulation	K_{min}	N	$\boldsymbol{S}^\top \boldsymbol{S}$
orthogonal	M	M	$\boldsymbol{I}_N$
biorthogonal	$M/2$	$M/2$	$\boldsymbol{I}_N$
transorthogonal	$M-1$	M	$\boldsymbol{I}_N - \frac{1}{N}\mathbf{1}_{N \times N}$

the factor $1 - 1/M$, than orthogonal modulation to maintain the same Euclidean distance among signal waveforms. Note that a transorthogonal signal set need not be constructed by translating an orthogonal signal set; a transorthogonal signal set merely needs to satisfy (1.3). Thus, since the rank of $\boldsymbol{J}_M$ is $M - 1$, we merely need $K \geq M - 1$.

1.3.4 Summary Of Modulations

Thus, symbols from each of these modulations can be expressed in the form of (1.1). In Table 1.2, we summarize the specification of $\boldsymbol{S}$ for each of the modulations. As we have seen, there is a minimum number of rows of $\boldsymbol{S}$ necessary for representation of each of these modulations, and these values K_{min} are summarized in the table. In addition, we have seen that the number of columns in the signal set matrix for orthogonal and transorthogonal modulations is M, while the number of columns in the signal set matrix for biorthogonal modulation is $M/2$. So, we define a new parameter N which is equal to the number of columns in $\boldsymbol{S}$ for a particular modulation, and so we can always write $\boldsymbol{S} \in \mathbb{R}^{K \times N}$. These values are also summarized in Table 1.2.

Lastly in our summary of the modulations, we recall that for orthogonal and

transorthogonal modulation,

$$\boldsymbol{a}_o[n], \boldsymbol{a}_t[n] \in \left\{ \begin{bmatrix} 1 \\ 0 \\ \vdots \\ 0 \end{bmatrix}, \begin{bmatrix} 0 \\ 1 \\ \vdots \\ 0 \end{bmatrix}, \ldots, \begin{bmatrix} 0 \\ 0 \\ \vdots \\ 1 \end{bmatrix} \right\}$$

while for biorthogonal modulation,

$$\boldsymbol{a}_b[n] \in \left\{ \pm \begin{bmatrix} 1 \\ 0 \\ \vdots \\ 0 \end{bmatrix}, \pm \begin{bmatrix} 0 \\ 1 \\ \vdots \\ 0 \end{bmatrix}, \ldots, \pm \begin{bmatrix} 0 \\ 0 \\ \vdots \\ 1 \end{bmatrix} \right\}$$

We can plot a K-chip signal constellation by plotting the value of each chip along an axis. For $K = 2$, we have plotted example constellations for each modulation, along with the optimal (i.e. maximum likelihood) decision regions in Fig. 1.2. We note that any rotation of these example constellations results in a permissible signal set.

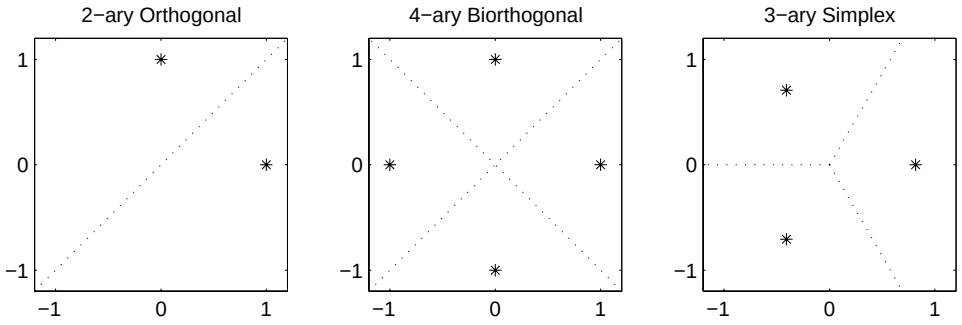

Figure 1.2: Example Constellations

In practice, the most popular choices of $\boldsymbol{S}$ for orthogonal modulation are: $\boldsymbol{S}_o = \boldsymbol{I}$ which corresponds to PPM, and the Hadamard matrix which is sometimes referred to as *Walsh modulation* [40]. The popularity of these choices is partly due to their ease of implementation, since $\boldsymbol{S}$ only contains 0 and ± 1 for these choices of $\boldsymbol{S}$. Another choice is the DFT matrix, which corresponds to FSK; however, this involves complex values, which are not considered in this dissertation (though, as mentioned, the extension is fairly straightforward). The identity and

Hadamard matrices are also popular choices of $\boldsymbol{S}$ for biorthogonal modulation, as these were the choices made in the standards proposals for IEEE 802.15.3a [9] and IEEE 802.11 [46], respectively.

1.4 The Optimal Detector in the AWGN Channel

Applying our sampled baseband model to the AWGN channel, we can express the received signal as

$$\boldsymbol{y}[n] = \boldsymbol{x}[n] + \boldsymbol{w}[n]. \tag{1.4}$$

The optimal (i.e. maximum likelihood) decision device for the AWGN channel is the minimum distance detector, which amounts to choosing the maximum output of M correlators matched to the M waveforms [29]. In the case of biorthogonal modulation, the correlation can be accomplished with only $M/2$ correlators, but the sign of the correlator output needs to be taken into account. We let $\mathcal{Q}(\cdot)$ denote the nonlinear operation that chooses the appropriate correlator output, so that the decision device output for each modulation can be written

$$\hat{\boldsymbol{a}}[n] \;\; = \;\; \mathcal{Q}(\boldsymbol{S}^{\top}\boldsymbol{y}[n]) \tag{1.5}$$

For orthogonal and transorthogonal modulation, $\mathcal{Q}(\cdot)$ is defined as

$$\mathcal{Q}_o(\boldsymbol{x}) = \mathcal{Q}_t(\boldsymbol{x}) = \boldsymbol{e}_i \tag{1.6}$$

where i is the index of the largest element in $\boldsymbol{x}$. For biorthogonal modulation,

$$\mathcal{Q}_b(\boldsymbol{x}) = \mathrm{sgn}(x_i)\boldsymbol{e}_i \tag{1.7}$$

where i is the index of the largest element in $|\boldsymbol{x}|$. To make this clear consider these examples:

$$\mathcal{Q}_o\left(\begin{bmatrix}0.2\\0.8\\-1.2\end{bmatrix}\right)=\begin{bmatrix}0\\1\\0\end{bmatrix} \quad \text{and} \quad \mathcal{Q}_b\left(\begin{bmatrix}0.2\\0.8\\-1.2\end{bmatrix}\right)=\begin{bmatrix}0\\0\\-1\end{bmatrix}$$

The decision regions for the minimum distance detector were included on the example constellations plotted in Fig. 1.2. The error performance of the ML detector is well known [36] for each of these modulations, and all of these modulations have the property that the bit error probability goes to zero as M grows large[2]. In Fig. 1.3 we plot the bit error rate (BER) in AWGN as a function of the SNR per bit when $M = 8$, and for comparison we include the BER of 8-PAM. Note

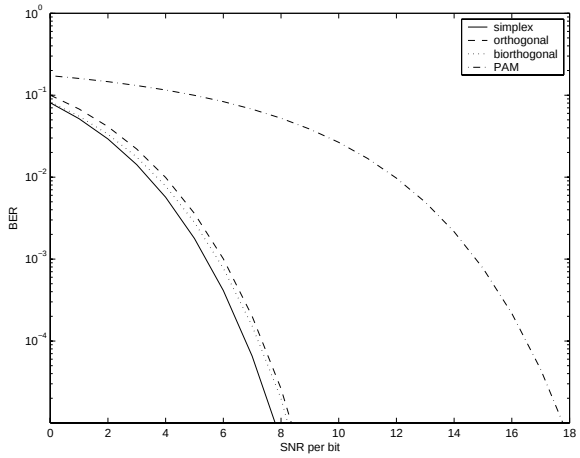

Figure 1.3: BER Comparison for 8-ary Modulations

that the BER depends on the chosen mapping of bits-to-waveforms; we have used the choices made in [36] (i.e. complementary bit encoding for biorthogonal modulation, arbitrary mapping for orthogonal and transorthogonal modulations, and

[2]This can be shown via the union bound [29], and requires that the SNR satisfy $\mathcal{E}_b/N_0 > \ln 2 \approx -1.6$dB which is precisely the Shannon limit.

Gray encoding for PAM). We see that, in an uncoded system without consideration for bandwidth, PAM is far less energy efficient than orthogonal, biorthogonal, and transorthogonal modulations.

1.5 Comparison with PAM

Pulse-amplitude modulation (PAM), which is in the class of those that are spectrally efficient, is one of the most studied modulations. Because of this, it is useful to point out several differences between M-ary PAM and the M-ary multipulse modulations considered in this dissertation.

As mentioned, the energy efficient modulations considered in this dissertation all attain zero probability of error as M grows large. This is not the case with PAM, as increasing the alphabet size with PAM results in a worse bit-error-rate as a function of the per-bit signal-to-noise ratio. However, for a fixed symbol rate, the bandwidth of a PAM system stays constant despite changes in M, which is not the case with orthogonal, biorthogonal, and transorthogonal modulations. Thus, in choosing between PAM and the multipulse modulations considered here, we see there is a tradeoff between energy efficiency and bandwidth efficiency. This tradeoff can be further adjusted with source coding techniques, but in this dissertation we only consider uncoded modulation.

PAM is a linear modulation where each symbol can be represented by a single sample. Furthermore, a PAM receiver can generate sufficient statistics by sampling only once every T seconds, where $1/T$ is the symbol rate. Often times, however, digital PAM receivers will sample the symbol more than once, a situation which is referred to as *oversampling* or *fractional sampling*, and the number of samples per symbol is referred to as the *oversampling rate*. In contrast to PAM, the energy

efficient multipulse modulations studied in this dissertation always require a vector of samples to represent a symbol, where the minimal number of samples per symbol K_{min} relates to the dimensionality of the signal set, and was given in Table 1.2. For energy efficient modulations, we say the receiver employs oversampling when the number of samples per symbol K is larger than K_{min}, and the oversampling rate is given by the ratio K/K_{min}.

1.6 Dissertation Organization

The dissertation is organized into six chapters. In Chapter 2, we present the generalized multirate system model which encapsulates all of these energy efficient modulations, and is general enough to accommodate both chip-spaced and fractionally-chip-spaced implementations. We note that the model includes BPSK as a special case, which is convenient because it provides us with a point of reference that allows us to make connections to known results and concepts. After analyzing some statistical properties of signals originating from these energy efficient modulations, we proceed to derive the MMSE settings for the first equalizer structure under consideration: the scalar chip-rate DFE, which is very similar to the classical DFE. For biorthogonal modulation, the MMSE settings follow directly from Wiener filter theory. However, for orthogonal modulation we propose a modification to standard the MSE definition that exploits a property of orthogonal modulation. Next, we present the conditions for "perfect equalization", which impose constraints on the equalizer length, channel disparity, and the signal waveform. We conclude the chapter by deriving the equations for trained and decision-directed LMS adaptation of the equalizer structure.

In Chapter 3, we derive the MMSE settings for the second equalizer struc-

ture: the block DFE implemented as a multirate filter bank that operates symbol-by-symbol. We mimic much of what was done in Chapter 2 for this new structure, again presenting several modulation-specific modifications to the equalization structure. We again review the conditions for perfect equalization and find that the block structure permits perfect equalization in a larger variety of situations. We conclude with a comparison of computational complexity between the scalar and block equalization structure, and show that the block structure permits a reduction in complexity.

Adaptive linear equalization of these modulations is the focus of the second half of the dissertation. We begin Chapter 4 by discussing the use of DD-LMS for adapting equalizers for these energy efficient modulations, and discover that it is unsuitable for cold startup (which agrees with conventional wisdom for, say, pulse amplitude modulation). This leads us to consider the use of the two most popular classical blind equalization algorithms – the Constant Modulus Algorithm (CMA) and the Shalvi-Weinstein Algorithm (SWA) – both of which we show to be similarly unsuitable in their pure form largely due to their reliance on i.i.d. source statistics. With the lack of a suitable blind algorithm, we proceed with a general discussion of blind algorithm development, including the desired properties of blind algorithm cost functions, a methodology for algorithm assessment, and guidelines for selecting cost functions.

In Chapter 5, we put to use the previous discussion of algorithm development/assessment, and present the first two blind algorithms beyond decision direction for biorthogonal modulation, which includes a discussion of their characteristics and convergence. The first algorithm, called LTBOMB, is CMA-like in spirit, and we show that the zero-forcing solutions are locally stable under ideal condi-

tions. The second algorithm, called TROMBONE, was designed with a SWA-like philosophy in mind, and thus relies on a spectral prewhitener before equalization. We show that the ZF solutions are stationary points of TROMBONE, and include simulations demonstrating the performance of the two blind algorithms. Finally, Chapter 6 concludes the dissertation with a summary of results and a listing of some immediate open issues revealed by this dissertation.

Chapter 2

Scalar Equalization of Energy Efficient Modulations

This chapter introduces the multirate system model we will use throughout the dissertation, investigates the first- and second-order statistics of sources driven by these modulations, and describes the proposed scalar MMSE DFE. Since the three modulation schemes under consideration are all in the class of multipulse modulations, we are able to develop a single system model that encapsulates all of these modulations at once. In addition, we present the conditions that permit perfect linear equalization, and we provide the equations for LMS adaptation of this structure.

2.1 System Model

We now consider the model shown in Fig. 2.1, and in particular we focus on the design of the feedforward filter $\boldsymbol{f}$ and the feedback filter $\boldsymbol{g}$. As described in Section 1.3, the output of the M-ary modulator is product of the signal set matrix $\boldsymbol{S}$ and the selection vector:

$$\boldsymbol{x}[n] = \boldsymbol{S}\boldsymbol{a}[n]. \tag{2.1}$$

While up to now we have considered only a symbol-rate model, it will be convenient at times to consider the chip-rate process, where we recall that there are K chips

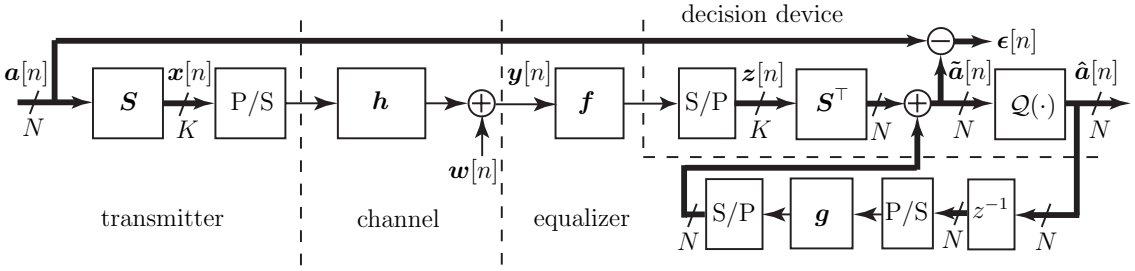

Figure 2.1: Scalar Equalizer System Model

per symbol. For this we use a polyphase representation, letting $x[Kn-k]$ denote the kth chip from the nth symbol, where $k \in \{0, \ldots, K-1\}$. In fact, this multirate system has three rates: the symbol rate $1/T$, the waveform chip rate K/T, and the rate of the corresponding chips of the selection vectors N/T.

The waveform chips $x[Kn-k]$ are transmitted through a causal linear time-invariant channel with finite impulse response $\boldsymbol{h} = [h[0], h[1], \ldots, h[N_h-1]]^\top$ (which includes the transmit and receiver filters) and are further corrupted by additive noise $w[Kn-k]$. While typically the noise will be modelled as AWGN, we only make the assumption that the noise is zero-mean and originates from a wide-sense stationary random process. We express the channel impulse response in matrix form by defining $\boldsymbol{H}[n] \in \mathbb{R}^{K \times K}$ where $[\boldsymbol{H}[n]]_{i,j} = h[Kn+j-i]$ are Tœplitz

matrices, so

$$\begin{aligned}
\boldsymbol{H}[0] &= \begin{bmatrix} h[0] & h[1] & \cdots & h[K-1] \\ 0 & h[0] & & \vdots \\ \vdots & & \ddots & h[1] \\ 0 & \cdots & 0 & h[0] \end{bmatrix} \\
\boldsymbol{H}[1] &= \begin{bmatrix} h[K] & h[K+1] & \cdots & h[2K-1] \\ h[K-1] & h[K] & & \vdots \\ \vdots & & \ddots & h[K+1] \\ h[1] & \cdots & h[K-1] & h[K] \end{bmatrix} \\
&\vdots
\end{aligned}$$

Then, the received symbol at time n is written

$$\boldsymbol{y}[n] = \sum_m \boldsymbol{H}[m]\boldsymbol{x}[n-m] + \boldsymbol{w}[n]. \tag{2.2}$$

The received chip stream $y[Kn-k]$ is passed through a linear feedforward equalizer with impulse response $\boldsymbol{f} = [f[0], f[1], \ldots, f[N_f-1]]^\top$. Similar to the definition of the channel matrix above, we express the feedforward equalizer impulse response in matrix form by defining $\boldsymbol{F}[n] \in \mathbb{R}^{K\times K}$ where $[\boldsymbol{F}[n]]_{i,j} = f[Kn+j-i]$. Then, the symbol output by the feedforward equalizer at time n is written

$$\boldsymbol{z}[n] = \sum_m \boldsymbol{F}[m]\boldsymbol{y}[n-m]. \tag{2.3}$$

The output of the feedforward equalizer passes through the correlator which projects the K-chip signal into the lower-dimensional N-chip space, to which we add the contribution from the feedback equalizer which has impulse response $\boldsymbol{g} = [g[0], g[1], \ldots, g[N_g-1]]^\top$. The feedback equalizer can be expressed in matrix form by defining $\boldsymbol{G}[n] \in \mathbb{R}^{N\times N}$ where $[\boldsymbol{G}[n]]_{i,j} = g[Nn+j-i]$. Thus, after adding

the contribution of the feedback equalizer we have a soft estimate of the selection vector $\tilde{\boldsymbol{a}}[n]$ given by

$$\tilde{\boldsymbol{a}}[n] \;=\; \boldsymbol{S}^{\top}\boldsymbol{z}[n] + \sum_{m} \boldsymbol{G}[m]\hat{\boldsymbol{a}}[n-m-1] \tag{2.4}$$

The decision device assumed throughout this dissertation is the naïve memoryless Euclidean distance detector, which was described in Section 1.4. As mentioned previously, we have broken the decision device into two operations: correlation and the nonlinear decision function $\mathcal{Q}(\cdot)$ defined in (1.6) and (1.7) for each modulation type. We have chosen this detector for its simplicity and low latency. The estimate of the selection vector is given by

$$\hat{\boldsymbol{a}}[n] \;=\; \mathcal{Q}(\tilde{\boldsymbol{a}}[n]) \tag{2.5}$$

As is typical of decision feedback equalizers, we have placed a one-symbol delay in the feedback path, which is evident in (2.4). The delay needs to be a full symbol since the decision device must wait until all K chips of the current symbol have been received before making a decision. Note that we could make tentative decisions as each chip is received, thereby reducing the feedback delay to a single chip rather than a whole symbol [2]; however, this technique will not be investigated here. When the equalizer is operating correctly, the decision device output is $\hat{\boldsymbol{a}}[n] \approx \boldsymbol{a}[n-\Delta]$ where Δ is the symbol delay through the combined channel and equalizer.

At times, it will be more convenient to use a formulation based on Hankel matrices that isolates the equalizer response vectors $\boldsymbol{f}$ and $\boldsymbol{g}$. In this case, the regressor matrix $\boldsymbol{Y}[n] \in \mathbb{R}^{N_f \times K}$ of received chips can be written

$$\boldsymbol{Y}[n] \;=\; \boldsymbol{\mathcal{H}}\boldsymbol{X}[n] + \boldsymbol{W}[n] \tag{2.6}$$

where $N_c \triangleq N_f + N_h - 1$ is the combined length of the channel and feedforward equalizer, $\boldsymbol{X}[n] \in \mathbb{R}^{N_c \times K}$ is the Hankel matrix of chips defined as $[\boldsymbol{X}[n]]_{i,j} = x[Kn - i - j]$, so

$$\boldsymbol{X}[n] = \begin{bmatrix} x[Kn] & x[Kn-1] & \cdots & x[Kn-K+1] \\ x[Kn-1] & x[Kn-2] & & \vdots \\ \vdots & & \ddots & x[Kn-N_c-K+3] \\ x[Kn-N_c+1] & \cdots & 0 & x[Kn-N_c-K+2] \end{bmatrix}$$

Similarly, $\boldsymbol{W}[n] \in \mathbb{R}^{N_f \times K}$ is the Hankel matrix of noise samples which is defined as $[\boldsymbol{W}[n]]_{i,j} = w[Kn - i - j]$, and $\boldsymbol{\mathcal{H}} \in \mathbb{R}^{N_f \times N_c}$ is the Tœplitz channel impulse response matrix defined as $[\boldsymbol{\mathcal{H}}]_{i,j} = h[j - i]$. Then, the symbol output by the feedforward equalizer at time n can be written

$$\boldsymbol{z}[n] = \boldsymbol{Y}^\top[n]\boldsymbol{f}. \tag{2.7}$$

and the soft estimates of the selection vector can be written

$$\tilde{\boldsymbol{a}}[n] = \boldsymbol{S}^\top \boldsymbol{z}[n] + \hat{\boldsymbol{A}}^\top[n-1]\boldsymbol{g} \tag{2.8}$$

where the Hankel matrix of selection vector estimates $\hat{\boldsymbol{A}}[n] \in \mathbb{R}^{N_g \times N}$ is defined as $[\hat{\boldsymbol{A}}[n]]_{i,j} = \hat{a}[Nn - i - j]$.

In the sequel, we will switch between the symbol-by-symbol model (2.2)-(2.4) and the equivalent block matrix model (2.6)-(2.8) whenever convenient. From time to time, we will also use the combined channel/feedforward equalizer response, which can be equivalently written as

$$\begin{aligned} \boldsymbol{c} &\triangleq \boldsymbol{\mathcal{H}}^\top \boldsymbol{f} \\ \boldsymbol{C}[n] &\triangleq \sum_m \boldsymbol{F}[m]\boldsymbol{H}[n-m]. \end{aligned}$$

Our sampled model assumes that carrier recovery has been dealt with before equalization, and thus its effect is not considered in our model. The effects of pulse shaping and imperfect chip sample timing acquisition can be lumped into the channel $\boldsymbol{h}$, however. In addition to chip timing, some means of symbol timing (i.e. aligning the chips so the block decision device operates on the symbol boundary) will be necessary. While our model does not assume that symbol timing has been accounted for before equalization, knowledge of the appropriate symbol timing can be incorporated into the equalizer by smart choice of combined channel/equalizer delay.

Finally, we note that this structure is quite general in that it includes many previously studied receivers as special cases. For example, the optimum receiver in AWGN for energy efficient modulations discussed in Section 1.4 is a special case. This can be seen by letting $\boldsymbol{h} = 1$ (i.e. the AWGN channel), and choosing $\boldsymbol{f} = 1$ and $\boldsymbol{g} = 0$. In this case $\boldsymbol{z}[n] = \boldsymbol{y}[n]$, and so equations for the AWGN channel model (1.4) and (1.5) apply to this model.

Another special case is that of baud-spaced and fractionally-spaced equalization of BPSK signals. As mentioned in Section 1.5, biorthogonal and transorthogonal modulation can be exactly BPSK when $M = 2$. In particular, for the following signal set matrices, our structure reduces to standard baud- and fractionally-spaced

equalization of BPSK:

$$\text{biorthogonal} \begin{cases} \boldsymbol{S}_b = 1 & \rightarrow \text{ baud-spaced BPSK} \\ \boldsymbol{S}_b = \begin{bmatrix} 1 \\ 0 \end{bmatrix} & \rightarrow \text{ fractionally-spaced BPSK} \end{cases}$$

$$\text{transorthogonal} \begin{cases} \boldsymbol{S}_t = \frac{1}{\sqrt{2}} \begin{bmatrix} 1 & -1 \end{bmatrix} & \rightarrow \text{ baud-spaced BPSK} \\ \boldsymbol{S}_t = \frac{1}{\sqrt{2}} \begin{bmatrix} 1 & -1 \\ 0 & 0 \end{bmatrix} & \rightarrow \text{ fractionally-spaced BPSK} \end{cases}$$

Fractionally-spaced DFEs typically have a downsampling operation following the linear portion of the equalizer. Downsampling is accomplished in our receiver by the correlator (i.e. multiplication with $\boldsymbol{S}^\top$) which reduces the number of samples per symbol from K to N. The correlator is a multirate block filter which can be viewed in polyphase representation as shown in Fig. 2.2, where $[\boldsymbol{S}]_i$ denotes the ith column of $\boldsymbol{S}$. Recall that our receiver is fractionally-spaced when $K > K_{min}$.

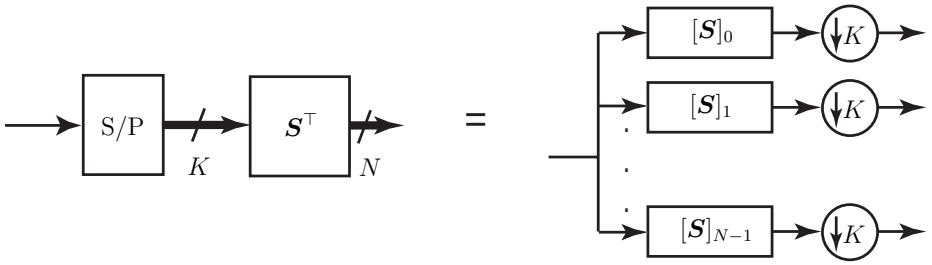

Figure 2.2: Block Filtering as Multirate System

2.2 Statistical Properties of the Source Signal

Before discussing methods for choosing the equalizer tap settings, we first discuss some of the statistical properties of signals originating from the modulations under

study. Throughout this dissertation, we make the assumption that the symbols are i.i.d. and equiprobable (note that, however, the chips within a symbol will not be i.i.d.). The first-order moments become

$$\begin{aligned} E[\boldsymbol{x}_o[n]] &= E[\boldsymbol{S}\boldsymbol{a}_o[n]] \\ &= \boldsymbol{S}E[\boldsymbol{a}_o[n]] \\ &= \frac{1}{N}\boldsymbol{S}\mathbf{1}_{N\times 1} \end{aligned} \tag{2.9}$$

$$\begin{aligned} E[\boldsymbol{x}_b[n]] &= \boldsymbol{S}E[\boldsymbol{a}_b[n]] \\ &= \mathbf{0}_{K\times 1} \end{aligned} \tag{2.10}$$

$$\begin{aligned} E[\boldsymbol{x}_t[n]] &= \boldsymbol{S}E[\boldsymbol{a}_t[n]] \\ &= \frac{1}{N}\boldsymbol{S}\mathbf{1}_{N\times 1} \\ &= \mathbf{0}_{K\times 1} \end{aligned} \tag{2.11}$$

The last line (2.11) showing that transorthogonal modulation is zero-mean may not be immediately obvious, but is due to the conditions on $\boldsymbol{S}$ for transorthogonal modulation, and can be seen by first showing that $||E[\boldsymbol{x}_t[n]]||_2^2 = 0$, which implies $E[\boldsymbol{x}_t[n]] = \mathbf{0}$. Thus, biorthogonal and transorthogonal modulations result in symbol vectors that are zero-mean, whereas symbols from orthogonal modulation are not zero-mean.

We now consider the second-order moments. For $n \neq m$, we have

$$\begin{aligned} E[\boldsymbol{x}_o[n]\boldsymbol{x}_o^\top[m]] &= E[\boldsymbol{x}_o[n]]E[\boldsymbol{x}_o^\top[m]] \\ &= \frac{1}{N^2}\boldsymbol{S}\mathbf{1}_{N\times N}\boldsymbol{S}^\top \\ E[\boldsymbol{x}_b[n]\boldsymbol{x}_b^\top[m]] &= E[\boldsymbol{x}_b[n]]E[\boldsymbol{x}_b^\top[m]] \\ &= \mathbf{0} \\ E[\boldsymbol{x}_t[n]\boldsymbol{x}_t^\top[m]] &= E[\boldsymbol{x}_t[n]]E[\boldsymbol{x}_t^\top[m]] \\ &= \mathbf{0} \end{aligned}$$

where we have used the fact that the symbols are i.i.d. For all modulations,

$$\begin{aligned} E[\boldsymbol{x}[n]\boldsymbol{x}^\top[n]] &= \boldsymbol{S}E[\boldsymbol{a}[n]\boldsymbol{a}^\top[n]]\boldsymbol{S}^\top \\ &= \frac{1}{N}\boldsymbol{S}\boldsymbol{S}^\top \end{aligned}$$

Thus, the second-order moments are given by

$$E[\boldsymbol{x}_o[n]\boldsymbol{x}_o^\top[m]] = \begin{cases} \frac{1}{N}\boldsymbol{S}\boldsymbol{S}^\top & n = m \\ \frac{1}{N^2}\boldsymbol{S}\mathbf{1}_{N\times N}\boldsymbol{S}^\top & n \neq m \end{cases} \tag{2.12}$$

$$E[\boldsymbol{x}_b[n]\boldsymbol{x}_b^\top[m]] = \begin{cases} \frac{1}{N}\boldsymbol{S}\boldsymbol{S}^\top & n = m \\ \mathbf{0}_{K\times K} & n \neq m \end{cases} \tag{2.13}$$

$$E[\boldsymbol{x}_t[n]\boldsymbol{x}_t^\top[m]] = \begin{cases} \frac{1}{N}\boldsymbol{S}\boldsymbol{S}^\top & n = m \\ \mathbf{0}_{K\times K} & n \neq m \end{cases} \tag{2.14}$$

2.3 The MMSE Equalizer

We now present the design equations for the equalizer based on minimizing the mean-squared error, which is a standard benchmark of equalizer performance. We address each of the modulation types separately in turn, and we start with

biorthogonal modulation since the others build upon ideas presented for biorthogonal modulation. The MMSE equalizer accepts one design parameter, Δ, which represents the desired symbol delay through the channel/equalizer chain.

2.3.1 Biorthogonal Modulation

Following the standard approach to MMSE equalizer design, we first form the error between the pre-decision device "soft-estimate" of the selection vector $\tilde{\boldsymbol{a}}[n]$ and the delayed transmitted selection vector $\boldsymbol{a}[n-\Delta]$, which is indicated by $\boldsymbol{\epsilon}[n]$ in Fig. 2.1. Since this error signal is a vector, the MSE metric we choose is the average of the sum of the squared components of the error vector, or the mean-square of the ℓ_2 norm of the error vector,

$$J_{MSE}(\boldsymbol{f},\boldsymbol{g},\Delta) \;=\; E\left[||\tilde{\boldsymbol{a}}[n]-\boldsymbol{a}[n-\Delta]||_2^2\right]. \tag{2.15}$$

Expanding (2.15) via (2.1), (2.6), and (2.7), we have

$$\begin{aligned}
J_{MSE}(\boldsymbol{f},\boldsymbol{g},\Delta)=&E\left[||\boldsymbol{S}^\top\boldsymbol{Y}^\top[n]\boldsymbol{f}+\hat{\boldsymbol{A}}^\top[n-1]\boldsymbol{g}-\boldsymbol{S}^\top\boldsymbol{x}[n-\Delta]||_2^2\right]\\
=&E\Big[||\boldsymbol{S}^\top\left(\boldsymbol{X}^\top[n]\boldsymbol{\mathcal{H}}^\top+\boldsymbol{W}^\top[n]\right)\boldsymbol{f}+\hat{\boldsymbol{A}}^\top[n-1]\boldsymbol{g}\\
&\qquad\qquad-\boldsymbol{S}^\top\boldsymbol{X}^\top[n]\boldsymbol{e}_{K\Delta}||_2^2\Big]\\
=&\boldsymbol{f}^\top\boldsymbol{\mathcal{H}}E\left[\boldsymbol{X}[n]\boldsymbol{S}\boldsymbol{S}^\top\boldsymbol{X}^\top[n]\right]\boldsymbol{\mathcal{H}}^\top\boldsymbol{f}+\boldsymbol{f}^\top\boldsymbol{\mathcal{H}}E\left[\boldsymbol{X}[n]\boldsymbol{S}\boldsymbol{S}^\top\boldsymbol{W}^\top[n]\right]\boldsymbol{f}\\
&+\boldsymbol{f}^\top\boldsymbol{\mathcal{H}}E\left[\boldsymbol{X}[n]\boldsymbol{S}\hat{\boldsymbol{A}}^\top[n-1]\right]\boldsymbol{g}-\boldsymbol{f}^\top\boldsymbol{\mathcal{H}}E\left[\boldsymbol{X}[n]\boldsymbol{S}\boldsymbol{S}^\top\boldsymbol{X}^\top[n]\right]\boldsymbol{e}_{K\Delta}\\
&+\boldsymbol{f}^\top E\left[\boldsymbol{W}[n]\boldsymbol{S}\boldsymbol{S}^\top\boldsymbol{X}^\top[n]\right]\boldsymbol{\mathcal{H}}^\top\boldsymbol{f}+\boldsymbol{f}^\top E\left[\boldsymbol{W}[n]\boldsymbol{S}\boldsymbol{S}^\top\boldsymbol{W}^\top[n]\right]\boldsymbol{f}\\
&+\boldsymbol{f}^\top E\left[\boldsymbol{W}[n]\boldsymbol{S}\hat{\boldsymbol{A}}^\top[n-1]\right]\boldsymbol{g}-\boldsymbol{f}^\top E\left[\boldsymbol{W}[n]\boldsymbol{S}\boldsymbol{S}^\top\boldsymbol{X}^\top[n]\right]\boldsymbol{e}_{K\Delta}\\
&+\boldsymbol{g}^\top E\left[\hat{\boldsymbol{A}}[n-1]\boldsymbol{S}^\top\boldsymbol{X}^\top[n]\right]\boldsymbol{\mathcal{H}}^\top\boldsymbol{f}+\boldsymbol{g}^\top E\left[\hat{\boldsymbol{A}}[n-1]\boldsymbol{S}^\top\boldsymbol{W}^\top[n]\right]\boldsymbol{f}\\
&+\boldsymbol{g}^\top E\left[\hat{\boldsymbol{A}}[n-1]\hat{\boldsymbol{A}}^\top[n-1]\right]\boldsymbol{g}-\boldsymbol{g}^\top E\left[\hat{\boldsymbol{A}}[n-1]\boldsymbol{S}^\top\boldsymbol{X}^\top[n]\right]\boldsymbol{e}_{K\Delta}\\
&-\boldsymbol{e}_{K\Delta}^\top E\left[\boldsymbol{X}[n]\boldsymbol{S}\boldsymbol{S}^\top\boldsymbol{X}^\top[n]\right]\boldsymbol{\mathcal{H}}^\top\boldsymbol{f}-\boldsymbol{e}_{K\Delta}^\top E\left[\boldsymbol{X}[n]\boldsymbol{S}\boldsymbol{S}^\top\boldsymbol{W}^\top[n]\right]\boldsymbol{f}\\
&-\boldsymbol{e}_{K\Delta}^\top E\left[\boldsymbol{X}[n]\boldsymbol{S}\hat{\boldsymbol{A}}^\top[n-1]\right]\boldsymbol{g}+\boldsymbol{e}_{K\Delta}^\top E\left[\boldsymbol{X}[n]\boldsymbol{S}\boldsymbol{S}^\top\boldsymbol{X}^\top[n]\right]\boldsymbol{e}_{K\Delta}\\
=&\boldsymbol{f}^\top\boldsymbol{\mathcal{H}}\boldsymbol{R}_{xx}\boldsymbol{\mathcal{H}}^\top\boldsymbol{f}+2\boldsymbol{f}^\top\boldsymbol{\mathcal{H}}\boldsymbol{R}_{x\hat{a}}\boldsymbol{g}-2\boldsymbol{f}^\top\boldsymbol{\mathcal{H}}\boldsymbol{R}_{xx}\boldsymbol{e}_{K\Delta}-2\boldsymbol{g}^\top\boldsymbol{R}_{x\hat{a}}^\top\boldsymbol{e}_{K\Delta}\\
&+\boldsymbol{f}^\top\boldsymbol{R}_{ww}\boldsymbol{f}+\boldsymbol{g}^\top\boldsymbol{R}_{\hat{a}\hat{a}}\boldsymbol{g}+\boldsymbol{e}_{K\Delta}^\top\boldsymbol{R}_{xx}\boldsymbol{e}_{K\Delta} \qquad (2.16)
\end{aligned}$$

where we have assumed the noise and data are uncorrelated, and we define

$$\boldsymbol{R}_{xx} \triangleq E\left[\boldsymbol{X}[n]\boldsymbol{S}\boldsymbol{S}^\top\boldsymbol{X}^\top[n]\right] \qquad (2.17)$$

$$\boldsymbol{R}_{\hat{a}\hat{a}} \triangleq E\left[\hat{\boldsymbol{A}}[n-1]\hat{\boldsymbol{A}}^\top[n-1]\right] \qquad (2.18)$$

$$\boldsymbol{R}_{x\hat{a}} \triangleq E\left[\boldsymbol{X}[n]\boldsymbol{S}\hat{\boldsymbol{A}}^\top[n-1]\right] \qquad (2.19)$$

$$\boldsymbol{R}_{ww} \triangleq E\left[\boldsymbol{W}[n]\boldsymbol{S}\boldsymbol{S}^\top\boldsymbol{W}^\top[n]\right]. \qquad (2.20)$$

Setting the gradient of $J_{MSE}(\boldsymbol{f}, \boldsymbol{g}, \Delta)$ with respect to $\boldsymbol{g}$ to zero gives

$$\begin{aligned} \frac{1}{2}\frac{J(\boldsymbol{f},\boldsymbol{g})}{\partial \boldsymbol{g}} &= \boldsymbol{R}_{x\hat{a}}^{\top}\boldsymbol{\mathcal{H}}^{\top}\boldsymbol{f} - \boldsymbol{R}_{x\hat{a}}^{\top}\boldsymbol{e}_{K\Delta} + \boldsymbol{R}_{\hat{a}\hat{a}}\boldsymbol{g} \\ &= 0 \\ \Longrightarrow\ \boldsymbol{g}^{*} &= \boldsymbol{R}_{\hat{a}\hat{a}}^{-1}\boldsymbol{R}_{x\hat{a}}^{\top}\left[\boldsymbol{e}_{K\Delta} - \boldsymbol{\mathcal{H}}^{\top}\boldsymbol{f}\right] \end{aligned} \tag{2.21}$$

Setting the gradient of $J_{MSE}(\boldsymbol{f}, \boldsymbol{g}^{*}, \Delta)$ with respect to $\boldsymbol{f}$ to zero gives

$$\begin{aligned} \frac{1}{2}\frac{\partial J(\boldsymbol{f},\boldsymbol{g}^{*})}{\partial \boldsymbol{f}} &= \boldsymbol{\mathcal{H}}\boldsymbol{R}_{xx}\boldsymbol{\mathcal{H}}^{\top}\boldsymbol{f} + \boldsymbol{\mathcal{H}}\boldsymbol{R}_{x\hat{a}}\boldsymbol{g}^{*} - \boldsymbol{\mathcal{H}}\boldsymbol{R}_{xx}\boldsymbol{e}_{K\Delta} + \boldsymbol{R}_{ww}\boldsymbol{f} \\ &= \left[\boldsymbol{\mathcal{H}}\left(\boldsymbol{R}_{xx} - \boldsymbol{R}_{x\hat{a}}\boldsymbol{R}_{\hat{a}\hat{a}}^{-1}\boldsymbol{R}_{x\hat{a}}^{\top}\right)\boldsymbol{\mathcal{H}}^{\top} + \boldsymbol{R}_{ww}\right]\boldsymbol{f} \\ &\quad + \boldsymbol{\mathcal{H}}\left(\boldsymbol{R}_{x\hat{a}}\boldsymbol{R}_{\hat{a}\hat{a}}^{-1}\boldsymbol{R}_{x\hat{a}}^{\top} - \boldsymbol{R}_{xx}\right)\boldsymbol{e}_{K\Delta} \\ &= 0 \\ \Longrightarrow\ \boldsymbol{f}^{*} &= \left[\boldsymbol{\mathcal{H}}\boldsymbol{\mathcal{R}}\boldsymbol{\mathcal{H}}^{\top} + \boldsymbol{R}_{ww}\right]^{-1}\boldsymbol{\mathcal{H}}\boldsymbol{\mathcal{R}}\boldsymbol{e}_{K\Delta} \end{aligned} \tag{2.22}$$

where

$$\boldsymbol{\mathcal{R}} \triangleq \boldsymbol{R}_{xx} - \boldsymbol{R}_{x\hat{a}}\boldsymbol{R}_{\hat{a}\hat{a}}^{-1}\boldsymbol{R}_{x\hat{a}}^{\top} \tag{2.23}$$

We adopt the standard MMSE DFE assumption that the decisions $\hat{\boldsymbol{a}}[n]$ in the feedback path are correct, so that $\hat{\boldsymbol{a}}[n] = \boldsymbol{a}[n-\Delta]$. The assumption of correct feedback is needed only in the calculation of $\boldsymbol{R}_{x\hat{a}}$ in (2.19). Unfortunately, the above correlation matrices (2.17)-(2.20) do not lend themselves to compact closed-form expressions, as expanding the expectations is rather tedious. However, under the assumption of correct feedback, these matrices only involve second-order statistics of the source sequence, so their calculation is straightforward if tedious, and the details are provided in Appendix A.

2.3.2 Orthogonal Modulation

At first glance it might seem like the previous development of the MMSE DFE for biorthogonal modulation ought to be exactly the same for orthogonal modulation, perhaps with minor changes to the correlation matrices. However, a slight modification to the MSE definition enables us to reap a gain with orthogonal modulation, as we will describe below. Before deriving the MMSE DFE for orthogonal modulation, we first prove two lemmas.

Lemma 2.1. *Properties of* $\mathcal{Q}_o(\cdot)$

The orthogonal modulation decision device function $\mathcal{Q}_o(\cdot)$ *defined in (1.6) satisfies*

$$\mathcal{Q}_o(\tilde{\boldsymbol{a}}[n]) \;=\; \mathcal{Q}_o\left(\boldsymbol{J}_N\tilde{\boldsymbol{a}}[n]\right)$$

for $\boldsymbol{J}_N \triangleq \boldsymbol{I}_N - 1/N\mathbf{1}_{N\times N}$ *and any* $\tilde{\boldsymbol{a}}[n] \in \mathbb{R}^{N\times 1}$.

Proof. The decision device amounts to simply choosing the index of the largest element of the input vector. Consequently, the decision device is clearly unaffected by the addition of a constant to all elements of the input vector. Thus, for any scalar b,

$$\mathcal{Q}_o(\tilde{\boldsymbol{a}}[n]) = \mathcal{Q}_o(\tilde{\boldsymbol{a}}[n] + \mathbf{1}_{N\times 1}b).$$

Note that this is true when b is any scalar — even one that is a function of $\tilde{\boldsymbol{a}}[n]$. Consider the particular choice $b = -1/N\mathbf{1}_{N\times 1}^{\top}\tilde{\boldsymbol{a}}[n]$, so that b equals the negated average of the elements of $\tilde{\boldsymbol{a}}[n]$. For this choice,

$$\begin{aligned}
\mathcal{Q}_o(\tilde{\boldsymbol{a}}[n]) &= \mathcal{Q}_o\left(\tilde{\boldsymbol{a}}[n] - \frac{1}{M}\mathbf{1}_{N\times 1}\mathbf{1}_{N\times 1}^{\top}\tilde{\boldsymbol{a}}[n]\right) \\
&= \mathcal{Q}_o\left(\left(\boldsymbol{I} - \frac{1}{M}\mathbf{1}_{N\times N}\right)\tilde{\boldsymbol{a}}[n]\right) \\
&= \mathcal{Q}_o\left(\boldsymbol{J}_N\tilde{\boldsymbol{a}}[n]\right).
\end{aligned}$$

Thus, pre-multiplication of the decision-device input by $\boldsymbol{J}_N$ has no effect on the decision. Recall from Section 1.3.3 that multiplication by $\boldsymbol{J}_N$ projects an orthogonal signal set into a transorthogonal signal set with identical Euclidean distance properties. We also note that any scalar multiple of the vector $\mathbf{1}_{N\times 1}$ describes the nullspace of $\boldsymbol{J}_N$ (and $\boldsymbol{J}_N^\top$), since $\boldsymbol{J}_N\mathbf{1}_{N\times 1} = \mathbf{0}_{N\times 1}$. ■

Lemma 2.2. *Decomposition of* $\boldsymbol{J}_N$

For any square symmetric semi-positive definite matrix $\boldsymbol{J}_N \in \mathbb{R}^{N\times N}$*, there exists a rectangular upper-triangular matrix* $\boldsymbol{U}_N \in \mathbb{R}^{r\times N}$ *such that*

$$\boldsymbol{U}_N^\top \boldsymbol{U}_N = \boldsymbol{J}_N$$

where $r \leq N$ *is the rank of* $\boldsymbol{J}_N$*.*

Proof. While we will typically use this lemma with our particular choice of $\boldsymbol{J}$ from Lemma 2.1, this lemma applies to any square symmetric semi-positive definite matrix. The Cholesky decomposition is typically only defined for strictly positive definite matrices [14], and here we extend the definition to semi-positive definite matrices. Since $\boldsymbol{J}_N$ is symmetric and semi-positive definite, the singular value decomposition can be written as

$$\boldsymbol{J}_N = \boldsymbol{V}^\top \boldsymbol{\Sigma} \boldsymbol{V}$$

where $\boldsymbol{\Sigma}$ is a diagonal matrix containing the non-negative singular values, assumed to be in decreasing order. Then $\boldsymbol{\Sigma}$ can be written as $\boldsymbol{\Sigma} = \boldsymbol{\Gamma}^\top \boldsymbol{\Gamma}$ where $\boldsymbol{\Gamma} \in \mathbb{R}^{r\times N}$ is the extraction of the first r rows of $\boldsymbol{\Sigma}^{(1/2)}$. Note that the remaining $N - r$ rows of $\boldsymbol{\Sigma}^{(1/2)}$ are all zeros, and are thrown out. Next, let $\boldsymbol{Q}$ and $\boldsymbol{U}_N$ be the QR-decomposition of $\boldsymbol{\Gamma V}$ defined as

$$\boldsymbol{Q}\boldsymbol{U}_N = \boldsymbol{\Gamma V} \tag{2.24}$$

where $\boldsymbol{Q} \in \mathbb{R}^{r \times r}$ is orthogonal and $\boldsymbol{U}_N \in \mathbb{R}^{r \times N}$ is upper triangular. Summarizing this development, then,

$$\begin{aligned} \boldsymbol{J}_N &= \boldsymbol{V}^\top \boldsymbol{\Sigma} \boldsymbol{V} \\ &= \boldsymbol{V}^\top \boldsymbol{\Gamma}^\top \boldsymbol{\Gamma} \boldsymbol{V} \\ &= \boldsymbol{U}_N^\top \boldsymbol{Q}^\top \boldsymbol{Q} \boldsymbol{U} \\ &= \boldsymbol{U}_N^\top \boldsymbol{U}_N \end{aligned}$$

where $\boldsymbol{U}_N$ is upper triangular and of appropriate dimension. ■

Recall from Lemma 1.1 that our particular choice of $\boldsymbol{J}_N = \boldsymbol{I}_N - 1/N \mathbf{1}_{N \times N}$ has rank $N-1$, and can thus can expressed as $\boldsymbol{J}_N = \boldsymbol{U}_N^\top \boldsymbol{U}_N$ where $\boldsymbol{U}_N \in \mathbb{R}^{N-1 \times N}$.

Lemma 2.3. *More Properties of* $\boldsymbol{U}$

For $\boldsymbol{U}_N \in \mathbb{R}^{N-1 \times N}$ *defined as the decomposition of*

$$\begin{aligned} \boldsymbol{U}_N^\top \boldsymbol{U}_N &= \boldsymbol{J}_N \\ &= \boldsymbol{I}_N - \frac{1}{N} \mathbf{1}_{N \times N} \end{aligned}$$

we have

$$\boldsymbol{U}_N \boldsymbol{U}_N^\top = \boldsymbol{I}_{N-1}$$

and

$$\boldsymbol{U}_N \mathbf{1}_{N \times 1} = \mathbf{0}_{N-1 \times 1}.$$

Proof. We know from Lemma 1.1 that $\boldsymbol{J}_N$ has rank $N-1$, with all but one of the eigenvalues equal to 1. Thus, continuing with the notation from Lemma 2.2, we know that $\boldsymbol{J}_N$ can be decomposed as $\boldsymbol{J}_N = (\boldsymbol{\Gamma V})^\top (\boldsymbol{\Gamma V})$ with

$$\boldsymbol{\Gamma} = \begin{bmatrix} \boldsymbol{I}_{N-1} & \mathbf{0}_{N-1 \times 1} \end{bmatrix}$$

for this particular choice of $\boldsymbol{J}$. Clearly $\boldsymbol{\Gamma}\boldsymbol{\Gamma}^\top = \boldsymbol{I}$. From (2.24) we can express $\boldsymbol{U}_N$ as

$$\boldsymbol{U}_N = \boldsymbol{Q}^\top \boldsymbol{\Gamma} \boldsymbol{V}$$

so that

$$\begin{aligned} \boldsymbol{U}_N \boldsymbol{U}_N^\top &= \boldsymbol{Q}^\top \boldsymbol{\Gamma} \boldsymbol{V} \boldsymbol{V}^\top \boldsymbol{\Gamma}^\top \boldsymbol{Q} \\ &= \boldsymbol{I}_{N-1} \end{aligned}$$

due to the orthogonality of $\boldsymbol{Q}$ and $\boldsymbol{V}$.

To prove the second statement, note that

$$\begin{aligned} ||\boldsymbol{U}_N \mathbf{1}_{N\times 1}||_2^2 &= \mathbf{1}_{1\times N} \boldsymbol{U}_N^\top \boldsymbol{U}_N \mathbf{1}_{N\times 1} \\ &= \mathbf{1}_{1\times N} \boldsymbol{J}_N \mathbf{1}_{N\times 1} \\ &= \mathbf{1}_{1\times N} \left(\boldsymbol{I}_N - \frac{1}{N} \mathbf{1}_{N\times N} \right) \mathbf{1}_{N\times 1} \\ &= N - N \\ &= 0 \\ \implies \boldsymbol{U}_N \mathbf{1}_{N\times 1} &= \mathbf{0}_{N-1\times 1} \end{aligned}$$

■

Following from these lemmas, then, we can insert such a $\boldsymbol{U}_N$ and $\boldsymbol{U}_N^\top$ before the decision device as shown in Fig. 2.3. Though the path between $\tilde{\boldsymbol{a}}[n]$ and $\hat{\boldsymbol{a}}[n]$ appears to have been modified, the input-output relationship of this new equalizer structure is mathematically equivalent to the original equalizer structure shown in Fig. 2.1, and all of the previous equations (2.1)-(2.5) describing the system model still apply. By exploiting properties of the detector, we are able to reduce the

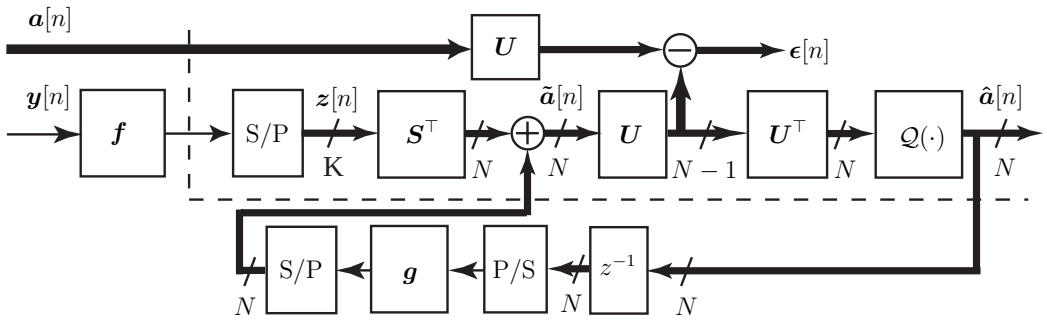

Figure 2.3: Equalizer with Modified Error Signal for Orthogonal Modulation

number of chips necessary to represent a symbol from N to $N-1$, and $\boldsymbol{U}$ effectively performs further downsampling of the signal.

Now, rather than forming the mean-squared error between $\tilde{\boldsymbol{a}}[n]$ and $\boldsymbol{a}[n-\Delta]$, we can form the error in a space of reduced dimension. It is pointless to account for the error in the larger space when subsequent multiplication of $\tilde{\boldsymbol{a}}[n]$ by $\boldsymbol{U}$ will project the signal into the smaller $(N-1)$-dimensional space. In analogy to traditional fractionally-spaced equalization of BPSK, we know that it is senseless to minimize the error between the upsampled, zero-padded transmit signal and the equalizer output prior to downsampling; such a choice of error signal would render useless the benefits of fractional-sampling. Thus, we use the MSE given by

$$\begin{aligned} J_{MSE}(\boldsymbol{f},\boldsymbol{g},\Delta) &= E\left[||\boldsymbol{U}(\tilde{\boldsymbol{a}}[n]-\boldsymbol{a}[n-\Delta])||_2^2\right] \\ &= E\Big[||\boldsymbol{U}\boldsymbol{S}^\top\left(\boldsymbol{X}^\top[n]\boldsymbol{\mathcal{H}}^\top+\boldsymbol{W}^\top[n]\right)\boldsymbol{f} \\ &\qquad +\boldsymbol{U}\hat{\boldsymbol{A}}^\top[n-1]\boldsymbol{g}-\boldsymbol{U}\boldsymbol{S}^\top\boldsymbol{X}^\top[n]\boldsymbol{e}_{K\Delta}||_2^2\Big] \\ &= \boldsymbol{f}^\top\boldsymbol{\mathcal{H}}\boldsymbol{R}_{xx}\boldsymbol{\mathcal{H}}^\top\boldsymbol{f}+2\boldsymbol{f}^\top\boldsymbol{\mathcal{H}}\boldsymbol{R}_{x\hat{a}}\boldsymbol{g}-2\boldsymbol{f}^\top\boldsymbol{\mathcal{H}}\boldsymbol{R}_{xx}\boldsymbol{e}_{K\Delta}-2\boldsymbol{g}^\top\boldsymbol{R}_{x\hat{a}}^\top\boldsymbol{e}_{K\Delta} \\ &\qquad +\boldsymbol{f}^\top\boldsymbol{R}_{ww}\boldsymbol{f}+\boldsymbol{g}^\top\boldsymbol{R}_{\hat{a}\hat{a}}\boldsymbol{g}+\boldsymbol{e}_{K\Delta}^\top\boldsymbol{R}_{xx}\boldsymbol{e}_{K\Delta} \end{aligned} \tag{2.25}$$

where we define

$$\boldsymbol{R}_{xx} \triangleq E\left[\boldsymbol{X}[n]\boldsymbol{S}\boldsymbol{J}\boldsymbol{S}^{\top}\boldsymbol{X}^{\top}[n]\right] \tag{2.26}$$

$$\boldsymbol{R}_{\hat{a}\hat{a}} \triangleq E\left[\hat{\boldsymbol{A}}[n-1]\boldsymbol{J}\hat{\boldsymbol{A}}^{\top}[n-1]\right] \tag{2.27}$$

$$\boldsymbol{R}_{x\hat{a}} \triangleq E\left[\boldsymbol{X}[n]\boldsymbol{S}\boldsymbol{J}\hat{\boldsymbol{A}}^{\top}[n-1]\right] \tag{2.28}$$

$$\boldsymbol{R}_{ww} \triangleq E\left[\boldsymbol{W}[n]\boldsymbol{S}\boldsymbol{J}\boldsymbol{S}^{\top}\boldsymbol{W}^{\top}[n]\right]. \tag{2.29}$$

With the newly defined correlation matrices, we see the MSE (2.25) has the same form as the MSE for the biorthogonal signal set in (2.15). Thus, the same design equations for $\boldsymbol{f}$ and $\boldsymbol{g}$ apply, so

$$\begin{aligned}\boldsymbol{g}^{*} &= \boldsymbol{R}_{\hat{a}\hat{a}}^{-1}\boldsymbol{R}_{x\hat{a}}^{\top}\left[\boldsymbol{e}_{K\Delta} - \boldsymbol{\mathcal{H}}^{\top}\boldsymbol{f}\right] \\ \boldsymbol{f}^{*} &= \left[\boldsymbol{\mathcal{H}}\boldsymbol{\mathcal{R}}\boldsymbol{\mathcal{H}}^{\top} + \boldsymbol{R}_{ww}\right]^{-1}\boldsymbol{\mathcal{H}}\boldsymbol{\mathcal{R}}\boldsymbol{e}_{K\Delta}\end{aligned}$$

where, as before,

$$\boldsymbol{\mathcal{R}} \triangleq \boldsymbol{R}_{xx} - \boldsymbol{R}_{x\hat{a}}\boldsymbol{R}_{\hat{a}\hat{a}}^{-1}\boldsymbol{R}_{x\hat{a}}^{\top}.$$

Again, calculation of the correlation matrices is rather tedious, and the procedure is outlined in Appendix A.

Lastly, we reëmphasize that we have really not modified the structure of the equalizer at all, though we *have* modified the definition of the error signal (i.e. the MSE), which in turn causes the MMSE equalizer setting to change. Though the equalizer in Fig. 2.3 differs from the original equalizer in Fig. 2.1 due to the appearance of $\boldsymbol{U}^{\top}\boldsymbol{U}$ in the signal path, we note that an actual implementation could forego the use of $\boldsymbol{U}^{\top}\boldsymbol{U}$ in the signal path. We have only included the $\boldsymbol{U}^{\top}\boldsymbol{U}$ in Fig. 2.3 to emphasize that this non-invertible transform can be inserted without affecting the equalizer, and that it is therefore not unreasonable to use $\boldsymbol{U}\tilde{\boldsymbol{a}}[n]$ in the construction of our error signal.

By exploiting the invariance of the decision device to a DC value added to all the chips of its input, we are able to project the orthogonal signal set into a transorthogonal signal set of reduced dimension. With the "choose max" decision device, there is no sense in penalizing DC offsets in the MSE since all that matters in the end is the relative amplitudes of the decision device input. While up to now our motivation for the addition of $\boldsymbol{U}$ to the MSE has been largely heuristic, we will explore its benefits further in Section 2.4. There, we will see the amazing result that inclusion of $\boldsymbol{U}$ in the MSE can in some cases allow for perfect linear equalization in situations where perfect equalization would not be possible without the redefined MSE.

2.3.3 Transorthogonal Modulation

As we saw in (1.6), transorthogonal modulation uses the same "choose max" decision device as orthogonal modulation. Thus, we can expect some benefit by using the same trick we used for orthogonal modulation, i.e. by inserting $\boldsymbol{U}$ into the MSE. The MMSE DFE design for transorthogonal modulation mimics the design for orthogonal modulation quite closely, but there are a few caveats worth mentioning. In particular, the insertion of $\boldsymbol{U}$ in the MSE plays a slightly different role, and it is interesting to point out some issues that would arise if we did not include $\boldsymbol{U}$ in the MSE.

First, we observe that when the equalizer is operating correctly, all of the modulations obey

$$\tilde{\boldsymbol{a}}[n] \approx \boldsymbol{S}^{\top}\boldsymbol{S}\boldsymbol{a}[n-\Delta]$$

where multiplication by $\boldsymbol{S}$ and $\boldsymbol{S}^{\top}$ represent the passage of the selection vector $\boldsymbol{a}[n-\Delta]$ through the modulator (at the transmitter) and the correlator (at the

receiver), respectively. For orthogonal and biorthogonal modulation, $\boldsymbol{S}_o^\top \boldsymbol{S}_o = \boldsymbol{S}_b^\top \boldsymbol{S}_b = \boldsymbol{I}$, so $\tilde{\boldsymbol{a}}_b[n] - \boldsymbol{a}_b[n-\Delta] \approx 0$, which motivated a MSE based on the difference $\tilde{\boldsymbol{a}}_b[n] - \boldsymbol{a}_b[n-\Delta]$ as in (2.16) and (2.25). However, for transorthogonal modulation $\boldsymbol{S}_t^\top \boldsymbol{S}_t = \boldsymbol{J}$ and $\tilde{\boldsymbol{a}}_t[n] - \boldsymbol{J}\boldsymbol{a}_t[n-\Delta] \approx 0$. Thus, for transorthogonal modulation, the ideal input to the decision device $\tilde{\boldsymbol{a}}_t[n]$ does not have the form of a selection vector (as was the case with orthogonal and biorthogonal modulation) but instead $\tilde{\boldsymbol{a}}_t[n]$ has the form of a column of $\boldsymbol{J}$. This suggests that a MSE criterion based on the difference $\tilde{\boldsymbol{a}}_b[n] - \boldsymbol{a}_b[n-\Delta]$ may not be a suitable choice for transorthogonal modulation, and that one based on $\tilde{\boldsymbol{a}}_t[n] - \boldsymbol{J}\boldsymbol{a}_t[n-\Delta]$ might make a better choice. By incorporating multiplication of $\boldsymbol{U}$ into the MSE, and noting that $\boldsymbol{U}\boldsymbol{J} = \boldsymbol{U}$ (due to the idempotency of $\boldsymbol{J}$) the resulting MSE is

$$\begin{aligned} J_{MSE}(\boldsymbol{f}, \boldsymbol{g}, \Delta) &= E\left[||\boldsymbol{U}(\tilde{\boldsymbol{a}}[n] - \boldsymbol{J}\boldsymbol{a}[n-\Delta])||_2^2\right] \\ &= E\left[||\boldsymbol{U}(\tilde{\boldsymbol{a}}[n] - \boldsymbol{a}[n-\Delta])||_2^2\right] \end{aligned} \tag{2.30}$$

where we see that the MSE simplifies to the expression for orthogonal modulation, and so multiplication of $\boldsymbol{a}[n-\Delta]$ by $\boldsymbol{J}$ is superfluous when making use of $\boldsymbol{U}$ in the MSE expression.

Secondly, from Table 1.2 we note that transorthogonal modulation is the only modulation of the three considered in this dissertation for which it is possible that $\boldsymbol{S}$ is wide (i.e. $K < N$). Whereas correlation at the receiver accomplished via multiplication by $\boldsymbol{S}^\top$ typically performs an operation analogous to downsampling (by projecting $\boldsymbol{z}[n]$ into lower dimensional signal $\tilde{\boldsymbol{a}}[n]$, thereby reducing the number of chips per symbol), it is possible with transorthogonal modulation that multiplication by $\boldsymbol{S}^\top$ actually *increases* the number of chips per symbol. This effect only occurs when $K < N$, and is seen best by looking at Fig. 2.3. With the use of $\boldsymbol{U}$ before the decision device, however, the waveform is projected back into the $M-1$

dimensional space as desired.

So, the use of $\boldsymbol{U}$ has several unforseen benefits that spare us from having to make any changes to the development of the MMSE DFE for transorthogonal modulation. The MMSE DFE design equations then follow automatically, with no change from the previous section:

$$\begin{aligned} \boldsymbol{g}^* &= \boldsymbol{R}_{\hat{a}\hat{a}}^{-1}\boldsymbol{R}_{x\hat{a}}^{\top}\left[\boldsymbol{e}_{K\Delta} - \boldsymbol{\mathcal{H}}^{\top}\boldsymbol{f}\right] \\ \boldsymbol{f}^* &= \left[\boldsymbol{\mathcal{H}}\boldsymbol{\mathcal{R}}\boldsymbol{\mathcal{H}}^{\top} + \boldsymbol{R}_{ww}\right]^{-1}\boldsymbol{\mathcal{H}}\boldsymbol{\mathcal{R}}\boldsymbol{e}_{K\Delta} \end{aligned}$$

where, as before,

$$\begin{aligned} \boldsymbol{\mathcal{R}} &\triangleq \boldsymbol{R}_{xx} - \boldsymbol{R}_{x\hat{a}}\boldsymbol{R}_{\hat{a}\hat{a}}^{-1}\boldsymbol{R}_{x\hat{a}}^{\top} \\ \boldsymbol{R}_{xx} &\triangleq E\left[\boldsymbol{X}[n]\boldsymbol{S}\boldsymbol{J}\boldsymbol{S}^{\top}\boldsymbol{X}^{\top}[n]\right] \\ \boldsymbol{R}_{\hat{a}\hat{a}} &\triangleq E\left[\hat{\boldsymbol{A}}[n-1]\boldsymbol{J}\hat{\boldsymbol{A}}^{\top}[n-1]\right] \\ \boldsymbol{R}_{x\hat{a}} &\triangleq E\left[\boldsymbol{X}[n]\boldsymbol{S}\boldsymbol{J}\hat{\boldsymbol{A}}^{\top}[n-1]\right] \\ \boldsymbol{R}_{ww} &\triangleq E\left[\boldsymbol{W}[n]\boldsymbol{S}\boldsymbol{J}\boldsymbol{S}^{\top}\boldsymbol{W}^{\top}[n]\right]. \end{aligned}$$

Again, calculation of the correlation matrices is rather tedious, and the procedure is outlined in Appendix A.

2.4 Conditions for Perfect Linear Equalization

It is interesting to consider what conditions, if any, permit a feedforward equalizer to perfectly invert the channel for these modulations. It is well known for equalization of PAM that a finite-length symbol-rate linear equalizer has no hope of perfectly inverting the channel. On the other hand, a finite-length fractionally-spaced linear equalizer for PAM *can* perfectly invert the channel in certain cases. For example, with a PAM equalizer operating at twice the symbol rate, channel

inversion is possible when the equalizer length satisfies $N_f \geq N_h - 1$ and the effective channel matrix is full rank [18]. As we have mentioned, fractionally-spaced equalization of BPSK is a special case of our equalizer structure, and so we expect perfect channel invertibility for at least some situations. In a PAM system, perfect equalization is attained when the effective combined channel/equalizer impulse response is a single spike. For our equalizer with energy efficient modulations, however, there may be other effective responses that result in perfect equalization due to the correlation of the source data. Finding a set of invertibility conditions is not quite as simple as it is for PAM systems.

Throughout this section, we assume that there is no feedback equalizer, and we assume there is no noise. We define "perfect linear equalization" (or equivalently "perfect channel inversion") as the situation where, in the absence of noise, and given any source sequence, the received soft-symbols at the input to the decision device have exactly the desired value (i.e. no ISI). Equivalently, we have perfect equalization when the MSE is zero in the absence of noise. The equalizer settings for which perfect equalization occurs are called the zero-forcing (ZF) solutions.

With no noise and no feedback section, the MSE reduces to

$$J_{MSE}(\boldsymbol{f}, \Delta) \;=\; \boldsymbol{f}^\top \boldsymbol{\mathcal{H}} \boldsymbol{R}_{xx} \boldsymbol{\mathcal{H}}^\top \boldsymbol{f} - 2\boldsymbol{f}^\top \boldsymbol{\mathcal{H}} \boldsymbol{R}_{xx} \boldsymbol{e}_{K\Delta} + \boldsymbol{e}_{K\Delta}^\top \boldsymbol{R}_{xx} \boldsymbol{e}_{K\Delta}. \quad (2.31)$$

From Lemma 2.2, we can decompose $\boldsymbol{R}_{xx}$ as

$$\boldsymbol{R}_{xx} = \boldsymbol{\Gamma}_{xx}^\top \boldsymbol{\Gamma}_{xx}$$

where $\boldsymbol{\Gamma}_{xx} \in \mathbb{R}^{r \times N_c}$ and $r \leq N_c$ is the rank of $\boldsymbol{R}_{xx}$. Defining $\boldsymbol{\mathcal{H}}_{eff} \triangleq (\boldsymbol{\mathcal{H}} \boldsymbol{\Gamma}_{xx}^\top) \in \mathbb{R}^{N_f \times r}$, (2.31) becomes

$$J_{MSE}(\boldsymbol{f}, \Delta) \;=\; \boldsymbol{f}^\top \boldsymbol{\mathcal{H}}_{eff} \boldsymbol{\mathcal{H}}_{eff}^\top \boldsymbol{f} - 2\boldsymbol{f}^\top \boldsymbol{\mathcal{H}}_{eff} \boldsymbol{\Gamma}_{xx} \boldsymbol{e}_{K\Delta} + \boldsymbol{e}_{K\Delta}^\top \boldsymbol{\Gamma}_{xx}^\top \boldsymbol{\Gamma}_{xx} \boldsymbol{e}_{K\Delta} \quad (2.32)$$

So, for perfect equalization (i.e. to attain zero MSE), $\boldsymbol{f}$ must satisfy

$$\boldsymbol{\mathcal{H}}_{eff}^{\top}\boldsymbol{f}^{*} \;=\; \boldsymbol{\Gamma}_{xx}\boldsymbol{e}_{K\Delta}. \tag{2.33}$$

In order for this expression to be solvable, we arrive at the following three related conditions on the length of the equalizer, the source statistics, and the rank of the effective channel matrix which guarantee perfect equalizability:

1. **Length Condition:** For $\boldsymbol{f}$ to satisfy (2.33) for arbitrary Δ, $\boldsymbol{\mathcal{H}}_{eff}$ must be a tall matrix. Hence, it is required that $N_f \geq \text{rank}(\boldsymbol{R}_{xx})$.

2. **Source Condition:** In the length condition above, the rank of $\boldsymbol{R}_{xx}$ itself depends on N_f. Since $N_f + N_h - 1 = \text{rank}(\boldsymbol{R}_{xx}) + \text{nullity}(\boldsymbol{R}_{xx})$, the length condition can be written equivalently as $N_h \leq \text{nullity}(\boldsymbol{R}_{xx}) - 1$. Since N_h itself must satisfy $N_h \geq 1$, we see that a necessary condition for perfect equalization is rank deficiency of $\boldsymbol{R}_{xx}$, a condition which may be impossible to satisfy for a given signal set.

3. **Disparity Condition:** For $\boldsymbol{f}$ to satisfy (2.33) for arbitrary Δ, $\boldsymbol{\mathcal{H}}_{eff}$ must have full column rank.

In fractionally-spaced PAM equalization, the source condition is guaranteed, the length condition is described by a simple inequality, and the disparity condition amounts to the condition that there are no common subchannel roots. Such simple and intuitive conditions are not possible in general here, since the conditions will change with the chosen modulation and signal set. However, calculation of the rank of $\boldsymbol{R}_{xx}$ for a particular modulation and signal set is fairly straightforward. To illustrate, we will consider several examples.

2.4.1 Example: Biorthogonal Modulation with $\boldsymbol{S} = [1, 0]^\top$

As mentioned previously, biorthogonal modulation with $\boldsymbol{S} = [1, 0]^\top$ corresponds to fractionally-spaced equalization of a BPSK signal. Thus, we expect the length and disparity conditions for this case to coincide with the known result for BPSK. We have

$$\boldsymbol{R}_{xx} = \begin{bmatrix} 1 & 0 & 0 & 0 & \dots & 0 & 0 \\ 0 & 0 & 0 & 0 & \dots & 0 & 0 \\ 0 & 0 & 1 & 0 & \dots & 0 & 0 \\ 0 & 0 & 0 & 0 & \dots & 0 & 0 \\ \vdots & & & & \ddots & & \vdots \\ 0 & 0 & 0 & 0 & \dots & 1 & 0 \\ 0 & 0 & 0 & 0 & \dots & 0 & 0 \end{bmatrix} \tag{2.34}$$

where the even elements of the diagonal equal 1 and the odd elements equal 0. Consequently, the rank is simply equal to half the number of rows (or columns) of $\boldsymbol{R}_{xx}$, so

$$\begin{aligned} r &= \operatorname{rank}(\boldsymbol{R}_{xx}) \\ &= \left\lceil \frac{N_f + N_h - 1}{2} \right\rceil \end{aligned}$$

The length condition $N_f \geq r$ becomes

$$N_f \geq N_h - 1$$

which indeed coincides with the known result for BPSK. In addition, $\boldsymbol{\mathcal{H}}_{eff}$ assumes the form of a column-decimated version of $\boldsymbol{\mathcal{H}}$. This, too, coincides with the known result for BPSK, requiring no common roots among the subchannels [18]. Lastly, we note that transorthogonal modulation with

$$\boldsymbol{S} = \begin{bmatrix} 1 & -1 \\ 0 & 0 \end{bmatrix}$$

also corresponds to fractionally-spaced BPSK, and leads to the same conditions.

2.4.2 Example: Comparison of Two Biorthogonal Signal Sets

Here, we consider biorthogonal with two very similar choices of $\boldsymbol{S}$, where $K = 4$ and $N = 2$:

$$\boldsymbol{S}_1 = \frac{1}{\sqrt{2}} \begin{bmatrix} +1 & +1 \\ 0 & 0 \\ +1 & -1 \\ 0 & 0 \end{bmatrix} \text{ and } \boldsymbol{S}_2 = \frac{1}{\sqrt{2}} \begin{bmatrix} +1 & 0 \\ 0 & +1 \\ +1 & 0 \\ 0 & -1 \end{bmatrix}.$$

Clearly both of these choices are valid biorthogonal constellations since $\boldsymbol{S}^\top \boldsymbol{S} = \boldsymbol{I}$. The first choice $\boldsymbol{S}_1$ corresponds to oversampled 4-ary biorthogonal Walsh modulation. The second choice $\boldsymbol{S}_2$ is simply a modified version of $\boldsymbol{S}_1$ with the second column shifted. Note that both signal sets effectively employ $2\times$ oversampling (as defined in Section 1.5) since $K/N = 2$. Thus, we might expect that both signal sets permit perfect equalization. Alas, this is not the case. For $\boldsymbol{S}_1$, the corresponding autocorrelation matrix $\boldsymbol{R}_{xx}$ is exactly as in (2.34) above for fractionally-spaced BPSK, and therefore has identical conditions as BPSK for perfect equalization. On the other hand, the autocorrelation matrix $\boldsymbol{R}_{xx}$ for $\boldsymbol{S}_2$ results in a matrix that is always full-rank, and so perfect equalization is not possible with a finite-length equalizer. Calculation of $\boldsymbol{R}_{xx}$ follows from use of (A.2) in Appendix A. However, (A.2) shows that $\boldsymbol{R}_{xx}$ is completely specified by $\boldsymbol{S}\boldsymbol{S}^\top$. The gross difference in equalizability in using $\boldsymbol{S}_1$ vs. $\boldsymbol{S}_2$ arises from the difference in $\boldsymbol{S}\boldsymbol{S}^\top$

$$\boldsymbol{S}_1\boldsymbol{S}_1^\top = \begin{bmatrix} 1 & 0 & 0 & 0 \\ 0 & 0 & 0 & 0 \\ 0 & 0 & 1 & 0 \\ 0 & 0 & 0 & 0 \end{bmatrix} \text{ and } \boldsymbol{S}_2\boldsymbol{S}_2^\top = \frac{1}{2} \begin{bmatrix} 1 & 0 & 1 & 0 \\ 0 & 1 & 0 & -1 \\ 1 & 0 & 1 & 0 \\ 0 & -1 & 0 & 1 \end{bmatrix}.$$

where the lack of nullity in using $\boldsymbol{S}_2$ arises from the non-zero off-diagonal elements of $\boldsymbol{S}_2\boldsymbol{S}_2^\top$ and the lack of zeros along the diagonal.

In light of the fact that both of these examples are seen as oversampled (in the sense that twice as many samples as necessary are used to represent each

symbol) it may come as a surprise that perfect equalization is not possible when employing $\boldsymbol{S}_2$. This is simply a consequence of the autocorrelation matrix $\boldsymbol{R}_x x$. In the next chapter, we will return to this example, and show that a modification to the equalizer structure results in perfect equalization for *both* of these signal sets.

2.4.3 Example: Binary Pulse Position Modulation

The source condition demonstrates the desirability of having $\boldsymbol{R}_{xx}$ be rank deficient. Obviously, $\boldsymbol{R}_{xx}$ can be made rank deficient through appropriate choice of signal set, as the previous example showed. However, in looking at the definition of $\boldsymbol{R}_{xx}$ for orthogonal modulation (2.26), we note the appearance of $\boldsymbol{J}$ which arose due to our use of $\boldsymbol{U}$ in the formation of the MSE. Recall that $\boldsymbol{J}$ is not full rank, and therefore serves to help reduce the rank of $\boldsymbol{R}_{xx}$.

We now consider the case of orthogonal modulation with the choice $\boldsymbol{S} = \boldsymbol{I}_2$, which corresponds to binary PPM. The autocorrelation matrix, calculated via (A.7) is

$$
\begin{aligned}
\boldsymbol{R}_{xx} &= E\left[\boldsymbol{X}[n]\boldsymbol{S}\boldsymbol{J}\boldsymbol{S}^{\top}\boldsymbol{X}^{\top}[n]\right] \\
&= \frac{1}{8}\begin{bmatrix}
4 & -2 & 0 & 0 & \cdots & & \\
-2 & 2 & -2 & 1 & 0 & \cdots & \\
0 & -2 & 4 & -2 & 0 & 0 & \cdots \\
0 & 1 & -2 & 2 & -2 & 1 & 0 & \cdots \\
\vdots & 0 & 0 & -2 & 4 & -2 & \ddots & \\
 & \vdots & 0 & 1 & -2 & \ddots & & \\
 & & \vdots & 0 & \ddots & & & \\
 & & & \vdots & & & &
\end{bmatrix}
\end{aligned}
$$

which has rank

$$r = \left\lceil \frac{N_f + N_h}{2} \right\rceil$$

leading to the length condition $N_f \geq N_h$. Thus, perfect equalization of binary PPM is possible, in spite of the fact that there is no oversampling *per se* (since $K = N$). We note that it is precisely the presence of $\boldsymbol{J}$ in the autocorrelation matrix which causes $\boldsymbol{R}_{xx}$ to be rank deficient, thereby permitting perfect equalization. If, in the equalizer for orthogonal modulation, we had instead formed the MSE between $\tilde{\boldsymbol{a}}[n]$ and $\boldsymbol{a}[n-\Delta]$ (i.e. without inclusion of $\boldsymbol{U}$, so that DC offsets were penalized), the autocorrelation matrix would have been

$$E\left[\boldsymbol{X}[n]\boldsymbol{S}\boldsymbol{S}^\top\boldsymbol{X}^\top[n]\right] = \frac{1}{8}\begin{bmatrix} 8 & 2 & 4 & 4 & \cdots \\ 2 & 8 & 2 & 4 & \\ 4 & 2 & \ddots & \ddots & \ddots \\ 4 & 4 & \ddots & & \\ \vdots & & \ddots & & \end{bmatrix}$$

which is full-rank, thus prohibiting perfect equalization under that definition of MSE.

2.4.4 Example: 3-ary Pulse Position Modulation

We now consider the case of orthogonal modulation with the choice $\boldsymbol{S} = \boldsymbol{I}_3$, corresponding to 3-ary PPM. The autocorrelation matrix is

$$\begin{aligned}\boldsymbol{R}_{xx} &= E\left[\boldsymbol{X}[n]\boldsymbol{S}\boldsymbol{J}\boldsymbol{S}^\top\boldsymbol{X}^\top[n]\right] \\ &= \frac{1}{27}\begin{bmatrix} 18 & -6 & -3 & 0 & 0 & 0 & \cdots & & & \\ -6 & 14 & -8 & -3 & 2 & 1 & 0 & \cdots & & \\ -3 & -8 & 14 & -6 & -2 & 2 & 0 & 0 & \cdots & \\ 0 & -3 & -6 & 18 & -6 & -3 & 0 & 0 & 0 & \cdots \\ 0 & 2 & -2 & -6 & 14 & -8 & -3 & 2 & 1 & 0 & \cdots \\ 0 & 1 & 2 & -3 & -8 & 14 & -6 & -2 & 2 & \ddots & \\ \vdots & 0 & 0 & 0 & -3 & -6 & 18 & -6 & \ddots & & \\ & \vdots & 0 & 0 & 2 & -2 & -6 & \ddots & & & \\ & & \vdots & 0 & 1 & 2 & \ddots & & & & \\ & & & \vdots & 0 & \ddots & & & & & \\ & & & & \vdots & & & & & & \end{bmatrix}\end{aligned}$$

which has full rank $r = N_f + N_h - 1$, leading to the condition $N_f \geq N_f + N_h - 1$ or $N_h \leq 1$. Thus, perfect equalization of 3-ary PPM is not possible except in the trivial case when the channel length is 1. We will revisit this example in the next chapter.

2.5 LMS Adaptation

While we have assumed up to now that the channel $\boldsymbol{H}$ and noise statistics $\boldsymbol{R}_{ww}$ are known, this is not likely to be the case in practice, and thus an adaptive scheme is desirable. Furthermore, direct computation of the equalizer coefficients may not be feasible, requiring the use of iterative or adaptive solutions. Fortunately, the mean-squared error is quadratic in the parameters $\boldsymbol{f}$ and $\boldsymbol{g}$, so we can use the LMS algorithm to calculate $\boldsymbol{f}^*$ and $\boldsymbol{g}^*$ adaptively when training data is available. The LMS algorithm is a stochastic gradient descent algorithm which uses the

instantaneous gradient [16] of the mean-squared error as an estimate for the true gradient (i.e. by ignoring the expectation operator).

For biorthogonal modulation, taking the instantaneous gradient of the MSE in (2.15) gives

$$\begin{aligned}\frac{1}{2}\hat{\nabla}_{\boldsymbol{f}} J_{MSE} &= \boldsymbol{Y}[n]\boldsymbol{S}\left[\tilde{\boldsymbol{a}}[n] - \boldsymbol{a}[n-\Delta]\right] \\ \frac{1}{2}\hat{\nabla}_{\boldsymbol{g}} J_{MSE} &= \hat{\boldsymbol{A}}[n-1]\left[\tilde{\boldsymbol{a}}[n] - \boldsymbol{a}[n-\Delta]\right].\end{aligned}$$

This results in the LMS update equations for biorthogonal modulation as

$$\begin{aligned}\boldsymbol{\epsilon}_{LMS}[n] &= \tilde{\boldsymbol{a}}[n] - \boldsymbol{a}[n-\Delta] \\ \boldsymbol{f}_{LMS}[n+1] &= \boldsymbol{f}_{LMS}[n] - \mu_1 \hat{\nabla}_{\boldsymbol{f}} J_{MSE} \\ &= \boldsymbol{f}_{LMS}[n] - \mu_1 \boldsymbol{Y}[n]\boldsymbol{S}\boldsymbol{\epsilon}_{LMS}[n] \\ \boldsymbol{g}_{LMS}[n+1] &= \boldsymbol{g}_{LMS}[n] - \mu_2 \hat{\nabla}_{\boldsymbol{g}} J_{MSE} \\ &= \boldsymbol{g}_{LMS}[n] - \mu_2 \hat{\boldsymbol{A}}[n-1]\boldsymbol{\epsilon}_{LMS}[n]\end{aligned}$$

where μ_1, μ_2 are small positive step-sizes which serves to average out the noise in the gradient estimate. With a small step-size, the algorithm exhibits mean transient and steady-state behavior very close to that of the exact gradient descent [16]. Note that the presence of $\boldsymbol{a}[n-\Delta]$ in the error term implies the availability of training data. When training data is unavailable, we can feed back the output of the decision device $\hat{\boldsymbol{a}}[n]$ instead, arriving at the decision-directed (DD) LMS update equations

$$\begin{aligned}\boldsymbol{\epsilon}_{DD}[n] &= \tilde{\boldsymbol{a}}[n] - \hat{\boldsymbol{a}}[n] \\ \boldsymbol{f}_{DD}[n+1] &= \boldsymbol{f}_{DD}[n] - \mu_1 \boldsymbol{Y}[n]\boldsymbol{S}\boldsymbol{\epsilon}_{DD}[n] \\ \boldsymbol{g}_{DD}[n+1] &= \boldsymbol{g}_{DD}[n] - \mu_2 \hat{\boldsymbol{A}}[n-1]\boldsymbol{\epsilon}_{DD}[n]\end{aligned}$$

The update equations for orthogonal and transorthogonal modulation follow similarly, though with the appearance of $\boldsymbol{U}$ in the update equations as

$$\begin{aligned}
\boldsymbol{\epsilon}_{LMS}[n] &= \boldsymbol{U}\left[\tilde{\boldsymbol{a}}[n] - \boldsymbol{a}[n-\Delta]\right] \\
\boldsymbol{f}_{LMS}[n+1] &= \boldsymbol{f}_{LMS}[n] - \mu_1 \boldsymbol{Y}[n]\boldsymbol{S}\boldsymbol{U}^{\top}\boldsymbol{\epsilon}_{LMS}[n] \\
\boldsymbol{g}_{LMS}[n+1] &= \boldsymbol{g}_{LMS}[n] - \mu_2 \hat{\boldsymbol{A}}[n-1]\boldsymbol{U}^{\top}\boldsymbol{\epsilon}_{LMS}[n]
\end{aligned}$$

Similarly, in the absence of training, $\boldsymbol{a}[n-\Delta]$ can be replaced with $\hat{\boldsymbol{a}}[n]$ to arrive at the DD-LMS equations.

Chapter 3

Block Equalization of Energy Efficient Modulations

In this chapter, we present an improvement upon the previous chapter by extending the equalizer from simple scalar filters into block (polyphase) filters. This new equalizer structure brings about several benefits, including: the ability to obtain perfect linear equalization for a larger class of signal sets, a reduced effective delay through the feedback equalizer, and a reduction in computational complexity. Portions of this work appeared in [21][22].

3.1 Motivation for Block Structure

The scalar equalizer of the previous chapter has several shortcomings. First, as demonstrated in Section 2.4.2, a linear equalizer is not able to perfectly equalize the channel even when the oversampling factor K/K_{min} is large. Secondly, the operation of the feedback portion of the equalizer has a feature that is quite undesirable. Upon reception of the symbol at time n, all of the chips from the symbol at time $n-1$ have been estimated and are available to the feedback equalizer. However, the chips are fed serially into the feedback equalizer, which needlessly introduces delay in the feedback path.

Also, as we have mentioned, the source sequence is not i.i.d. at the chip level.

Furthermore, the chip process is not wide-sense-stationary (WSS) in general, since the autocorrelation $E\left[x[n]x[m]\right] \neq E\left[x[n+p]x[m+p]\right]$ for all p. However, the chip process is cyclostationary since $E\left[x[n]x[m]\right] = E\left[x[n+Kp]x[m+Kp]\right]$. These properties follow directly from the second-order moments (2.12)-(2.14). Since the autocorrelation is different for each of the K polyphases, we might expect improved performance from an equalizer that exploited this fact that was ignored by the scalar equalizer of the previous chapter.

3.2 System Model

We now consider a block equalizer, where the scalar chip-rate filters $\boldsymbol{f}$ and $\boldsymbol{g}$ of the previous chapter are replaced with block filters $\boldsymbol{\mathcal{F}} \in \mathbb{R}^{N_f \times N}$ and $\boldsymbol{\mathcal{G}} \in \mathbb{R}^{N_g \times N}$, using polyphase representation. The scalar equalizer was a single equalizer operating on a chip-by-chip basis, whereas the block equalizer here is a bank of N equalizers operating on a symbol-by-symbol basis. These block filters can be expressed in an equivalent multirate form as was shown in Fig. 2.2. The resulting equalizer structure under consideration is shown in Fig. 3.1. The equations to describe

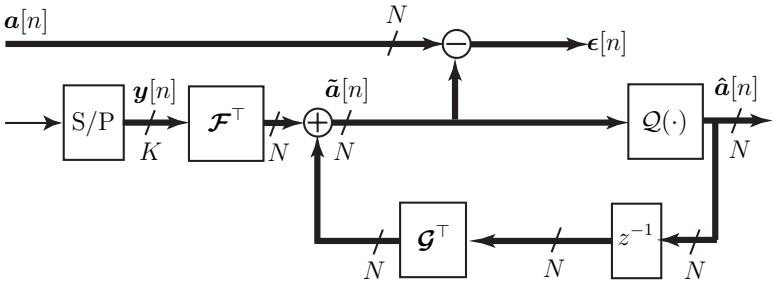

Figure 3.1: Block Equalizer System Model

this system model are quite similar to those from Chapter 2, with a few minor changes.

As before, we consider two models: a symbol-by-symbol model based on matrix convolutions, and a block formulation that isolates the equalizer coefficients $\boldsymbol{\mathcal{F}}$ and $\boldsymbol{\mathcal{G}}$. The symbol-by-symbol model is largely unchanged from the previous section, and is described by the following equations

$$\begin{aligned}
\boldsymbol{x}[n] &= \boldsymbol{S}\boldsymbol{a}[n] && (3.1)\\
\boldsymbol{y}[n] &= \sum_m \boldsymbol{H}[m]\boldsymbol{x}[n-m] + \boldsymbol{w}[n] && (3.2)\\
\tilde{\boldsymbol{a}}[n] &= \sum_m \boldsymbol{F}[m]\boldsymbol{y}[n-m] + \sum_m \boldsymbol{G}[m]\hat{\boldsymbol{a}}[n-m-1] && (3.3)\\
\hat{\boldsymbol{a}}[n] &= \mathcal{Q}(\tilde{\boldsymbol{a}}[n]). && (3.4)
\end{aligned}$$

The receiver input $\boldsymbol{y}[n]$ is identical to that from the previous chapter, and as before the Tœplitz channel impulse response matrices $\boldsymbol{H}[n] \in \mathbb{R}^{K\times K}$ are expressed in terms of the channel coefficients as $[\boldsymbol{H}[n]]_{i,j} = h[Kn + j - i]$. In contrast to the scalar model where $\boldsymbol{F}[n]$ and $\boldsymbol{G}[n]$ were Tœplitz, the block equalizer here does not impose this requirement. In addition, we have absorbed the correlation operation (multiplication with $\boldsymbol{S}^\top$) into the feedforward equalizer. The set of matrices $\boldsymbol{F}[n] \in \mathbb{R}^{N\times K}$ and $\boldsymbol{G}[n] \in \mathbb{R}^{N\times N}$ can be expressed in terms of $\boldsymbol{\mathcal{F}}$ and $\boldsymbol{\mathcal{G}}$ via

$$\begin{aligned}
[\boldsymbol{F}[n]]_{i,j} &= [\boldsymbol{\mathcal{F}}]_{Kn+j,i}\\
[\boldsymbol{G}[n]]_{i,j} &= [\boldsymbol{\mathcal{G}}]_{Nn+j,i}
\end{aligned}$$

Again, we have a one-symbol delay in the feedback path, which is evident in (3.3). However, as opposed to the scalar equalizer where the relative chip delay through the feedback path was fixed at N chips, the relative chip delay through the feedback path is now different for each polyphase. For example, consider the equalization of the ith chip from the nth symbol, denoted $\tilde{a}[Nn-i]$. At this time,

the entire $(n-1)$th symbol estimate (i.e. $\hat{\boldsymbol{a}}[n-1] = [\hat{a}[Nn-N],\ \hat{a}[Nn-N-1]\ \ldots, \hat{a}[Nn-2N+1]]^\top$) is in the feedback path, with the most "recent" chip being $\hat{a}[Nn-N]$. So, the feedback path chip delay for the ith chip from the nth symbol is $(Nn-i)-(Nn-N) = N-i$, where $0 \leq i \leq N-1$. Hence, the feedback delay can be as low as 1 chip (for the first received chip of a symbol, corresponding to the $(N-1)$th polyphase), to as large as N chips (for the last received chip of a symbol, corresponding to the 0th polyphase). The reason for this reduction in delay relative to the scalar equalizer relates to the serial operation of the scalar model which imposed a Tœplitz structure on $\boldsymbol{G}[n]$. The Tœplitz structure required the lower triangular portion of $\boldsymbol{G}[0]$ to be zero which effectively introduced unnecessary delay in the feedback path. Since $\boldsymbol{G}[n]$ is not required to be Tœplitz in the block model, we are able to reduce the feedback path delay.

We note that the block equalizer is a generalization that includes the scalar equalizer of the previous chapter as a special case. Specifically, consider some scalar equalizer where $\boldsymbol{F}_{scalar}[n] \in \mathbb{R}^{K\times K}$ and $\boldsymbol{G}_{scalar}[n] \in \mathbb{R}^{N\times N}$ are Tœplitz matrices which were defined in Chapter 2 as $[\boldsymbol{F}_{scalar}[n]]_{i,j} = f[Kn+j-i]$ and $[\boldsymbol{G}_{scalar}[n]]_{i,j} = g[Nn+j-i]$. The particular block equalizer with identical functionality to this scalar equalizer is obtained when $\boldsymbol{F}[n]$ and $\boldsymbol{G}[n]$ for the block equalizer are set to

$$\boldsymbol{F}[n] = \boldsymbol{S}^\top \boldsymbol{F}_{scalar}[n] \tag{3.5}$$

$$\boldsymbol{G}[n] = \boldsymbol{G}_{scalar}[n] \tag{3.6}$$

Since the scalar equalizer is a special case of the block equalizer, we can be assured that the block equalizer will as good or better than the scalar equalizer (in terms of MSE).

At times, it will be more convenient to use a formulation that isolates the equalizer response matrices $\boldsymbol{\mathcal{F}}$ and $\boldsymbol{\mathcal{G}}$. In this case, the stacked regressor vector of

transmitted symbols $\bar{\boldsymbol{x}}[n] \in \mathbb{R}^{N_c}$ can be written as

$$\bar{\boldsymbol{x}}[n] \;=\; (\boldsymbol{I}_{\frac{N_c}{K}} \otimes \boldsymbol{S})\bar{\boldsymbol{a}}[n] \tag{3.7}$$

where $\otimes$ denotes the Kronecker product, $N_c \triangleq N_f + N_h - 1$ is the combined length of the channel and feedforward equalizer, and $\bar{\boldsymbol{a}}[n] \in \mathbb{R}^{N_c N/K}$ contains the stacked selection vectors so that

$$\bar{\boldsymbol{a}}[n] \;=\; \begin{bmatrix} \boldsymbol{a}[n] \\ \boldsymbol{a}[n-1] \\ \vdots \end{bmatrix}.$$

Note that $\bar{\boldsymbol{x}}[n]$ may include a partial symbol if N_c is not a multiple of K. For simplicity, we will assume that N_c is always a multiple of K, which can be accomplished without loss of generality by appending zeros to $\boldsymbol{h}$ to sufficiently increase N_c until it is a multiple of K. Next, the vector $\bar{\boldsymbol{y}}[n] \in \mathbb{R}^{N_f}$ of received chips can be written

$$\bar{\boldsymbol{y}}[n] \;=\; \boldsymbol{\mathcal{H}}\bar{\boldsymbol{x}}[n] + \bar{\boldsymbol{w}}[n] \tag{3.8}$$

where $\bar{\boldsymbol{w}}[n] \in \mathbb{R}^{N_f}$ is the vector of noise samples defined as $\bar{\boldsymbol{w}}[n] = [w[Kn], w[Kn-1], \ldots]^\top$. Then, the the soft estimates of the selection vector output by the equalizer at time n can be written

$$\tilde{\boldsymbol{a}}[n] \;=\; \boldsymbol{\mathcal{F}}^\top \bar{\boldsymbol{y}}[n] + \boldsymbol{\mathcal{G}}^\top \bar{\hat{\boldsymbol{a}}}[n-1] \tag{3.9}$$

where the regressor vector of stacked selection vector estimates $\bar{\hat{\boldsymbol{a}}}[n] \in \mathbb{R}^{N_g}$ is defined as $\bar{\hat{\boldsymbol{a}}}[n] = [\hat{\boldsymbol{a}}[n]^\top,\, \hat{\boldsymbol{a}}[n-1]^\top, \cdots]^\top$. In the sequel, we will switch between the symbol-by-symbol model (3.1)-(3.3) and the equivalent block matrix model (3.7)-(3.9) whenever convenient.

Lastly, to simplify expressions in the sequel, we make the following assumptions about the sizes of the channel and equalizers:

- N_c is a multiple of K.
- $N_g \leq N(N_c/K - \Delta - 1)$.
- N_g is a multiple of N.

By artificially appending zeros to $\boldsymbol{h}$, thus increasing N_c, the first two assumptions can be trivially satisfied without loss of generality for any set of system parameters. The third assumption is reasonable since it effectively requires feedback of whole symbols.

3.3 Block MMSE Equalizer

We now present the design equations for the block equalizer coefficients based on minimizing the mean-squared error. Again, the MMSE equalizer accepts one design parameter, Δ, which represents the desired symbol delay through the channel/equalizer chain. By defining

$$\boldsymbol{E}_{N\Delta} \triangleq \begin{bmatrix} \boldsymbol{0}_{N\Delta \times N} \\ \boldsymbol{I}_N \\ \boldsymbol{0}_{N(N_c/K-\Delta-1)\times N} \end{bmatrix}$$

so that $\boldsymbol{E}_{N\Delta} \in \mathbb{R}^{N_c N/K \times N}$, we can express the delayed symbol vector as

$$\boldsymbol{a}[n-\Delta] = \boldsymbol{E}_{N\Delta}^{\top} \bar{\boldsymbol{a}}[n]. \tag{3.10}$$

The block equalizer structure permits much less tedious calculation of the correlation matrices, and allows us to express most formulae in terms of the selection vectors (and not a mix of selection vectors $\boldsymbol{a}[n]$ and waveform chips $\boldsymbol{x}[n]$, as was the case for the scalar equalizer). While the second-order statistics of the transmitted chips $\boldsymbol{x}[n]$ were given in (2.12)-(2.12), here we will be primarily interested in the

second-order statistics of the selection vectors $\boldsymbol{a}[n]$, which we recall are related to the chips via the simple linear relation $\boldsymbol{x}[n] = \boldsymbol{S}\boldsymbol{a}[n]$. Recall that for orthogonal and transorthogonal modulation,

$$\boldsymbol{a}_o[n], \boldsymbol{a}_t[n] \in \left\{ \begin{bmatrix} 1 \\ 0 \\ \vdots \\ 0 \end{bmatrix}, \begin{bmatrix} 0 \\ 1 \\ \vdots \\ 0 \end{bmatrix}, \ldots, \begin{bmatrix} 0 \\ 0 \\ \vdots \\ 1 \end{bmatrix} \right\}$$

while for biorthogonal modulation,

$$\boldsymbol{a}_b[n] \in \left\{ \pm \begin{bmatrix} 1 \\ 0 \\ \vdots \\ 0 \end{bmatrix}, \pm \begin{bmatrix} 0 \\ 1 \\ \vdots \\ 0 \end{bmatrix}, \ldots, \pm \begin{bmatrix} 0 \\ 0 \\ \vdots \\ 1 \end{bmatrix} \right\}.$$

Obviously, the second-order statistics of the selection vectors for orthogonal and transorthogonal modulations will be identical. For $n \neq m$, we have

$$\begin{aligned} E[\boldsymbol{a}_o[n]\boldsymbol{a}_o^\top[m]] = E[\boldsymbol{a}_t[n]\boldsymbol{a}_t^\top[m]] &= E[\boldsymbol{a}_o[n]]E[\boldsymbol{a}_o^\top[m]] \\ &= \frac{1}{N^2}\mathbf{1}_{N\times N} \\ E[\boldsymbol{a}_b[n]\boldsymbol{a}_b^\top[m]] &= E[\boldsymbol{a}_b[n]]E[\boldsymbol{a}_b^\top[m]] \\ &= \mathbf{0} \end{aligned}$$

where we have used the fact that the symbols are i.i.d. For all modulations,

$$E[\boldsymbol{a}[n]\boldsymbol{a}^\top[n]] = \frac{1}{N}\boldsymbol{I}_N$$

Thus, the second-order moments are given by

$$E[\boldsymbol{a}_o[n]\boldsymbol{a}_o^\top[m]] = E[\boldsymbol{a}_t[n]\boldsymbol{a}_t^\top[m]] = \begin{cases} \frac{1}{N}\boldsymbol{I}_N & n = m \\ \frac{1}{N^2}\mathbf{1}_{N\times N} & n \neq m \end{cases}$$

$$E[\boldsymbol{a}_b[n]\boldsymbol{a}_b^\top[m]] = \begin{cases} \frac{1}{N}\boldsymbol{I}_N & n = m \\ \mathbf{0}_{N\times N} & n \neq m \end{cases}$$

from which is follows that the vectors of stacked selection vectors have second order

moments

$$\begin{aligned} E[\bar{\boldsymbol{a}}_o[n]\bar{\boldsymbol{a}}_o^\top[m]] &= E[\bar{\boldsymbol{a}}_t[n]\bar{\boldsymbol{a}}_t^\top[m]] \\ &= \frac{1}{N^2}\begin{bmatrix} N\boldsymbol{I}_N & \mathbf{1}_{N\times N} & \mathbf{1}_{N\times N} & \cdots \\ \mathbf{1}_{N\times N} & N\boldsymbol{I}_N & \mathbf{1}_{N\times N} & \\ \mathbf{1}_{N\times N} & \mathbf{1}_{N\times N} & \ddots & \\ \vdots & & & \end{bmatrix} \\ &= \frac{1}{N^2}\left[\mathbf{1}_{\frac{N_cN}{K}\times\frac{N_cN}{K}} + (\boldsymbol{I}_{\frac{N_c}{K}} \otimes (N\boldsymbol{I}_N - \mathbf{1}_{N\times N}))\right] \qquad (3.11) \\ E[\bar{\boldsymbol{a}}_b[n]\bar{\boldsymbol{a}}_b^\top[m]] &= \frac{1}{N}\boldsymbol{I}_{\frac{N_cN}{K}} \qquad (3.12) \end{aligned}$$

We now prove a lemma that applies to $E[\bar{\boldsymbol{a}}_o[n]\bar{\boldsymbol{a}}_o^\top[m]]$ (and $E[\bar{\boldsymbol{a}}_t[n]\bar{\boldsymbol{a}}_t^\top[m]]$).

Lemma 3.1. *Properties of* $\mathbf{1}_{bN\times bN} + (\boldsymbol{I}_b \otimes (N\boldsymbol{I}_N - \mathbf{1}_{N\times N}))$

For positive integers b *and* N*, the symmetric matrix*

$$\mathbf{1}_{bN\times bN} + (\boldsymbol{I}_b \otimes (N\boldsymbol{I}_N - \mathbf{1}_{N\times N}))$$

has singular value decomposition given by $\boldsymbol{V}\boldsymbol{D}\boldsymbol{V}^\top$ *where*

$$\boldsymbol{V} = \left[\frac{1}{\sqrt{bN}}\mathbf{1}_{bN\times 1} \quad (\boldsymbol{I}_b \otimes \boldsymbol{U}_N^\top) \quad \frac{1}{\sqrt{N}}(\boldsymbol{U}_b^\top \otimes \mathbf{1}_{N\times 1})\right]$$

and $\boldsymbol{D} = \mathrm{diag}([bN, \underbrace{N, \ldots, N}_{b(N-1)}, \underbrace{0, \ldots, 0}_{b-1}])$.

Proof. Recall that $\boldsymbol{U}_N \in \mathbb{R}^{N-1\times N}$ was defined in Lemmas 1.1 and 2.2 as the decomposition of the matrix

$$\boldsymbol{U}_N^\top\boldsymbol{U}_N = \boldsymbol{I}_N - \frac{1}{N}\mathbf{1}_{N\times N}$$

and $\boldsymbol{U}_b \in \mathbb{R}^{b-1\times b}$ is defined identically with appropriate size.

Clearly $\boldsymbol{D}$ is diagonal with non-negative entries. To complete the proof, we need to show that $\boldsymbol{V}$ is orthogonal, and that $\mathbf{1}_{bN\times bN} + (\boldsymbol{I}_b \otimes (N\boldsymbol{I}_N - \mathbf{1}_{N\times N})) = \boldsymbol{V}\boldsymbol{D}\boldsymbol{V}^\top$.

To show that $\boldsymbol{V}$ is orthogonal, we have

$$\begin{aligned}
\boldsymbol{V}\boldsymbol{V}^\top &= \left[\frac{1}{\sqrt{bN}}\mathbf{1}_{bN\times 1} \quad (\boldsymbol{I}_b \otimes \boldsymbol{U}_N^\top) \quad \frac{1}{\sqrt{N}}(\boldsymbol{U}_b^\top \otimes \mathbf{1}_{N\times 1})\right] \begin{bmatrix} \frac{1}{\sqrt{bN}}\mathbf{1}_{1\times bN} \\ (\boldsymbol{I}_b \otimes \boldsymbol{U}_N) \\ \frac{1}{\sqrt{N}}(\boldsymbol{U}_b \otimes \mathbf{1}_{1\times N}) \end{bmatrix} \\
&= \frac{1}{bN}\mathbf{1}_{bN\times bN} + (\boldsymbol{I}_b \otimes \boldsymbol{J}_N) + (\boldsymbol{J}_b \otimes \frac{1}{N}\mathbf{1}_{N\times N}) \\
&= \boldsymbol{I}_{bN}
\end{aligned}$$

where the last line follows from substitution of the definition of $\boldsymbol{J}$. Hence, $\boldsymbol{V}$ is orthogonal. Now, partition $\boldsymbol{D}$ as

$$\boldsymbol{D} = \begin{bmatrix} \boldsymbol{D}_1 & \boldsymbol{D}_2 & \boldsymbol{D}_3 \end{bmatrix}$$

where

$$\boldsymbol{D}_1 = bN \begin{bmatrix} 1 \\ \mathbf{0}_{bN-1\times 1} \end{bmatrix}, \qquad \boldsymbol{D}_2 = N \begin{bmatrix} \mathbf{0}_{1\times b(N-1)} \\ \boldsymbol{I}_{b(N-1)} \\ \mathbf{0}_{b-1\times b(N-1)} \end{bmatrix}, \qquad \boldsymbol{D}_3 = \mathbf{0}_{bN\times b-1}$$

Then we have

$$\begin{aligned}
\boldsymbol{V}\boldsymbol{D}\boldsymbol{V}^\top &= \boldsymbol{V}\left(\frac{1}{\sqrt{bN}}\boldsymbol{D}_1\mathbf{1}_{1\times bN} + \boldsymbol{D}_2(\boldsymbol{I}_b \otimes \boldsymbol{U}_N)\right) \\
&= \sqrt{bN}\left[\frac{1}{\sqrt{bN}}\mathbf{1}_{bN\times 1} \ (\boldsymbol{I}_b \otimes \boldsymbol{U}_N^\top) \ \frac{1}{\sqrt{N}}(\boldsymbol{U}_b^\top \otimes \mathbf{1}_{N\times 1})\right]\left[\begin{smallmatrix} 1 \\ \mathbf{0}_{bN-1\times 1} \end{smallmatrix}\right]\mathbf{1}_{1\times bN} \\
&\quad + N\left[\frac{1}{\sqrt{bN}}\mathbf{1}_{bN\times 1} \ (\boldsymbol{I}_b \otimes \boldsymbol{U}_N^\top) \ \frac{1}{\sqrt{N}}(\boldsymbol{U}_b^\top \otimes \mathbf{1}_{N\times 1})\right]\begin{bmatrix} \mathbf{0}_{1\times b(N-1)} \\ \boldsymbol{I}_{b(N-1)} \\ \mathbf{0}_{b-1\times b(N-1)} \end{bmatrix}(\boldsymbol{I}_b \otimes \boldsymbol{U}_N) \\
&= \mathbf{1}_{bN\times bN} + N(\boldsymbol{I}_b \otimes \boldsymbol{U}_N^\top)\boldsymbol{I}_{b(N-1)}(\boldsymbol{I}_b \otimes \boldsymbol{U}_N) \\
&= \mathbf{1}_{bN\times bN} + N(\boldsymbol{I}_b \otimes \boldsymbol{J}_N) \\
&= \mathbf{1}_{bN\times bN} + (\boldsymbol{I}_b \otimes N\boldsymbol{I}_N - \mathbf{1}_{N\times N}).
\end{aligned}$$

■

We now present the MMSE DFE design equations for each of the modulation types separately in turn.

3.3.1 Biorthogonal Modulation

As before with the scalar equalizer, we again form the error between the pre-decision device "soft-estimate" of the selection vector $\tilde{\boldsymbol{a}}[n]$ and the delayed transmitted selection vector $\boldsymbol{a}[n-\Delta]$. Expanding the MSE via (3.7)-(3.10) gives

$$
\begin{aligned}
J_{MSE}(\boldsymbol{\mathcal{F}},\boldsymbol{\mathcal{G}},\Delta) &= E\left[||\tilde{\boldsymbol{a}}[n]-\boldsymbol{a}[n-\Delta]||_2^2\right] \qquad (3.13)\\
&= E\left[\left|\left|\boldsymbol{\mathcal{F}}^\top\left(\boldsymbol{\mathcal{H}}(\boldsymbol{I}_{\frac{N_c}{K}}\otimes\boldsymbol{S})\bar{\boldsymbol{a}}[n]+\bar{\boldsymbol{w}}[n]\right)\right.\right.\\
&\qquad\left.\left.+\boldsymbol{\mathcal{G}}^\top\bar{\tilde{\boldsymbol{a}}}[n-1]-\boldsymbol{E}_{N\Delta}^\top\bar{\boldsymbol{a}}[n]\right|\right|_2^2\Big]\\
&= \mathrm{tr}\Big(\boldsymbol{\mathcal{F}}^\top\boldsymbol{\mathcal{H}}(\boldsymbol{I}_{\frac{N_c}{K}}\otimes\boldsymbol{S})E[\bar{\boldsymbol{a}}[n]\bar{\boldsymbol{a}}^\top[n]](\boldsymbol{I}_{\frac{N_c}{K}}\otimes\boldsymbol{S})^\top\boldsymbol{\mathcal{H}}^\top\boldsymbol{\mathcal{F}}\\
&\quad+\boldsymbol{\mathcal{F}}^\top\boldsymbol{\mathcal{H}}(\boldsymbol{I}_{\frac{N_c}{K}}\otimes\boldsymbol{S})E[\bar{\boldsymbol{a}}[n]\bar{\boldsymbol{w}}^\top[n]]\boldsymbol{\mathcal{F}}\\
&\quad+\boldsymbol{\mathcal{F}}^\top\boldsymbol{\mathcal{H}}(\boldsymbol{I}_{\frac{N_c}{K}}\otimes\boldsymbol{S})E[\bar{\boldsymbol{a}}[n]\bar{\tilde{\boldsymbol{a}}}^\top[n]]\boldsymbol{\mathcal{G}}\\
&\quad-\boldsymbol{\mathcal{F}}^\top\boldsymbol{\mathcal{H}}(\boldsymbol{I}_{\frac{N_c}{K}}\otimes\boldsymbol{S})E[\bar{\boldsymbol{a}}[n]\bar{\boldsymbol{a}}^\top[n]]\boldsymbol{E}_{N\Delta}\\
&\quad+\boldsymbol{\mathcal{F}}^\top E[\bar{\boldsymbol{w}}[n]\bar{\boldsymbol{a}}^\top[n]](\boldsymbol{I}_{\frac{N_c}{K}}\otimes\boldsymbol{S})^\top\boldsymbol{\mathcal{H}}^\top\boldsymbol{\mathcal{F}}\\
&\quad+\boldsymbol{\mathcal{F}}^\top E[\bar{\boldsymbol{w}}[n]\bar{\boldsymbol{w}}^\top[n]]\boldsymbol{\mathcal{F}}+\boldsymbol{\mathcal{F}}^\top E[\bar{\boldsymbol{w}}[n]\bar{\tilde{\boldsymbol{a}}}^\top[n]]\boldsymbol{\mathcal{G}}\\
&\quad-\boldsymbol{\mathcal{F}}^\top E[\bar{\boldsymbol{w}}[n]\bar{\boldsymbol{a}}^\top[n]]\boldsymbol{E}_{N\Delta}+\boldsymbol{\mathcal{G}}^\top E[\bar{\tilde{\boldsymbol{a}}}[n]\bar{\boldsymbol{a}}^\top[n]](\boldsymbol{I}_{\frac{N_c}{K}}\otimes\boldsymbol{S})^\top\boldsymbol{\mathcal{H}}^\top\boldsymbol{\mathcal{F}}\\
&\quad+\boldsymbol{\mathcal{G}}^\top E[\bar{\tilde{\boldsymbol{a}}}[n]\bar{\boldsymbol{w}}^\top[n]]\boldsymbol{\mathcal{F}}+\boldsymbol{\mathcal{G}}^\top E[\bar{\tilde{\boldsymbol{a}}}[n]\bar{\tilde{\boldsymbol{a}}}^\top[n]]\boldsymbol{\mathcal{G}}\\
&\quad-\boldsymbol{\mathcal{G}}^\top E[\bar{\tilde{\boldsymbol{a}}}[n]\bar{\boldsymbol{a}}^\top[n]]\boldsymbol{E}_{N\Delta}-\boldsymbol{E}_{N\Delta}^\top E[\bar{\boldsymbol{a}}[n]\bar{\boldsymbol{a}}^\top[n]](\boldsymbol{I}_{\frac{N_c}{K}}\otimes\boldsymbol{S})^\top\boldsymbol{\mathcal{H}}^\top\boldsymbol{\mathcal{F}}\\
&\quad-\boldsymbol{E}_{N\Delta}^\top E[\bar{\boldsymbol{a}}[n]\bar{\boldsymbol{w}}^\top[n]]\boldsymbol{\mathcal{F}}-\boldsymbol{E}_{N\Delta}^\top E[\bar{\boldsymbol{a}}[n]\bar{\tilde{\boldsymbol{a}}}^\top[n]]\boldsymbol{\mathcal{G}}\\
&\quad+\boldsymbol{E}_{N\Delta}^\top E[\bar{\boldsymbol{a}}[n]\bar{\boldsymbol{a}}^\top[n]]\boldsymbol{E}_{N\Delta}\Big)\\
&= \mathrm{tr}\Big(\boldsymbol{\mathcal{F}}^\top\left[\boldsymbol{\mathcal{H}}(\boldsymbol{I}_{\frac{N_c}{K}}\otimes\boldsymbol{S})\boldsymbol{R}_{aa}(\boldsymbol{I}_{\frac{N_c}{K}}\otimes\boldsymbol{S})^\top\boldsymbol{\mathcal{H}}^\top+\boldsymbol{R}_{ww}\right]\boldsymbol{\mathcal{F}}\\
&\quad+2\boldsymbol{\mathcal{F}}^\top\boldsymbol{\mathcal{H}}(\boldsymbol{I}_{\frac{N_c}{K}}\otimes\boldsymbol{S})\boldsymbol{R}_{a\hat{a}}\boldsymbol{\mathcal{G}}-2\boldsymbol{\mathcal{F}}^\top\boldsymbol{\mathcal{H}}(\boldsymbol{I}_{\frac{N_c}{K}}\otimes\boldsymbol{S})\boldsymbol{R}_{aa}\boldsymbol{E}_{N\Delta}\\
&\quad+\boldsymbol{\mathcal{G}}^\top\boldsymbol{R}_{\hat{a}\hat{a}}\boldsymbol{\mathcal{G}}-2\boldsymbol{\mathcal{G}}^\top\boldsymbol{R}_{a\hat{a}}^\top\boldsymbol{E}_{N\Delta}+\boldsymbol{E}_{N\Delta}^\top\boldsymbol{R}_{aa}\boldsymbol{E}_{N\Delta}\Big)
\end{aligned}
$$

where we have assumed the noise and data are uncorrelated, and we define

$$\begin{aligned}
\boldsymbol{R}_{aa} &\triangleq E[\bar{\boldsymbol{a}}[n]\bar{\boldsymbol{a}}^{\top}[n]] && (3.14)\\
\boldsymbol{R}_{a\hat{a}} &\triangleq E[\bar{\boldsymbol{a}}[n]\bar{\hat{\boldsymbol{a}}}^{\top}[n-1]] && (3.15)\\
\boldsymbol{R}_{\hat{a}\hat{a}} &\triangleq E[\bar{\hat{\boldsymbol{a}}}[n-1]\bar{\hat{\boldsymbol{a}}}^{\top}[n-1]] && (3.16)\\
\boldsymbol{R}_{ww} &\triangleq E[\bar{\boldsymbol{w}}[n]\bar{\boldsymbol{w}}^{\top}[n]]. && (3.17)
\end{aligned}$$

To find the optimal feedback filter, we take the derivative with respect to $\boldsymbol{\mathcal{G}}$, set to zero and solve for $\boldsymbol{\mathcal{G}}$, giving

$$\begin{aligned}
\frac{1}{2}\frac{\partial J_{MSE}(\boldsymbol{\mathcal{F}},\boldsymbol{\mathcal{G}},\Delta)}{\partial \boldsymbol{\mathcal{G}}} &= \boldsymbol{R}_{a\hat{a}}^{\top}(\boldsymbol{I}_{\frac{N_c}{K}}\otimes\boldsymbol{S})^{\top}\boldsymbol{\mathcal{H}}^{\top}\boldsymbol{\mathcal{F}}+\boldsymbol{R}_{\hat{a}\hat{a}}\boldsymbol{\mathcal{G}}-\boldsymbol{R}_{a\hat{a}}^{\top}\boldsymbol{E}_{N\Delta}\\
&= \boldsymbol{0}\\
\implies \boldsymbol{\mathcal{G}}^{*} &= \boldsymbol{R}_{\hat{a}\hat{a}}^{-1}\boldsymbol{R}_{a\hat{a}}^{\top}\left[\boldsymbol{E}_{N\Delta}-(\boldsymbol{I}_{\frac{N_c}{K}}\otimes\boldsymbol{S})^{\top}\boldsymbol{\mathcal{H}}^{\top}\boldsymbol{\mathcal{F}}\right]. \qquad (3.18)
\end{aligned}$$

Taking the derivative with respect to $\boldsymbol{\mathcal{F}}$, substituting $\boldsymbol{\mathcal{G}}^{*}$, and setting to zero gives

$$\begin{aligned}
\frac{1}{2}\frac{\partial J_{MSE}(\boldsymbol{\mathcal{F}},\boldsymbol{\mathcal{G}}^{*},\Delta)}{\partial \boldsymbol{\mathcal{F}}} &= \boldsymbol{\mathcal{H}}(\boldsymbol{I}_{\frac{N_c}{K}}\otimes\boldsymbol{S})\boldsymbol{R}_{aa}(\boldsymbol{I}_{\frac{N_c}{K}}\otimes\boldsymbol{S})^{\top}\boldsymbol{\mathcal{H}}^{\top}\boldsymbol{\mathcal{F}}+\boldsymbol{R}_{ww}\boldsymbol{\mathcal{F}}\\
&\quad +\boldsymbol{\mathcal{H}}(\boldsymbol{I}_{\frac{N_c}{K}}\otimes\boldsymbol{S})\boldsymbol{R}_{a\hat{a}}\boldsymbol{\mathcal{G}}^{*}-\boldsymbol{\mathcal{H}}(\boldsymbol{I}_{\frac{N_c}{K}}\otimes\boldsymbol{S})\boldsymbol{R}_{aa}\boldsymbol{E}_{N\Delta}\\
&= \left(\boldsymbol{\mathcal{H}}(\boldsymbol{I}_{\frac{N_c}{K}}\otimes\boldsymbol{S})\boldsymbol{\mathcal{R}}(\boldsymbol{I}_{\frac{N_c}{K}}\otimes\boldsymbol{S})^{\top}\boldsymbol{\mathcal{H}}^{\top}+\boldsymbol{R}_{ww}\right)\boldsymbol{\mathcal{F}}\\
&\quad -\boldsymbol{\mathcal{H}}(\boldsymbol{I}_{\frac{N_c}{K}}\otimes\boldsymbol{S})\boldsymbol{\mathcal{R}}\boldsymbol{E}_{N\Delta}\\
&= \boldsymbol{0}\\
\implies \boldsymbol{\mathcal{F}}^{*} &= \left(\boldsymbol{\mathcal{H}}(\boldsymbol{I}_{\frac{N_c}{K}}\otimes\boldsymbol{S})\boldsymbol{\mathcal{R}}(\boldsymbol{I}_{\frac{N_c}{K}}\otimes\boldsymbol{S})^{\top}\boldsymbol{\mathcal{H}}^{\top}+\boldsymbol{R}_{ww}\right)^{-1}\\
&\qquad \cdot\boldsymbol{\mathcal{H}}(\boldsymbol{I}_{\frac{N_c}{K}}\otimes\boldsymbol{S})\boldsymbol{\mathcal{R}}\boldsymbol{E}_{N\Delta} \qquad (3.19)
\end{aligned}$$

where

$$\boldsymbol{\mathcal{R}} \triangleq \boldsymbol{R}_{aa}-\boldsymbol{R}_{a\hat{a}}\boldsymbol{R}_{\hat{a}\hat{a}}^{-1}\boldsymbol{R}_{a\hat{a}}^{\top}. \qquad (3.20)$$

Under the assumption of correct feedback, $\hat{\boldsymbol{a}}[n] = \boldsymbol{a}[n-\Delta]$, or

$$\bar{\hat{\boldsymbol{a}}}[n-1] = \underbrace{\left[\mathbf{0}_{N_g \times N(\Delta+1)} \quad \boldsymbol{I}_{N_g} \quad \mathbf{0}_{N_g \times N(N_c/K-\Delta-1)-N_g}\right]}_{\triangleq \boldsymbol{\Sigma}_{N\Delta} \in \mathbb{R}^{N_g \times N_c N/K}} \bar{\boldsymbol{a}}[n] \tag{3.21}$$

where $\boldsymbol{\Sigma}_{N\Delta}$ effectively selects the appropriate elements of $\bar{\boldsymbol{a}}[n]$ to construct $\bar{\hat{\boldsymbol{a}}}[n-1]$. We note that $\boldsymbol{\Sigma}_{N\Delta}\boldsymbol{\Sigma}_{N\Delta}^{\top} = \boldsymbol{I}_{N_g}$ and $\boldsymbol{\Sigma}_{N\Delta}\boldsymbol{E}_{N\Delta} = \mathbf{0}_{N_g \times N}$. It then follows that under correct feedback

$$\begin{aligned} \boldsymbol{R}_{a\hat{a}} &= E[\bar{\boldsymbol{a}}[n]\bar{\boldsymbol{a}}^{\top}[n]\boldsymbol{\Sigma}_{N\Delta}^{\top}] \\ &= \boldsymbol{R}_{aa}\boldsymbol{\Sigma}_{N\Delta}^{\top} \qquad (3.22) \\ \boldsymbol{R}_{\hat{a}\hat{a}} &= E[\boldsymbol{\Sigma}_{\boldsymbol{N\Delta}}\bar{\boldsymbol{a}}[n]\bar{\boldsymbol{a}}^{\top}[n]\boldsymbol{\Sigma}_{N\Delta}^{\top}] \\ &= \boldsymbol{\Sigma}_{\boldsymbol{N\Delta}}\boldsymbol{R}_{aa}\boldsymbol{\Sigma}_{N\Delta}^{\top}. \qquad (3.23) \end{aligned}$$

From the second-order moments of the selection vectors given in (3.12), we see that $\boldsymbol{R}_{aa} = \boldsymbol{I}$ for biorthogonal modulation. Thus,

$$\begin{aligned} \boldsymbol{R}_{aa} &= \boldsymbol{I} \\ \boldsymbol{R}_{a\hat{a}} &= \boldsymbol{\Sigma}_{N\Delta}^{\top} \\ \boldsymbol{R}_{\hat{a}\hat{a}} &= \boldsymbol{I}. \end{aligned}$$

Substituting the correlation matrices into (3.18) and (3.19) gives the simplified MMSE DFE design equations for biorthogonal modulation:

$$\boldsymbol{\mathcal{G}}^{*} = -\boldsymbol{\Sigma}_{N\Delta}\boldsymbol{\mathcal{H}}_{eff}^{\top}\boldsymbol{\mathcal{F}} \tag{3.24}$$

$$\boldsymbol{\mathcal{F}}^{*} = \left(\boldsymbol{\mathcal{H}}_{eff}(\boldsymbol{I} - \boldsymbol{\Sigma}_{N\Delta}^{\top}\boldsymbol{\Sigma}_{N\Delta})\boldsymbol{\mathcal{H}}_{eff}^{\top} + \boldsymbol{R}_{ww}\right)^{-1}\boldsymbol{\mathcal{H}}_{eff}\boldsymbol{E}_{N\Delta} \tag{3.25}$$

where

$$\boldsymbol{\mathcal{H}}_{eff} = \boldsymbol{\mathcal{H}}(\boldsymbol{I}_{\frac{N_c}{K}} \otimes \boldsymbol{S}). \tag{3.26}$$

We note that when the noise is AWGN with variance σ_w^2, we have

$$\boldsymbol{R}_{ww} \;=\; \sigma_w^2 \boldsymbol{I}_{N_c}$$

We also note that in trivial case where there is no ISI (i.e. when $\boldsymbol{H} = \boldsymbol{I}$) but Gaussian noise, the feedforward equalizer reduces to the ML detector for the AWGN channel in the absence of a feedback section.

3.3.2 Orthogonal Modulation

As we saw in Section 2.3.2, the decision device for orthogonal modulation is invariant to a DC component added to all chips in a symbol. For the scalar equalizer, we redefined the MSE so that it did not penalize DC offsets, and this extra degree of freedom permitted us to obtain perfect equalization in situations where it would not have otherwise been possible. The same trick can be applied to the block equalizer, and in fact the benefit is even greater here since we incur a computational savings. Recall from Lemma 2.1 that the decision device is unaffected when the input signal is multiplied by $\boldsymbol{J}_N$. Since $\boldsymbol{J}_N$ is rank deficient, we are able

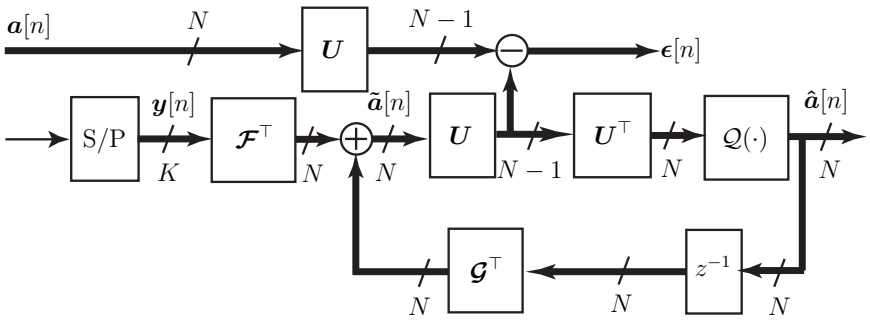

Figure 3.2: Equalizer with Modified Error Signal for Orthogonal Modulation

to decompose $\boldsymbol{J}_N$ as $\boldsymbol{J}_N = \boldsymbol{U}_N^\top \boldsymbol{U}_N$, thereby using $\boldsymbol{U}$ to map the N chips of the estimated selection vector to a transorthogonal signal set with only $N-1$ chips per

symbol. This is shown in Fig. 3.2, where the structure generates identical outputs to the original block equalizer structure shown in Fig. 3.1.

However, in the block equalizer, we can absorb $\boldsymbol{U}$ into the feedforward and feedback equalizers, thus eliminating one column from each block equalizer so that the size of the equalizers is reduced to $\boldsymbol{\mathcal{F}} \in \mathbb{R}^{N_f \times N-1}$ and $\boldsymbol{\mathcal{G}} \in \mathbb{R}^{N_g \times N-1}$ (and, similarly, $\boldsymbol{F}[n] \in \mathbb{R}^{N-1 \times K}$ and $\boldsymbol{G}[n] \in \mathbb{R}^{N-1 \times N}$). The new structure, shown in Fig. 3.3, requires a slight modification to the equations that describe the system model to account for the new sizes. In particular, the equation for the decision device

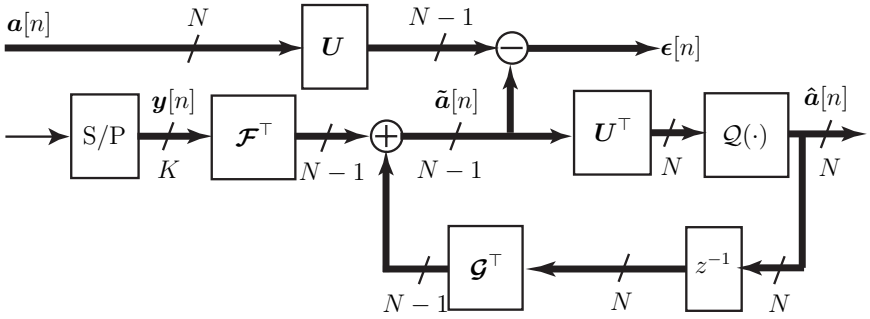

Figure 3.3: Modified Equalizer with Absorption of $\boldsymbol{U}^\top$

has changed to

$$\hat{\boldsymbol{a}}[n] \;=\; \mathcal{Q}(\boldsymbol{U}^\top \tilde{\boldsymbol{a}}[n]). \tag{3.27}$$

Note that, with the scalar equalizer for orthogonal modulation, we did not make any change to the equalizer structure — we simply modified the MSE metric. Here, however, we have modified the structure since we have absorbed $\boldsymbol{U}$ into the block equalizer. Also, we note that now $\tilde{\boldsymbol{a}}[n]$ is a vector with only $N-1$ elements, and so any comparison with the (delayed) transmitted selection vectors will require that $\boldsymbol{a}[n-\Delta]$ be mapped into the equivalent signal space via multiplication with $\boldsymbol{U}$. This is shown in the formation of the error signal in Fig. 3.3.

The MSE is then

$$\begin{aligned} J_{MSE}(\boldsymbol{\mathcal{F}},\boldsymbol{\mathcal{G}},\Delta) &= E\left[||\tilde{\boldsymbol{a}}[n]-\boldsymbol{U}\boldsymbol{a}[n-\Delta]||_2^2\right] \qquad (3.28)\\ &= E\left[\left|\left|\boldsymbol{\mathcal{F}}^\top\left(\boldsymbol{\mathcal{H}}(\boldsymbol{I}_{\frac{N_c}{K}}\otimes\boldsymbol{S})\bar{\boldsymbol{a}}[n]+\bar{\boldsymbol{w}}[n]\right)\right.\right.\\ &\qquad\left.\left.+\boldsymbol{\mathcal{G}}^\top\bar{\tilde{\boldsymbol{a}}}[n-1]-\boldsymbol{U}\boldsymbol{E}_{N\Delta}^\top\bar{\boldsymbol{a}}[n]\right|\right|_2^2\right]\\ &= \mathrm{tr}\left(\boldsymbol{\mathcal{F}}^\top\left[\boldsymbol{\mathcal{H}}(\boldsymbol{I}_{\frac{N_c}{K}}\otimes\boldsymbol{S})\boldsymbol{R}_{aa}(\boldsymbol{I}_{\frac{N_c}{K}}\otimes\boldsymbol{S})^\top\boldsymbol{\mathcal{H}}^\top+\boldsymbol{R}_{ww}\right]\boldsymbol{\mathcal{F}}\right.\\ &\quad+2\boldsymbol{\mathcal{F}}^\top\boldsymbol{\mathcal{H}}(\boldsymbol{I}_{\frac{N_c}{K}}\otimes\boldsymbol{S})\boldsymbol{R}_{a\hat{a}}\boldsymbol{\mathcal{G}}-2\boldsymbol{\mathcal{F}}^\top\boldsymbol{\mathcal{H}}(\boldsymbol{I}_{\frac{N_c}{K}}\otimes\boldsymbol{S})\boldsymbol{R}_{aa}\boldsymbol{E}_{N\Delta}\boldsymbol{U}^\top\\ &\quad\left.+\boldsymbol{\mathcal{G}}^\top\boldsymbol{R}_{\hat{a}\hat{a}}\boldsymbol{\mathcal{G}}-2\boldsymbol{\mathcal{G}}^\top\boldsymbol{R}_{a\hat{a}}^\top\boldsymbol{E}_{N\Delta}\boldsymbol{U}^\top+\boldsymbol{U}\boldsymbol{E}_{N\Delta}^\top\boldsymbol{R}_{aa}\boldsymbol{E}_{N\Delta}\boldsymbol{U}^\top\right). \end{aligned}$$

where as before,

$$\begin{aligned} \boldsymbol{R}_{aa} &\triangleq E[\bar{\boldsymbol{a}}[n]\bar{\boldsymbol{a}}^\top[n]]\\ \boldsymbol{R}_{a\hat{a}} &\triangleq E[\bar{\boldsymbol{a}}[n]\bar{\tilde{\boldsymbol{a}}}^\top[n-1]]\\ \boldsymbol{R}_{\hat{a}\hat{a}} &\triangleq E[\bar{\tilde{\boldsymbol{a}}}[n-1]\bar{\tilde{\boldsymbol{a}}}^\top[n-1]]\\ \boldsymbol{R}_{ww} &\triangleq E[\bar{\boldsymbol{w}}[n]\bar{\boldsymbol{w}}^\top[n]]. \qquad (3.29) \end{aligned}$$

Under the assumption of correct feedback, we substitute (3.11), (3.22), and (3.23) to give

$$\begin{aligned} \boldsymbol{R}_{aa} &= \frac{1}{N^2}\left[\mathbf{1}_{\frac{N_cN}{K}\times\frac{N_cN}{K}}+(\boldsymbol{I}_{\frac{N_c}{K}}\otimes(N\boldsymbol{I}_N-\mathbf{1}_{N\times N}))\right] \qquad (3.30)\\ \boldsymbol{R}_{a\hat{a}} &= \boldsymbol{R}_{aa}\boldsymbol{\Sigma}_{N\Delta}^\top \qquad (3.31)\\ \boldsymbol{R}_{\hat{a}\hat{a}} &= \boldsymbol{\Sigma}_{\boldsymbol{N\Delta}}\boldsymbol{R}_{aa}\boldsymbol{\Sigma}_{N\Delta}^\top \qquad (3.32)\\ &= \frac{1}{N^2}\left[\mathbf{1}_{N_g\times N_g}+(\boldsymbol{I}_{\frac{N_g}{N}}\otimes(N\boldsymbol{I}_N-\mathbf{1}_{N\times N}))\right]. \qquad (3.33) \end{aligned}$$

where the definition of $\boldsymbol{\Sigma}_{N\Delta}$ was given in (3.21). To find the optimal feedback

filter, we take the derivative with respect to $\boldsymbol{\mathcal{G}}$, set to zero and solve for $\boldsymbol{\mathcal{G}}$, giving

$$\begin{aligned}\frac{1}{2}\frac{\partial J_{MSE}(\boldsymbol{\mathcal{F}},\boldsymbol{\mathcal{G}},\Delta)}{\partial \boldsymbol{\mathcal{G}}} &= \boldsymbol{R}_{a\hat{a}}^{\top}(\boldsymbol{I}_{\frac{N_c}{K}}\otimes \boldsymbol{S})^{\top}\boldsymbol{\mathcal{H}}^{\top}\boldsymbol{\mathcal{F}} + \boldsymbol{R}_{\hat{a}\hat{a}}\boldsymbol{\mathcal{G}} - \boldsymbol{R}_{a\hat{a}}^{\top}\boldsymbol{E}_{N\Delta}\boldsymbol{U}^{\top} \\ &= \boldsymbol{0} \\ \implies \boldsymbol{R}_{\hat{a}\hat{a}}\boldsymbol{\mathcal{G}}^{*} &= \boldsymbol{R}_{a\hat{a}}^{\top}\left[\boldsymbol{E}_{N\Delta}\boldsymbol{U}^{\top} - (\boldsymbol{I}_{\frac{N_c}{K}}\otimes \boldsymbol{S})^{\top}\boldsymbol{\mathcal{H}}^{\top}\boldsymbol{\mathcal{F}}\right]. \end{aligned} \tag{3.34}$$

However, solving this expression for $\boldsymbol{\mathcal{G}}^{*}$ requires inversion of $\boldsymbol{R}_{\hat{a}\hat{a}}$. The matrix $\boldsymbol{R}_{\hat{a}\hat{a}}$ has exactly the form addressed by Lemma 3.1 (for $b = N_g/N$); thus, $\boldsymbol{R}_{\hat{a}\hat{a}}$ has nullity $N_g/N - 1$. However, the linear system (3.34) is consistent since the right side of the equation is in the column space of $\boldsymbol{R}_{\hat{a}\hat{a}}$, which follows from the definitions of the correlation matrices in (3.31) and (3.32). Thus, (3.34) is an underdetermined system with an infinite number of solutions. Consequently, we have flexibility in our a choice of $\boldsymbol{\mathcal{G}}^{*}$. We now consider two such choices, both of which lend themselves to simple adaptive implementations.

One possibility is to find a solution that attempts to minimize the effects of error propagation. As discussed in [19], large taps in the feedback portion of DFEs have a tendency to enhance the effects of error propagation. A sensible approach, then, is to use the minimum ℓ_2 norm solution of $\boldsymbol{\mathcal{G}}^{*}$, which is found easily by multiplying both sides of (3.34) with the Moore-Penrose pseudo-inverse of $\boldsymbol{R}_{\hat{a}\hat{a}}$. This solution may give a small performance improvement in environments with significant symbol errors.

Alternatively, we can make another choice of $\boldsymbol{\mathcal{G}}^{*}$ which incurs a computational savings, by constraining entire rows of $\boldsymbol{\mathcal{G}}^{*}$ to be zero.

Lemma 3.2. *Existence of $\boldsymbol{\mathcal{G}}^{*}$ with zeroed rows*

For some $\boldsymbol{\mathcal{G}}^{**} \in \mathbb{R}^{N_g \times N-1}$ satisfying (3.34), there exists another $\boldsymbol{\mathcal{G}}^{*}$ that also satisfies (3.34), but where the $N_g/N - 1$ rows of $\boldsymbol{\mathcal{G}}^{*}$ with indices Ni for $i \in$

$\{1, 2, \ldots, N_g/N - 1\}$ *are all zero.*

Proof. We show a proof by construction. Consider constructing $\boldsymbol{\mathcal{G}}^*$ from $\boldsymbol{\mathcal{G}}^{**}$ via the transformation

$$\boldsymbol{\mathcal{G}}^* = \left(\boldsymbol{I}_{N_g} + \boldsymbol{A}\right)\boldsymbol{\mathcal{G}}^{**}$$

where $\boldsymbol{A} \in \mathbb{R}^{N_g \times N_g}$ is a matrix of all zeros with the exception of the *columns* indexed by Ni, for i given above. These columns of $\boldsymbol{A}$ equal the vector

$$\boldsymbol{v}_{Ni} = \begin{bmatrix} \mathbf{1}_{N\times 1} \\ \mathbf{0}_{N(i-1)\times 1} \\ -\mathbf{1}_{N\times 1} \\ \mathbf{0}_{N_g - N(i+1)\times 1} \end{bmatrix} = \begin{bmatrix} 1 \\ \mathbf{0}_{i-1\times 1} \\ -1 \\ \mathbf{0}_{N_g/N - i - 1} \end{bmatrix} \otimes \mathbf{1}_{N\times 1}.$$

Under this construction, the Nith row of $\boldsymbol{A}$ is all zeros except for a -1 in the Nith column. Thus, the rows of $\left(\boldsymbol{I}_{N_g} + \boldsymbol{A}\right)$ indexed by Ni are all zeros, and therefore $\boldsymbol{\mathcal{G}}^*$ has zeros in the desired location under this transformation. Now, we only need to show that $\boldsymbol{\mathcal{G}}^*$ still satisfies (3.34). Note that

$$\begin{aligned} \boldsymbol{R}_{\hat{a}\hat{a}}\boldsymbol{v}_{Ni} &= \frac{1}{N^2}\left[\mathbf{1}_{N_g\times N_g} + (\boldsymbol{I}_{\frac{N_g}{N}} \otimes (N\boldsymbol{I}_N - \mathbf{1}_{N\times N}))\right]\boldsymbol{v}_{Ni} \\ &= \frac{1}{N^2}(\boldsymbol{I}_{\frac{N_g}{N}} \otimes (N\boldsymbol{I}_N - \mathbf{1}_{N\times N}))\boldsymbol{v}_{Ni} \\ &= \mathbf{0}_{N_g\times 1} \end{aligned}$$

so all the columns of $\boldsymbol{A}$ are in the nullspace of $\boldsymbol{R}_{\hat{a}\hat{a}}$. Consequently,

$$\begin{aligned} \boldsymbol{R}_{\hat{a}\hat{a}}\boldsymbol{\mathcal{G}}^* &= \boldsymbol{R}_{\hat{a}\hat{a}}\left(\boldsymbol{I}_{N_g} + \boldsymbol{A}\right)\boldsymbol{\mathcal{G}}^{**} \\ &= \boldsymbol{R}_{\hat{a}\hat{a}}\boldsymbol{\mathcal{G}}^{**}. \end{aligned}$$

■

Thus, for any feedback equalizer of length N_g, only $N_g - N_g/N + 1$ of the taps need to be in use. We note that any choice of $\boldsymbol{\mathcal{G}}^*$ satisfying (3.34) will have the same performance (under the assumption of correct feedback), so constraining some taps to zero as described by Lemma 3.2 seems the most sensible since it incurs a reduction in complexity. To clarify, for a $\boldsymbol{\mathcal{G}}^*$ constructed this way, the first row of each $N \times N - 1$ sub-block will be all zero, with the exception of the very first row of the matrix. Using $\times$ to indicated non-zero values, $\boldsymbol{\mathcal{G}}^*$ can then be made to have the following form, where the partitions occur every N rows:

$$\left[\begin{array}{cccc}
\times & \times & \cdots & \times \\
\times & \times & \cdots & \times \\
\vdots & & & \\
\times & \times & \cdots & \times \\
\hline
0 & 0 & \cdots & 0 \\
\times & \times & \cdots & \times \\
\vdots & & & \\
\times & \times & \cdots & \times \\
\hline
 & \vdots & & \\
 & \vdots & & \\
\hline
0 & 0 & \cdots & 0 \\
\times & \times & \cdots & \times \\
\vdots & & & \\
\times & \times & \cdots & \times
\end{array}\right]$$

Note that, rather than use a feedback filter with zeroed rows, a practical implementation could equivalently decimate the unneeded elements in the input regressor, $\bar{\hat{\boldsymbol{a}}}[n-1]$.

We define $\boldsymbol{R}_{\hat{a}\hat{a}}^{-}$ to be the matrix 1-inverse[1] of $\boldsymbol{R}_{\hat{a}\hat{a}}$ that results in the desired rows of $\boldsymbol{\mathcal{G}}^*$ being zeroed, and this matrix can be found using the construction in Lemma 3.2. Thus,

$$\boldsymbol{\mathcal{G}}^* \;=\; \boldsymbol{R}_{\hat{a}\hat{a}}^{-}\boldsymbol{R}_{a\hat{a}}^{\top}\left[\boldsymbol{E}_{N\Delta}\boldsymbol{U}^{\top} - (\boldsymbol{I}_{\frac{N_c}{K}} \otimes \boldsymbol{S})^{\top}\boldsymbol{\mathcal{H}}^{\top}\boldsymbol{\mathcal{F}}\right]. \tag{3.35}$$

Now, for the feedforward taps, we proceed by taking the derivative of the MSE with respect to $\boldsymbol{\mathcal{F}}$, substituting $\boldsymbol{\mathcal{G}}^*$, and setting to zero to give

$$\begin{aligned}
\frac{1}{2}\frac{\partial J_{MSE}(\boldsymbol{\mathcal{F}},\boldsymbol{\mathcal{G}}^*,\Delta)}{\partial \boldsymbol{\mathcal{F}}} &= \boldsymbol{\mathcal{H}}(\boldsymbol{I}_{\frac{N_c}{K}} \otimes \boldsymbol{S})\boldsymbol{R}_{aa}(\boldsymbol{I}_{\frac{N_c}{K}} \otimes \boldsymbol{S})^{\top}\boldsymbol{\mathcal{H}}^{\top}\boldsymbol{\mathcal{F}} + \boldsymbol{R}_{ww}\boldsymbol{\mathcal{F}} \\
&\quad + \boldsymbol{\mathcal{H}}(\boldsymbol{I}_{\frac{N_c}{K}} \otimes \boldsymbol{S})\boldsymbol{R}_{a\hat{a}}\boldsymbol{\mathcal{G}}^* - \boldsymbol{\mathcal{H}}(\boldsymbol{I}_{\frac{N_c}{K}} \otimes \boldsymbol{S})\boldsymbol{R}_{aa}\boldsymbol{E}_{N\Delta}\boldsymbol{U}^{\top} \\
&= \left(\boldsymbol{\mathcal{H}}(\boldsymbol{I}_{\frac{N_c}{K}} \otimes \boldsymbol{S})\boldsymbol{\mathcal{R}}(\boldsymbol{I}_{\frac{N_c}{K}} \otimes \boldsymbol{S})^{\top}\boldsymbol{\mathcal{H}}^{\top} + \boldsymbol{R}_{ww}\right)\boldsymbol{\mathcal{F}} \\
&\quad - \boldsymbol{\mathcal{H}}(\boldsymbol{I}_{\frac{N_c}{K}} \otimes \boldsymbol{S})\boldsymbol{\mathcal{R}}\boldsymbol{E}_{N\Delta}\boldsymbol{U}^{\top} \\
&= \boldsymbol{0} \\
\Longrightarrow \boldsymbol{\mathcal{F}}^* &= \left(\boldsymbol{\mathcal{H}}(\boldsymbol{I}_{\frac{N_c}{K}} \otimes \boldsymbol{S})\boldsymbol{\mathcal{R}}(\boldsymbol{I}_{\frac{N_c}{K}} \otimes \boldsymbol{S})^{\top}\boldsymbol{\mathcal{H}}^{\top} + \boldsymbol{R}_{ww}\right)^{-1} \\
&\qquad \cdot \boldsymbol{\mathcal{H}}(\boldsymbol{I}_{\frac{N_c}{K}} \otimes \boldsymbol{S})\boldsymbol{\mathcal{R}}\boldsymbol{E}_{N\Delta}\boldsymbol{U}^{\top}
\end{aligned} \tag{3.36}$$

where

$$\boldsymbol{\mathcal{R}} \;\triangleq\; \boldsymbol{R}_{aa} - \boldsymbol{R}_{a\hat{a}}\boldsymbol{R}_{\hat{a}\hat{a}}^{-}\boldsymbol{R}_{a\hat{a}}^{\top}$$

3.3.3 Transorthogonal Modulation

For transorthogonal modulation, the selection vectors $\boldsymbol{a}[n]$ have identical statistics to orthogonal modulation; the only difference is that now $\boldsymbol{S}^{\top}\boldsymbol{S} \neq \boldsymbol{I}_N$, but instead $\boldsymbol{S}^{\top}\boldsymbol{S} = \boldsymbol{J}_N$. However, this does not change the MMSE equalizer design equations

[1] An $n \times m$ matrix $\boldsymbol{A}^{-}$ is a 1-inverse of a $m \times n$ matrix $\boldsymbol{A}$ for which $\boldsymbol{A}\boldsymbol{A}^{-}\boldsymbol{A} = \boldsymbol{A}$.

at all. For completeness, we repeat the DFE MMSE design equations:

$$\boldsymbol{\mathcal{G}}^* = \boldsymbol{R}_{\hat{a}\hat{a}}^{-}\boldsymbol{R}_{\hat{a}\hat{a}}^{\top}\left[\boldsymbol{E}_{N\Delta}\boldsymbol{U}^{\top} - (\boldsymbol{I}_{\frac{N_c}{K}} \otimes \boldsymbol{S})^{\top}\boldsymbol{\mathcal{H}}^{\top}\boldsymbol{\mathcal{F}}\right] \tag{3.37}$$

$$\boldsymbol{\mathcal{F}}^* = \left(\boldsymbol{\mathcal{H}}(\boldsymbol{I}_{\frac{N_c}{K}} \otimes \boldsymbol{S})\boldsymbol{\mathcal{R}}(\boldsymbol{I}_{\frac{N_c}{K}} \otimes \boldsymbol{S})^{\top}\boldsymbol{\mathcal{H}}^{\top} + \boldsymbol{R}_{ww}\right)^{-1} \cdot\boldsymbol{\mathcal{H}}(\boldsymbol{I}_{\frac{N_c}{K}} \otimes \boldsymbol{S})\boldsymbol{\mathcal{R}}\boldsymbol{E}_{N\Delta}\boldsymbol{U}^{\top} \tag{3.38}$$

where

$$\boldsymbol{\mathcal{R}} \triangleq \boldsymbol{R}_{aa} - \boldsymbol{R}_{a\hat{a}}\boldsymbol{R}_{\hat{a}\hat{a}}^{-}\boldsymbol{R}_{a\hat{a}}^{\top}$$

$$\boldsymbol{R}_{aa} = \frac{1}{N^2}\left[\boldsymbol{1}_{\frac{N_cN}{K}\times\frac{N_cN}{K}} + (\boldsymbol{I}_{\frac{N_c}{K}} \otimes (N\boldsymbol{I}_N - \boldsymbol{1}_{N\times N}))\right] \tag{3.39}$$

$$\boldsymbol{R}_{a\hat{a}} = \boldsymbol{R}_{aa}\boldsymbol{\Sigma}_{N\Delta}^{\top} \tag{3.40}$$

$$\boldsymbol{R}_{\hat{a}\hat{a}} = \frac{1}{N^2}\left[\boldsymbol{1}_{N_g\times N_g} + (\boldsymbol{I}_{\frac{N_g}{N}} \otimes (N\boldsymbol{I}_N - \boldsymbol{1}_{N\times N}))\right] \tag{3.41}$$

$$\boldsymbol{R}_{ww} \triangleq E[\bar{\boldsymbol{w}}[n]\bar{\boldsymbol{w}}^{\top}[n]] \tag{3.42}$$

and $\boldsymbol{R}_{\hat{a}\hat{a}}^{-}$ is the 1-inverse of $\boldsymbol{R}_{\hat{a}\hat{a}}$ obtained via Lemma 3.2.

3.4 Conditions for Perfect Linear Equalization

For the block equalizer, we consider the conditions that permit a feedforward equalizer to perfectly invert the channel for these modulations. As we did for the scalar equalizer, we assume in this section that there is no feedback equalizer, no noise, and therefore perfect equalization arises when the MSE is zero.

3.4.1 Biorthogonal Modulation

With no noise and no feedback section, the MSE reduces to

$$\begin{aligned} J_{MSE}(\boldsymbol{f},\Delta) &= \mathrm{tr}\left(\boldsymbol{\mathcal{F}}^{\top}\boldsymbol{\mathcal{H}}_{eff}\boldsymbol{\mathcal{H}}_{eff}^{\top}\boldsymbol{\mathcal{F}} - 2\boldsymbol{\mathcal{F}}^{\top}\boldsymbol{\mathcal{H}}_{eff}\boldsymbol{E}_{N\Delta} + \boldsymbol{E}_{N\Delta}^{\top}\boldsymbol{E}_{N\Delta}\right) \\ &= \mathrm{tr}\left(\left[\boldsymbol{\mathcal{F}}^{\top}\boldsymbol{\mathcal{H}}_{eff} - \boldsymbol{E}_{N\Delta}\right]\left[\boldsymbol{\mathcal{F}}^{\top}\boldsymbol{\mathcal{H}}_{eff} - \boldsymbol{E}_{N\Delta}\right]^{\top}\right) \\ &= ||\boldsymbol{\mathcal{F}}^{\top}\boldsymbol{\mathcal{H}}_{eff} - \boldsymbol{E}_{N\Delta}||_{fro}^2 \end{aligned}$$

where $||\cdot||_{fro}$ denotes the Frobenius matrix norm and

$$\boldsymbol{\mathcal{H}}_{eff} \;=\; \boldsymbol{\mathcal{H}}(\boldsymbol{I}_{\frac{N_c}{K}} \otimes \boldsymbol{S}). \tag{3.43}$$

For the MSE to be zero, then, we require

$$\boldsymbol{\mathcal{H}}_{eff}^{\top}\boldsymbol{\mathcal{F}} = \boldsymbol{E}_{N\Delta}^{\top} \tag{3.44}$$

and therefore $\boldsymbol{\mathcal{H}}_{eff} \in \mathbb{R}^{N_f \times N_c N/K}$ must be tall and full rank, leading to the following three conditions for perfect equalization:

1. **Length Condition:** For $\boldsymbol{\mathcal{F}}$ to satisfy (3.44) for arbitrary Δ, $\boldsymbol{\mathcal{H}}_{eff}$ must be a tall matrix. Hence, it is required that $N_f \geq (N_f + N_h - 1)N/K$, or

$$N_f \geq \frac{N}{K-N}(N_h - 1). \tag{3.45}$$

2. **Source Condition:** In the length condition above, we note the presence of $K - N$ in the denominator. For biorthogonal modulation, all of the signal sets require $K \geq N$ (from Table 1.2). However, if a signal set is employed where $K = N$, the length condition goes to infinity, and equalization with a finite length linear equalizer is not possible. Thus, we require $K > N$.

3. **Disparity Condition:** For $\boldsymbol{\mathcal{F}}$ to satisfy (3.44) for arbitrary Δ, $\boldsymbol{\mathcal{H}}_{eff}$ must have full column rank.

3.4.2 Orthogonal and Transorthogonal Modulation

With no noise and no feedback section, the MSE reduces to

$$\begin{aligned} J_{MSE}(\boldsymbol{f}, \Delta) \;=\; & \mathrm{tr}\Big(\boldsymbol{\mathcal{F}}^{\top}\Big[\boldsymbol{\mathcal{H}}(\boldsymbol{I}_{\frac{N_c}{K}} \otimes \boldsymbol{S})\boldsymbol{R}_{aa}(\boldsymbol{I}_{\frac{N_c}{K}} \otimes \boldsymbol{S})^{\top}\boldsymbol{\mathcal{H}}^{\top}\Big]\boldsymbol{\mathcal{F}} \\ & -2\boldsymbol{\mathcal{F}}^{\top}\boldsymbol{\mathcal{H}}(\boldsymbol{I}_{\frac{N_c}{K}} \otimes \boldsymbol{S})\boldsymbol{R}_{aa}\boldsymbol{E}_{N\Delta}\boldsymbol{U}^{\top} + \boldsymbol{U}\boldsymbol{E}_{N\Delta}^{\top}\boldsymbol{R}_{aa}\boldsymbol{E}_{N\Delta}\boldsymbol{U}^{\top}\Big). \end{aligned}$$

From Lemma 3.1, the nullity of $\boldsymbol{R}_{aa} \in \mathbb{R}^{N_c N/K \times N_c N/K}$ is $N_c/K - 1$, and there exists a decomposition $\boldsymbol{\Gamma}_{aa}^{\top}\boldsymbol{\Gamma}_{aa} = \boldsymbol{R}_{aa}$ where $\boldsymbol{\Gamma} \in \mathbb{R}^{N_c(N-1)/K+1 \times N_c N/K}$. Letting

$$\boldsymbol{\mathcal{H}}_{eff} \;=\; \boldsymbol{\mathcal{H}}(\boldsymbol{I}_{\frac{N_c}{K}} \otimes \boldsymbol{S})\boldsymbol{\Gamma}_{aa}^{\top}$$

the MSE becomes

$$\begin{aligned} J_{MSE}(\boldsymbol{f}, \Delta) &= \operatorname{tr}\left(\boldsymbol{\mathcal{F}}^{\top}\boldsymbol{\mathcal{H}}_{eff}\boldsymbol{\mathcal{H}}_{eff}^{\top}\boldsymbol{\mathcal{F}} - 2\boldsymbol{\mathcal{F}}^{\top}\boldsymbol{\mathcal{H}}_{eff}\boldsymbol{\Gamma}_{aa}\boldsymbol{E}_{N\Delta}\boldsymbol{U}^{\top}\right. \\ &\qquad \left. + \boldsymbol{U}\boldsymbol{E}_{N\Delta}^{\top}\boldsymbol{\Gamma}_{aa}^{\top}\boldsymbol{\Gamma}_{aa}\boldsymbol{E}_{N\Delta}\boldsymbol{U}^{\top}\right) \\ &= \operatorname{tr}\left(\left[\boldsymbol{\mathcal{F}}^{\top}\boldsymbol{\mathcal{H}}_{eff} - \boldsymbol{U}\boldsymbol{E}_{N\Delta}^{\top}\boldsymbol{\Gamma}_{aa}^{\top}\right]\left[\boldsymbol{\mathcal{F}}^{\top}\boldsymbol{\mathcal{H}}_{eff} - \boldsymbol{U}\boldsymbol{E}_{N\Delta}^{\top}\boldsymbol{\Gamma}_{aa}^{\top}\right]^{\top}\right) \\ &= \left|\left|\boldsymbol{\mathcal{F}}^{\top}\boldsymbol{\mathcal{H}}_{eff} - \boldsymbol{U}\boldsymbol{E}_{N\Delta}^{\top}\boldsymbol{\Gamma}_{aa}^{\top}\right|\right|_{fro}^{2} \end{aligned}$$

yielding the condition for perfect equalization as

$$\boldsymbol{\mathcal{H}}_{eff}^{\top}\boldsymbol{\mathcal{F}} = \boldsymbol{\Gamma}_{aa}\boldsymbol{E}_{N\Delta}\boldsymbol{U}^{\top}. \tag{3.46}$$

and therefore $\boldsymbol{\mathcal{H}}_{eff} \in \mathbb{R}^{N_f \times N_c(N-1)/K+1}$ must be tall and full rank, leading to the following three conditions for perfect equalization:

1. **Length Condition:** For $\boldsymbol{\mathcal{F}}$ to satisfy (3.46) for arbitrary Δ, $\boldsymbol{\mathcal{H}}_{eff}$ must be a tall matrix. Hence, it is required that

$$N_f \geq \frac{N_h(N-1)}{K-N+1} - 1 \tag{3.47}$$

2. **Source Condition (Transorthogonal Modulation only):** In the length condition above, we note the presence of $K - N - 1$ in the denominator. For orthogonal modulation, all of the signal sets require $K \geq N$ (from Table 1.2), so the denominator can never be zero, and perfect equalization is possible with *all* orthogonal signal sets. For transorthogonal modulation, signal sets require $K \geq N - 1$, Thus, if a transorthogonal signal set is employed where

$K = N - 1$, the length condition goes to infinity, and equalization with a finite length linear equalizer is not possible. Hence, for transorthogonal modulation, we require $K \geq N$.

3. **Disparity Condition:** For $\boldsymbol{\mathcal{F}}$ to satisfy (3.46) for arbitrary Δ, $\boldsymbol{\mathcal{H}}_{eff}$ must have full column rank.

Interestingly, we need not impose a source condition on $\boldsymbol{S}$ for orthogonal modulation. So long as the length and disparity conditions are satisfied, any orthogonal signal set admits an $\boldsymbol{\mathcal{F}}$ yielding perfect linear equalization.

3.4.3 Example: Biorthogonal Modulation

Here, we revisit the example presented in Section 2.4.2 where we saw that perfect equalization was not possible with the scalar equalizer. We have

$$\boldsymbol{S} = \frac{1}{\sqrt{2}} \begin{bmatrix} +1 & 0 \\ 0 & +1 \\ +1 & 0 \\ 0 & -1 \end{bmatrix}.$$

so that $K = 4$ and $N = 2$. This satisfies the source condition for block equalization of biorthogonal modulation, i.e. $K > N$.

Thus, the block equalizer enables perfect equalization for a larger class of signal sets. From (3.45), the equalizer length condition then becomes

$$N_f \geq N_h - 1.$$

3.4.4 Example: 3-ary Pulse Position Modulation

Here, we revisit an example presented in Section 2.4.4 where perfect equalization was not possible. We consider orthogonal modulation with $\boldsymbol{S} = \boldsymbol{I}_3$, corresponding to 3-ary PPM. As we have mentioned in Section 3.4.2, all orthogonal signal sets lead

to perfect equalization, so long as the length and disparity conditions are satisfied. While the disparity condition will be channel-dependent, the length condition from (3.47) becomes, for $N = K = 3$,

$$N_f \geq 2N_h - 1 \tag{3.48}$$

thus requiring the equalizer to be twice as long as the channel. If $2\times$ oversampling were employed with 3-ary PPM, resulting in the zero-padded orthogonal signal set

$$\boldsymbol{S}' = \begin{bmatrix} 1 & 0 & 0 \\ 0 & 0 & 0 \\ 0 & 1 & 0 \\ 0 & 0 & 0 \\ 0 & 0 & 1 \\ 0 & 0 & 0 \end{bmatrix}$$

where $K' = 6$ and $N' = 3$, the feedforward equalizer length condition becomes

$$N_f' \geq \frac{N_h'}{2} - 1$$

effectively requiring the equalizer to be half the length of the fractionally spaced channel of length N_h'. However, to compare the two systems fairly on the same bandlimited channel, it is important to note that the length of the fractionally sampled channel N_h' would be effectively twice the length of the chip-spaced channel N_h. Thus, the use of a fractionally-spaced equalizer gives significant benefit since it only needs to be roughly equal in length to the chip-spaced channel (i.e. $N_f' \geq N_h'/2 - 1 \approx N_h - 1$), whereas the chip-spaced equalizer needs to be twice the length (i.e. $N_f \geq 2N_h - 1$).

3.5 LMS Adaptation

Since the mean-squared error is again quadratic, we can use the LMS algorithm to calculate the matrices $\boldsymbol{\mathcal{F}}^*$ and $\boldsymbol{\mathcal{G}}^*$ adaptively when training data is available. To derive the update equation, we first take the instantaneous derivative of the MSE as described in Section 2.5. For biorthogonal modulation, taking the instantaneous derivative of (3.13) results in the matrices

$$\begin{aligned}\frac{1}{2}\frac{\partial \hat{J}_{MSE}}{\partial \boldsymbol{\mathcal{F}}} &= \bar{\boldsymbol{y}}[n]\left[\tilde{\boldsymbol{a}}[n]-\boldsymbol{a}[n-\Delta]\right]^\top \\ \frac{1}{2}\frac{\partial \hat{J}_{MSE}}{\partial \boldsymbol{\mathcal{G}}} &= \bar{\tilde{\boldsymbol{a}}}[n-1]\left[\tilde{\boldsymbol{a}}[n]-\boldsymbol{a}[n-\Delta]\right]^\top .\end{aligned}$$

This results in the LMS update equations for biorthogonal modulation as

$$\begin{aligned}\boldsymbol{\epsilon}_{LMS}[n] &= \tilde{\boldsymbol{a}}[n]-\boldsymbol{a}[n-\Delta] \\ \boldsymbol{\mathcal{F}}_{LMS}[n+1] &= \boldsymbol{\mathcal{F}}_{LMS}[n]-\mu_1\frac{\partial \hat{J}_{MSE}}{\partial \boldsymbol{\mathcal{F}}} \\ &= \boldsymbol{\mathcal{F}}_{LMS}[n]-\mu_1\bar{\boldsymbol{y}}[n]\boldsymbol{\epsilon}_{LMS}^\top[n] \\ \boldsymbol{\mathcal{G}}_{LMS}[n+1] &= \boldsymbol{\mathcal{G}}_{LMS}[n]-\mu_2\frac{\partial \hat{J}_{MSE}}{\partial \boldsymbol{\mathcal{G}}} \\ &= \boldsymbol{\mathcal{G}}_{LMS}[n]-\mu_2\bar{\tilde{\boldsymbol{a}}}[n-1]\boldsymbol{\epsilon}_{LMS}^\top[n]\end{aligned}$$

where μ_1, μ_2 are small positive step-sizes which serves to average out the noise in the gradient estimate. Again, the presence of $\boldsymbol{a}[n-\Delta]$ in the error term implies the availability of training data. When training data is unavailable, we can feed back the output of the decision device $\hat{\boldsymbol{a}}[n]$ instead, arriving at the DD-LMS update equations for the block equalizer,

$$\begin{aligned}\boldsymbol{\epsilon}_{DD}[n] &= \tilde{\boldsymbol{a}}[n]-\hat{\boldsymbol{a}}[n] \\ \boldsymbol{\mathcal{F}}_{DD}[n+1] &= \boldsymbol{\mathcal{F}}_{DD}[n]-\mu_1\bar{\boldsymbol{y}}[n]\boldsymbol{\epsilon}_{DD}^\top[n] \\ \boldsymbol{\mathcal{G}}_{DD}[n+1] &= \boldsymbol{\mathcal{G}}_{DD}[n]-\mu_2\bar{\tilde{\boldsymbol{a}}}[n-1]\boldsymbol{\epsilon}_{DD}^\top[n]\end{aligned}$$

The LMS update equations for orthogonal and transorthogonal modulation follow similarly, with a minor change to the error term:

$$\boldsymbol{\epsilon}_{LMS}[n] \;=\; \tilde{\boldsymbol{a}}[n] - \boldsymbol{U}\boldsymbol{a}[n-\Delta]$$

We recall that $\boldsymbol{R}_{\hat{a}\hat{a}}$ is non-invertible for orthogonal and transorthogonal modulation, and consequently the the optimal feedback filter $\boldsymbol{\mathcal{G}}$ can assume an infinite number of possibilities. In Section 3.3.2, we presented a particular choice of $\boldsymbol{\mathcal{G}}$ that involved constraining some of the rows to zero (or, equivalently, decimating the input to the feedback equalizer). During adaptation with LMS, this constraint can be imposed, as well, to benefit from the computational savings it provides. Without a constraint, the system is underdetermined and $\boldsymbol{\mathcal{G}}_{LMS}[n]$ may wander through the subspace of allowable MMSE solutions.

From an error propagation perspective, however, it may be preferable not to impose a constraint. While the choice of constraint has no affect on the performance of the DFE in the absence of decision errors, some constraints may be better than others in the presence of decision errors. It was reported in [12] that the MMSE adaptation mechanism in the presence of error propagation may find a better answer than the solution computed in the absence of decision errors.

3.6 Computational Complexity Comparison

We now compare the computational complexity of the scalar equalizer from Chapter 2 to that of the block equalizer by evaluating the number of scalar multiply operations required to equalize one symbol. We assume that the equalizer taps have already been calculated, and focus our complexity comparison on the operation of the equalizer.

To equalize one chip with the scalar equalizer, the feedforward section requires N_f multiplies. Since there are K chips per symbol, the feedforward section requires KN_f multiplies per symbol. The feedback section of the scalar equalizer requires N_g multiplies per selection vector chip. Since there are N chips per selection vector, the feedback section requires NN_g multiplies per symbol. The scalar equalizer also needs to perform a correlation via multiplication with $\boldsymbol{S}^\top$. In practice, $\boldsymbol{S}^\top$ will likely contain only $\{-1, 0, 1\}$, and thus no multiplication is required. However, if this is not the case, the correlation will require KN multiplies per symbol (since there are KN elements in $\boldsymbol{S}$). Thus, the total cost in multiply operations of equalizing one symbol with the scalar equalizer is

$$\text{scalar equalizer (all modulations)} : \quad \underbrace{KN_f}_{\text{feedforward}} + \underbrace{NN_g}_{\text{feedback}} + \underbrace{KN}_{\text{correlation}} .$$

The block equalizer structure is slightly different for biorthogonal modulation vs. orthogonal and transorthogonal modulation. First, we consider the computation involved for block equalization of biorthogonal modulation. The feedforward equalizer requires NN_f multiplies per symbol, while the feedback equalizer requires NN_g multiplies per symbol. Hence, for block equalization of biorthogonal modulation, the number of multiplies is

$$\text{block equalizer (biorthogonal)} : \quad \underbrace{NN_f}_{\text{feedforward}} + \underbrace{NN_g}_{\text{feedback}} .$$

Since we always have $N \leq K$ for biorthogonal modulation, the complexity of the block equalizer is always less than or equal to the complexity of the scalar equalizer.

Now, we consider block equalization of orthogonal and transorthogonal modulations. Due to the absorption of $\boldsymbol{U}$ into the equalizer for these modulations, $\boldsymbol{\mathcal{F}}$ and $\boldsymbol{\mathcal{G}}$ each have one less column. In addition, we were able to constrain $N_g/N - 1$

rows of $\boldsymbol{\mathcal{G}}$ to be zero. Hence, for orthogonal and transorthogonal modulation, the number of multiplies is

$$\text{block equalizer (orthogonal and transorthogonal)}: \quad \underbrace{(N-1)N_f}_{\text{feedforward}} + \underbrace{(N-1)(N_g - N_g/N + 1)}_{\text{feedback}}$$

which is less than that for biorthogonal modulation.

3.7 Simulated Example

Here, we compare the performance of our equalizer to one proposed in [2]. We use the same simulation setup used in [2], where orthogonal modulation is used with $\boldsymbol{S} = \boldsymbol{I}_2$, $\boldsymbol{h} = [1 \quad -1 \quad 1]^\top/\sqrt{3}$, and the noise is AWGN. For our MMSE equalizer, we chose $N_f = 5$, $N_g = 2$, and $\Delta = 1$. The results are shown in Fig. 3.4, and the

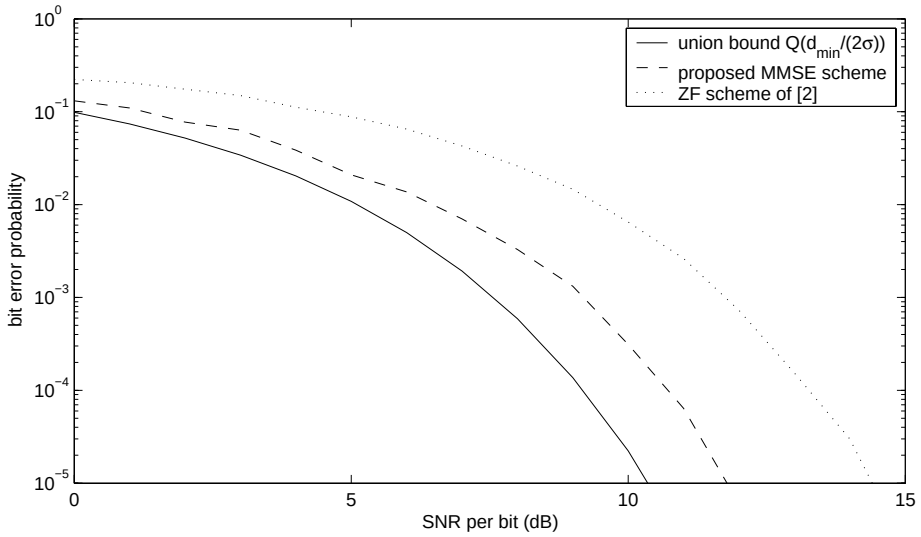

Figure 3.4: Comparison of ZF and MMSE bit error rate.

proposed MMSE equalizer demonstrates approximately a 3 dB performance gain over the ZF scheme of [2], even at high SNR.

Typically ZF equalizers have similar performance to MMSE equalizers in an ISI-dominated regime where the SNR is high. However, this is not the case here

because our proposed structure is fundamentally different in the way we perform the feedforward equalization. In the scheme of [2], the feedfoward equalizer $\boldsymbol{F}$ will always be a square lower triangular Tœplitz matrix, so the $(N-1)$-th chip of each symbol effectively has no feedforward equalization – only a gain. Since our proposed scheme does not impose this structure, it has a better ability to suppress ISI in addition to having less noise enhancement. We note that the equalization parameters were chosen so that the two schemes have equivalent computational complexity.

Chapter 4

Blind Equalization of Energy Efficient Modulations

The previous chapters largely assumed that the communication channel was known, or that sufficient training data was available so that LMS could be used to adaptively determine the equalizer coefficients. The one exception was the decision-directed LMS algorithm, which can be used in the absence of training data. However, decision-directed algorithms are notoriously sensitive to initialization [26]. In this chapter, we demonstrate the unsuitability in using DD-LMS for cold startup of the equalizer. We will highlight some specific examples where DD-LMS fails, and will revisit these examples in the next chapter when we investigate new blind algorithms. We then consider the use of existing stochastic blind algorithms with these modulations, and show that they, too, are unsuitable for use with energy efficient modulations. Finally, we provide a general discussion of blind algorithm development, including the desired properties of blind algorithm cost functions, a methodology for algorithm assessment, and guidelines for selecting cost functions.

4.1 Preliminaries

In this chapter, we focus on the use of stochastic gradient-descent algorithms for use in situations where the channel is unknown and training data is not available

(or is insufficient). There has been a flurry of research activity in the related area of subspace algorithms based on second-order statistics. However, such algorithms are known to suffer from robustness problems [7] and require multiple receive antennas, oversampling, or some other technique to make the effective channel matrix be tall,; consequently, we restrict our attention to stochastic gradient descent-based schemes.

We focus on the scalar equalizer of Chapter 2, and consider blind adaptation of the linear feedforward portion of the equalizer only. Though the performance of the scalar equalizer is inferior to the block equalizer in some situations, the scalar equalizer is simpler since there is only a single filter to adapt rather than a bank of filters. Removing the feedback filter simplifies the system considerably, as well, since we do not need to be concerned with the effects of error propagation[1]. If we find a blind algorithm that succeeds in opening the eye with the scalar equalizer, we could reap the additional benefits of the block equalizer by using the scalar-to-block mapping (3.5)-(3.6), and then continuing adaptation with DD-LMS. The system model is shown in Fig. 4.1. The equations to described the system model

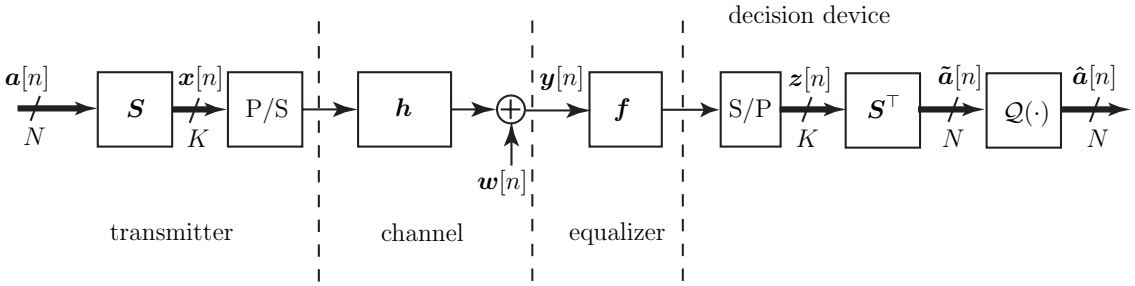

Figure 4.1: System Model for Blind Adaptation

[1]Though we focus on linear equalizers for the remained of the dissertation, Appendix F contains an extension of an algorithm studied in Chapter 5 that includes a decision feedback equalizer.

are identical to those in Chapter 2, but with the removal of the feedback filter, giving

$$\boldsymbol{Y}[n] = \boldsymbol{\mathcal{H}}\boldsymbol{X}[n] + \boldsymbol{W}[n] \tag{4.1}$$

$$\boldsymbol{z}[n] = \boldsymbol{Y}^{\top}[n]\boldsymbol{f} \tag{4.2}$$

$$\tilde{\boldsymbol{a}}[n] = \boldsymbol{S}^{\top}\boldsymbol{z}[n]. \tag{4.3}$$

We recall that $\boldsymbol{X}[n]$ and $\boldsymbol{Y}[n]$ are Hankel matrices containing the transmitted and received waveform chips, respectively. Thus, we are only concerned with blind adaptation of a single filter, $\boldsymbol{f}$.

In blind equalization, we assume that the receiver has no knowledge of the channel taps. We do assume, however, that the receiver has knowledge of the modulation scheme and signal set $\boldsymbol{S}$ in use. Consequently, the receiver must adapt the equalizer based only on the received signal, $\boldsymbol{Y}[n]$.

We note that blind equalizers have several inherent ambiguities:

- **Sign Ambiguity (biorthogonal modulation only):** Consider two channels $\boldsymbol{H}_1$ and $\boldsymbol{H}_2$ where $\boldsymbol{H}_2 = -\boldsymbol{H}_1$. Next, consider a sequence of biorthogonal chips generated at the transmitter, denoted $\boldsymbol{X}_1[n]$, and another sequence $\boldsymbol{X}_2[n]$ constructed as $\boldsymbol{X}_2[n] = -\boldsymbol{X}_1[n]$. If $\boldsymbol{X}_1[n]$ is a valid biorthogonal chip sequence, then so is $\boldsymbol{X}_2[n]$. In the absence of noise, the corresponding received signals are

$$\begin{aligned}
\boldsymbol{Y}_1[n] &= \boldsymbol{H}_1\boldsymbol{X}_1[n] \\
\boldsymbol{Y}_2[n] &= \boldsymbol{H}_2\boldsymbol{X}_2[n] \\
&= (-\boldsymbol{H}_1)(-\boldsymbol{X}_1[n]) \\
&= \boldsymbol{Y}_1[n].
\end{aligned}$$

Clearly, then, two different sequences passing through two different channels can generate the same received signal. Thus, there is no hope that a blind equalizer will be able to recover the sign information when it only has knowledge of $\boldsymbol{Y}[n]$.

- **Whole Symbol Delay Ambiguity:** Consider two chips steams, $\boldsymbol{X}_1[n]$ and $\boldsymbol{X}_2[n]$ where $\boldsymbol{X}_2[n] = \boldsymbol{X}_1[n+\Delta]$ is an advanced version of $\boldsymbol{X}_1[n]$. Next, consider two channels $\boldsymbol{H}_1$ and $\boldsymbol{H}_2$ where $\boldsymbol{H}_2$ is a delayed version of $\boldsymbol{H}_1$, where the delay is $K\Delta$ chips (i.e. Δ symbols). Subsequently, $\boldsymbol{Y}_1[n] = \boldsymbol{Y}_2[n]$, so again two different sequences passing through two different channels can generate the same received signal, thus implying the inability of a blind equalizer to recover the channel delay.

- **Partial Symbol Delay Ambiguity (biorthogonal modulation only):** To construct the whole symbol delay above, we chose the chip delay to be a multiple of K. However, depending on the choice of $\boldsymbol{S}$, some signal sets will exhibit a partial symbol delay ambiguity. Consider, for example, biorthogonal modulation where $\boldsymbol{S}$ is the 2×2 Hadamard matrix,

$$\boldsymbol{S} = \frac{1}{\sqrt{2}} \begin{bmatrix} 1 & 1 \\ 1 & -1 \end{bmatrix}.$$

The possible symbols are then

$$\sqrt{2}\boldsymbol{x}[n] \in \left\{ \begin{bmatrix} 1 \\ 1 \end{bmatrix}, \begin{bmatrix} 1 \\ -1 \end{bmatrix}, \begin{bmatrix} -1 \\ 1 \end{bmatrix}, \begin{bmatrix} -1 \\ -1 \end{bmatrix} \right\}$$

which comprise all possible combinations of ± 1, so that a chip stream originating from this signal set can contain *any* sequence of ± 1. Thus, for any signal originating from this signal set, a 1-chip delay is also a valid biorthogonal signal for the same choice of $\boldsymbol{S}$. For example, the following two sequences

are both valid, where the second is a 1-chip delay of the first and signal boundaries are indicated by |:

$$+1,-1\,\Big|\,+1,+1\,\Big|\,-1,+1\,\Big|\,-1,-1\,\Big|\,-1,+1\,\Big|\,-1,+1\,\Big|\,+1$$
$$+1\,\Big|\,-1,+1\,\Big|\,+1,-1\,\Big|\,+1,-1\,\Big|\,-1,-1\,\Big|\,+1,-1\,\Big|\,+1+1$$

Thus, we see there are several ambiguities which we cannot expect the blind equalizer to recover.

On a related note, we point out the decision device can make two types of errors:

- **Type I error:** This error occurs when the decision device decides that the wrong waveform (i.e. wrong column of $\boldsymbol{S}$) was transmitted.
- **Type II error:** This error occurs when the decision chooses the correct waveform, but chooses the wrong sign. This can only happen with biorthogonal modulation.

Consequently, in a blind scenario, we must accept the situation where the decision device *consistently* makes Type II errors (due to the sign ambiguity). However, such a situation is not serious since it can be overcome through a variety of techniques, such as differential encoding.

4.2 Unsuitability of DD-LMS for Cold Startup

4.2.1 Biorthogonal Modulation

Decision directed adaptive equalizers are notoriously sensitive to initialization [26], and generally require a nearly open eye initialization to ensure a sufficiently low

symbol error rate. An open eye condition is the situation where the decision device makes no errors in the absence of noise. Unfortunately, the open eye regime for energy efficient modulations can be smaller than the open eye regime for traditional BPSK. The open eye condition for BPSK requires the channel coefficients satisfy $|h[n]| > \sum_{m \neq n} |h[m]|$ where $h[n]$ is the dominant tap. The open eye condition for the energy efficient modulations depends on the underlying orthonormal basis vectors $\boldsymbol{S}$, and therefore a simple inequality is not possible. However, we consider several examples.

For the particular choice of parameters $\boldsymbol{S} = \boldsymbol{I}_2$ and $N_h = 3$, the open eye conditions can be found by considering all of the possible channel outputs. For an open eye, one of the following 3 conditions must be satisfied (depending on which tap is the dominant tap):

$$\begin{aligned} & \begin{cases} |h[0]| > 2|h[1]| - h[2]\,\mathrm{sgn(h[0])} \\ |h[0]| > |h[1]| + |h[2]| \end{cases} \\ \text{or} \quad & \begin{cases} |h[1]| > 2|h[0]| + |h[2]| \\ |h[1]| > |h[0]| + 2|h[2]| \end{cases} \\ \text{or} \quad & \begin{cases} |h[2]| > -h[0]\,\mathrm{sgn(h[2])} + 2|\mathrm{h[1]}| \\ |h[2]| > |h[0]| + |h[1]| \end{cases} \end{aligned} \tag{4.4}$$

where sgn is the signum function. A 2-D slice of the open eye region for both BPSK and biorthogonal modulation when $h[0]$ is the dominant tap is compared in Fig. 4.2. As shown, the open eye region for biorthogonal modulation is smaller than that for BPSK. Intuition as to why the open eye regime is smaller in general for biorthogonal modulation comes about by considering that biorthogonal modulation can make both Type I and Type II errors, whereas BPSK can only make Type II errors. In order to prevent both types of errors, the allowable channel

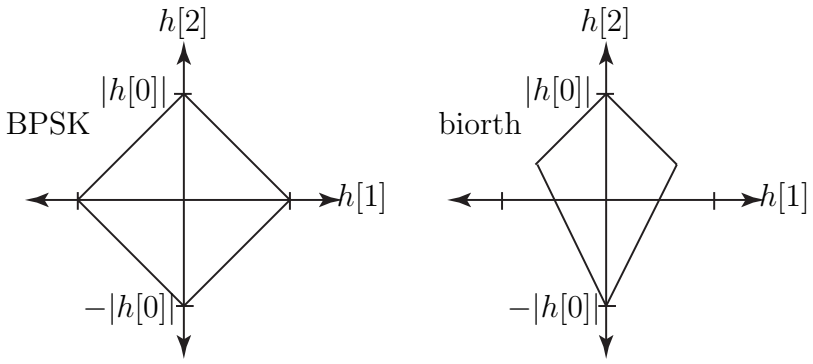

Figure 4.2: Example Open Eye Regions for BPSK and Biorthogonal Modulation

coefficients for an open eye in BOM have to satisfy a greater number of inequalities to ensure that K adjacent chips are relatively ISI-free. Decision directed adaptation is generally not a good choice for cold startup of BPSK equalizers [26], and the situation may only be worse for biorthogonal signals.

To further illustrate the fact that DD-LMS is indeed sensitive to initialization, we consider a specific low-dimensional example which permits an exact expression of the cost in terms of $\boldsymbol{c}$, the combined channel/equalizer coefficients. Recall the DD-LMS update equation from Section 2.5,

$$\boldsymbol{f}_{DD}[n+1] \;=\; \boldsymbol{f}_{DD}[n] - \mu_1 \boldsymbol{Y}[n]\boldsymbol{S}(\tilde{\boldsymbol{a}}[n] - \hat{\boldsymbol{a}}[n]).$$

While the trained LMS algorithm was obtained by taking the instantaneous gradient of the MSE, we note the interesting fact that the cost function

$$J_{DD}(\boldsymbol{f}) = E\left[||\boldsymbol{S}^\top \boldsymbol{z}[n]||_2^2 - 2||\boldsymbol{S}^\top \boldsymbol{z}[n]||_\infty + 1\right] \tag{4.5}$$

has instantaneous gradient that coincides exactly with decision directed LMS when using the Euclidean distance detector.

For our example, we ignore the AWGN, we let $\boldsymbol{S} = \boldsymbol{I}_2$, and we consider only two taps (i.e. $N_c = 2$) so that we can visualize the cost surface. Though this choice

of system parameters may seem too simplistic to be practical, analysis of decision-directed equalizers is particularly difficult due to the presence of discontinuous functions (i.e. the decision device) [26], and this example is only meant to demonstrate that the DD-LMS algorithm has false local minima even in low-dimensional noiseless scenarios.

For this choice of system parameters, the cost (4.5) becomes

$$J_{DD}(\boldsymbol{c}) = -\frac{1}{8}\big(4|c[0]+c[1]| + 4|c[0]-c[1]| + |c[0]+2c[1]| \\ +6|c[0]| + |c[0]-2c[1]|\big) + c[0]^2 + c[1]^2 + 1$$

which is plotted in the combined channel/equalizer space in Fig. 4.3, with the minima indicated by asterisks. Ideally, this cost function would only have minima

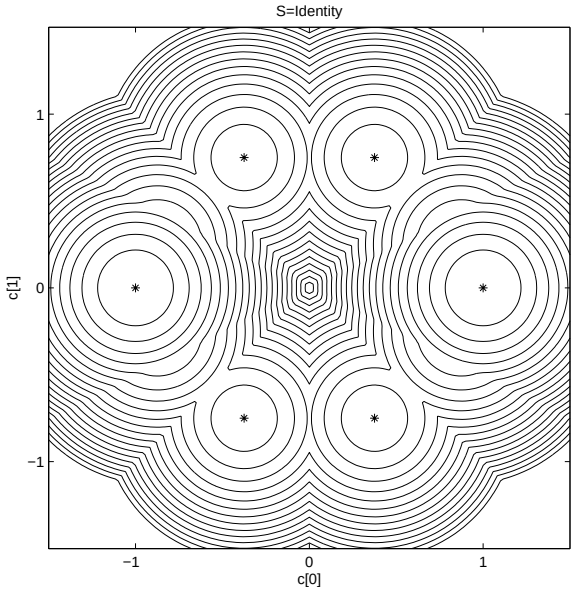

Figure 4.3: Example cost surface for DD-LMS

at single spike solutions; indeed, we note the appearance of local minima at the desired location $\boldsymbol{c} = \pm[1,\, 0]^\top$. However, we also note that there are false minima at $\boldsymbol{c} = \pm[3/8,\, 3/4]^\top$ and $\boldsymbol{c} = \pm[3/8,\, -3/4]^\top$. This verifies our claim that DD-LMS is

sensitive to initialization. As the length of the channel/equalizer space is increased, the number of false local minima of the highly faceted DD-LMS cost surface only grows. This motivates the search for blind methods of equalizer adaptation for biorthogonal modulation other than decision direction.

The ideal blind algorithm would be globally convergent, so that all local minima of the multimodal cost surface achieve the same globally optimized performance cost. If such an ideal algorithm cannot be found, however, we would settle for an algorithm with some false minima so long as the regions of attraction of the desirable local minima were larger than for DD-LMS.

4.2.2 Orthogonal and Transorthogonal Modulation

As we have mentioned, we must accept a sign ambiguity for biorthogonal modulation, and in some sense a simple sign flip is "okay" because the decision device makes consistent Type II errors. Signals from orthogonal and transorthogonal modulation do not exhibit sign ambiguities, and Type II errors have no meaning. Consequently, an uncorrected sign flip causes the decision device for orthogonal and transorthogonal modulation to *always* make (inconsistent) Type I errors.

To see this, consider the example of 3-ary PPM, which arises when $\boldsymbol{S} = \boldsymbol{I}_3$. Let the channel be a simple phase change so that $\boldsymbol{h} = -1$. An example received signal is then

$$\text{transmitted: } \boldsymbol{x}[n] = \begin{bmatrix} 0 \\ 1 \\ 0 \end{bmatrix} \qquad \text{received: } \boldsymbol{y}[n] = \begin{bmatrix} 0 \\ -1 \\ 0 \end{bmatrix}$$

However, if the sign is not corrected, the "choose max" decision device will clearly make a wrong decision, by deciding that either $[1, 0, 0]^\top$ or $[0, 0, 1]^\top$ was sent with

equal probability. Continuing with this 3-ary PPM example, we now consider a channel of length $N_h = 3$. The open-eye region for this case becomes

$$\begin{aligned}
&\begin{cases} h[0] > |h[1] - h[2]| \\ h[0] > h[1] \\ h[0] > h[2] \end{cases} \\
\text{or} \quad &\begin{cases} h[1] > |h[0] - h[2]| \\ h[1] > |h[0]| \\ h[1] > |h[2]| \\ h[1] > h[0] + h[2] \end{cases} \\
\text{or} \quad &\begin{cases} h[2] > |h[0] - h[2]| \\ h[2] > h[0] \\ h[2] > h[1] \end{cases}
\end{aligned} \tag{4.6}$$

As opposed to the open eye region for biorthogonal modulation (4.4), we note that here the dominant tap *must* be positive. Thus, the region is considerably smaller since the eye is always closed when the dominant tap is negative. Since the decision device always makes errors in cases when the dominant tap is negative, decision directed LMS is highly sensitive to initialization when used with orthogonal and biorthogonal modulations.

To verify the poor performance of DD-LMS in the presence of a negative tap, we ran a simulation of the 3-ary PPM setup with a simple phase-change channel where $\boldsymbol{h} = -1$. We set the number of equalizer taps to $N_f = 3$ with the initialization $\boldsymbol{f} = [1, 0, 0]^\top$. Thus, at the initialization, the combined channel/equalizer response is a simple phase-change with no ISI. The desired equalizer setting (resulting in zero errors and zero MSE) is given by $\boldsymbol{f}^* = [-1, 0, 0]^\top$, which inverts the phase change introduced by the channel. We ran the simulation in the absence of noise,

and the equalizer converged to $\boldsymbol{f} = [0.4724, 0.6175, -0.3885]^\top$ as shown in Fig. 4.4. This equalizer setting results in ISI enhancement, and so DD-LMS is quite useless in this case.

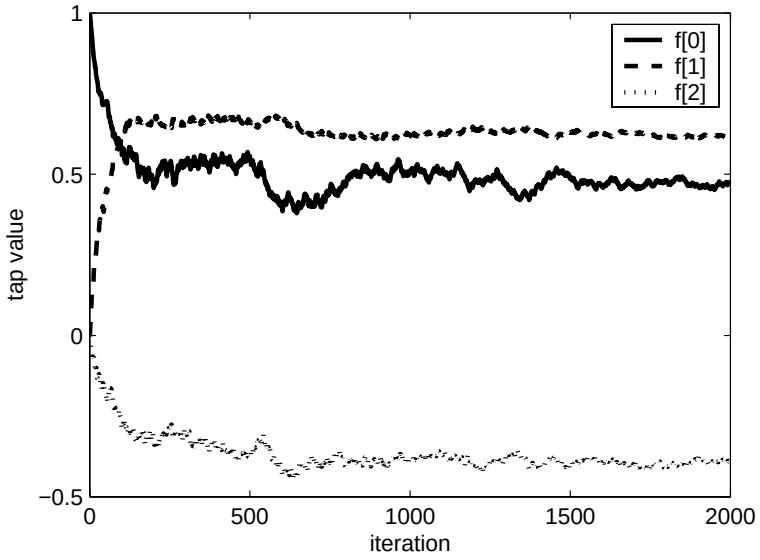

Figure 4.4: Convergence of DD-LMS to False Minima

4.3 Unsuitability in Using Classical Blind Approaches

When faced with the task of designing a blind adaptive equalization algorithm for a new modulation scheme, a natural path is to consider the use of classical approaches to blind equalization. In the realm of stochastic gradient descent-based blind algorithms, two most common algorithms are the constant modulus algorithm (CMA) [13][42] and the Shalvi-Weinstein algorithm (SWA) [33].

As mentioned in Section 1.5, binary biorthogonal and binary transorthogonal modulation reduce to BPSK. Likewise, in biorthogonal modulation when $K = 2$ and $\boldsymbol{S}$ is chosen to be the Hadamard matrix (as was considered when addressing partial symbol delays in Section 4.1), the chips have statistics identical to a BPSK

source. Thus, we can expect the classical blind algorithms to work fine for some very particular choices of K and $\boldsymbol{S}$. However, the classical blind algorithms will not work in general, as we now explain with several examples.

4.3.1 The Constant Modulus Algorithm

The CMA performs gradient descent of the cost

$$J_{CMA}(\boldsymbol{f}) \;=\; E\left[(z^2[Kn-k]-1)^2\right] \tag{4.7}$$

where the underlying random source $x[Kn-k]$ is assumed to be i.i.d. As we have mentioned, the i.i.d. assumption does not hold in general for (bi/trans)orthogonal modulation, and so standard convergence analyses of the CMA are not applicable. However, we overlook this detail for now. The fourth-order cumulant (or kurtosis) of a zero-mean real-valued random process, defined as

$$\mathcal{C}_4(x[Kn-k]) \;\triangleq\; E[x^4[Kn-k]] - 3E[x^2[Kn-k]]^2$$

is a frequently encountered quantity in the analysis of blind algorithms. First, considering a biorthogonal system with $\boldsymbol{S}=\boldsymbol{I}$, we have $\mathcal{C}_4(x[Kn-k]) = 1/K - 3/K^2$, which is leptokurtic (i.e. greater than zero) for $K > 3$. It is well known [18][23] that for leptokurtic sources, the CMA results in ISI enhancement. Thus, due to the non-i.i.d. and leptokurtic nature of the biorthogonal signal, the CMA is not a suitable choice as for blind equalization of biorthogonal signals. Orthogonal and transorthogonal signals, in addition to not satisfying the i.i.d. requirement, have correlation among adjacent chips. Thus, since the CMA suffers from spurious local minima when used with correlated sources [23], the CMA is not suitable for these modulations, either.

4.3.2 The Shalvi-Weinstein Algorithm

The SWA, on the other hand, maximizes the magnitude of the kurtosis of the equalizer output,

$$J_{SWA}(\boldsymbol{f}) \;=\; |\mathcal{C}_4(z[Kn-k])| \tag{4.8}$$

with a unit-norm constraint on the equalizer taps, and is suitable for use on sources that are leptokurtic. Note that the SWA is a constrained algorithm and has the additional requirement that pre-whitening be performed before equalization so that the effective channel is white. The rationale for this criterion (4.8) is based on the fact (see theorem in [33]) that when the equalizer output power equals the power of the source process, the magnitude of the channel/equalizer output kurtosis is less than or equal to the magnitude of the source kurtosis, or $|\mathcal{C}_4(z[Kn-k])| \leq |\mathcal{C}_4(x[Kn-k])|$. Equality occurs when ISI has been eliminated, and so constrained maximization of (4.8) seems like a sensible approach. As is the case with the CMA, however, the standard analysis [33] of the SWA also assumes that the source is i.i.d. Again using biorthogonal modulation for illustration with $\boldsymbol{S} = \boldsymbol{I}$ but $K = 2$, we have source kurtosis $|\mathcal{C}_4(x[Kn-k])| = 1/4$. Up to now all kurtosis values have not depended on a time index due to coincidental choice of system parameters, but in general the kurtosis of a non-i.i.d. random process is time-varying. In the case of a biorthogonal signal, the kurtosis is periodically time-varying and is generally different for each of the K polyphases. Let the combined channel/equalizer response be $\boldsymbol{c} = [1,\ 1]^\top/\sqrt{2}$, giving $z[Kn-k] = (x[Kn-k] + x[Kn-k-1])/\sqrt{2}$ where we have satisfied the condition that the equalizer output

power equals the power of the source process. After some algebra, we then have

$$|\mathcal{C}_4(z[Kn-k])| \;=\; \begin{cases} 1/2 & k=0 \\ 1/8 & k=1 \end{cases},$$

giving $|\mathcal{C}_4(z[Kn-1])| < |\mathcal{C}_4(x[Kn-k])| < |\mathcal{C}_4(z[Kn])|$ which violates the fact upon which the motivation for SWA was based. Thus, the non-i.i.d. nature of the biorthogonal signal renders the SWA unsuitable as a candidate algorithm. Transorthogonal and orthogonal modulation fail for the same reasons – the lack of an i.i.d. source, and the time-varying nature of the kurtosis.

While these two algorithms are both unsuitable for BOM signals, it is worth pointing out that conventional use of both of these algorithms (say, with BPSK) results in global convergence under the assumptions of an infinite length equalizer and the absence of noise, which is a desirable feature of any candidate algorithm.

Furthermore, while these two algorithms are unsuitable in their pure form for use with energy efficient modulations, we will investigate similar algorithms that use the same underlying approach in Chapter 5. These new algorithms may appear quite similar to the conventional CMA and SWA, but are not the same in a substantial, structural sense.

4.4 Desirable Properties of Blind Equalization Algorithms

In the search for blind algorithms that are suitable for use with (bi/trans)orthogonal modulation, it is worthwhile to consider the desirable properties of such algorithms. A first step in algorithm development is the selection of a cost function. Guidelines for selecting such cost functions, as well as a methodology for evaluating cost functions will be addressed in subsequent sections. Here, we simply consider the desirable properties of such cost functions. Along with each property, we review

the related known results of blind equalization algorithms for M-PAM. This comparison is useful because it serves as a historical reference point to help shape our expectations for any potential blind algorithm.

In this list of desired cost function (and resulting algorithm) properties, we note that the items on this list are more-or-less incompatible with one another: satisfaction of one property may preclude the other properties from making sense. However, we have placed the most desirable (if unreasonable) properties at the top of the list. We generally adopt the MSE as the performance metric.

- *Convex cost function whose single minimum occurs at* $\min_{\boldsymbol{f},\Delta} J_{MSE}(\boldsymbol{f},\Delta)$. While this is the holy grail of equalizer algorithm design, it is highly doubtful that such a cost function exists (except perhaps in trivial cases with no noise, unity channel, and single tap equalizer). No such blind algorithm has been found for M-PAM.

- *Multimodal cost function where all local minima of the cost surface achieve the same globally optimized performance cost.* Ideally, the locations of the minima would coincide with (or be near) the MMSE solutions. Blind equalization of M-PAM (and M-QAM) via the CMA has this property in the absence of noise under the following two scenarios:

  - Doubly infinite length equalizer [11]
  - Finite-length fractionally-spaced equalizer with no noise or common subchannel roots[24]

  We note that the multiple minima in CMA correspond to different delays Δ.

- *Multimodal cost function where all local minima yield acceptable performance, though some minima have better performance.* Again, the locations of the

minima would ideally coincide with (or be near) the MMSE solutions. The CMA exhibits this property when used for fractionally-spaced equalization of M-PAM when modest noise is present (and there are no common subchannel roots). For finite-length equalizers in the presence of noise, the MMSE equalizer does not have the same cost at each delay, so it is reasonable to expect the CMA to have different cost at each local minimum (i.e. delay), too. Additionally, we note that the CMA minima do indeed stay near the MMSE solutions [8][48] for moderate noise levels.

- *Multimodal cost function with the presence of spurious local minima that can often be avoided in practice.* While this is certainly the least desired property, it is perhaps the most common situation. False local minima can often be avoided in practice, particularly if they have shallow regions of attraction. Often times, the techniques for avoiding (or escaping) such false minima are rather *ad hoc* and difficult to analyze. Finite-length baud-spaced equalization of M-PAM with CMA has this property, for example, where the spurious local minima arise because of "end effects" when significant tap energy is clustered toward one end of the equalizer [6]. Nevertheless, these spurious local minima have not stopped practitioners from embracing CMA for baud-spaced equalization. Several techniques for avoiding the spurious minima have been proposed, for example the tap-centering technique in [11].

So that our blind algorithm works in the widest range of scenarios, we also desire the algorithm to have some level of robustness to such non-idealities as channel noise, "bad" or peculiar channels impulse responses, and equalizers length effects. Additionally, we desire the algorithm to converge to the desired solutions in a reasonable amount of time.

4.5 Methodology for Assessment of Blind Algorithms

We now describe a general strategy for the value assessment of blind adaptive equalization algorithms based on gradient descent of multimodal cost functions. Blind algorithms of this kind typically rely on some form of property restoral [43], by attempting to recover properties of the original source signal that are altered or destroyed by the communication channel. Thus, a candidate cost function is chosen to penalize deviation from these desired properties. However, there is no guarantee that arbitrary cost functions chosen in this way will exhibit acceptable performance. And while algorithm performance can be verified with simulation to some degree, a purely simulation-based value assessment provides little generalizable knowledge of algorithm behavior.

Analysis of the candidate cost function in the most ideal situations is a typical first step, since any resulting algorithm that performs poorly in the most idealized scenarios would not generally be expected to perform any better in more practical scenarios. Thus, in the early stages of algorithm analysis, it is reasonable to ignore the effects of AWGN. In addition, another reasonable assumption is that the equalizer is sufficiently long so that the desired points in the channel/equalizer space are reachable with arbitrary precision. In most cases, the desired points in the absence of noise amount to single-spike impulse responses, which we have previously labelled the zero-forcing (ZF) solutions. Yet another assumption is that the algorithm step-size is sufficiently small so that the stochastic gradient descent algorithm exhibits mean transient and steady-state behavior very close to that of the exact gradient descent.

Under these ideal assumptions, then, the first stage of the algorithm assessment is concerned with whether the ZF solutions are indeed stationary points of the

candidate cost function. For gradient descent algorithms, this amounts to verifying that the gradient of the cost function with respect to the equalizer coefficients is indeed zero at the ZF solutions. After demonstrating that the ZF solutions are stationary points, the next stage of algorithm assessment is to confirm that these stationary points are locally stable. For unconstrained gradient descent algorithms, this amounts to verifying that the Hessian of the cost function is positive definite at the ZF solutions. For constrained algorithms, the classification of the stationary points can be considerably more involved since it requires perturbation analysis or re-parameterization of the constrained cost function as an unconstrained cost function (see, for example, [30]). At this point in the assessment, any candidate algorithm that does not exhibit local stability around the desired solutions should be modified or discarded.

The next phase of algorithm assessment evaluates the existence of other stationary points, particularly those that are false local minima. Typically, such a search for stationary points of the algorithm is conducted under the assumption of an infinitely long equalizer [11], so that we can invoke the assumption of an invertible relationship between the combined channel/equalizer response and the equalizer coefficients. Unfortunately, identification of all classes of stationary points of arbitrary length is not always tractable. When such intractability persists, we are forced to resort to searching for classes of stationary points that occur as impulse responses with finite time support, i.e. with some finite number of contiguous non-zero taps. Under this approach, we still assume that the equalizer has infinite length, but we set all but a finite number N_c of combined taps in the gradient to be zero; this allows us to work with systems of polynomials with a finite number of terms. One technique that is indispensable in finding the stationary points of

such systems of polynomials is the method of Gröbner bases [4], a powerful device that generalizes Gaussian elimination to polynomial elimination, resulting in the exact location of all stationary points.

We thus start by considering the class of all channel/equalizer combinations with, say, $N_c = 2$ non-zero coefficients. The resulting gradient has only 2 variables, so we can quite easily calculate the location of all stationary points using Gröbner bases, and can then classify them as maxima, minima, or saddle points by examining the eigenvalues of the Hessian (with required re-parameterization in the case of constrained algorithms). Assuming no false minima are found for this low-dimensional example, we proceed by successively increasing the number of non-zero taps in the channel/equalizer combination, and continue categorizing the stationary points. The standard algorithm for computing Gröbner bases is known as Buchberger's Algorithm [4]; the algorithm requires significant computational power even for low-dimensional examples, and at some point N_c will be too large to expect Buchberger's Algorithm to converge in a reasonable amount of time. Thus, once we grow N_c beyond a certain point, we will be forced to use a numerical search for stationary points.

In general, stationary points found in low-dimensional examples will persist into higher dimensions, and additionally, delayed versions obtained by adding zeros to the front of such impulse responses will generally be stationary points, as well. That stationary points found in low-dimensional examples persist into higher dimensions is fairly obvious, since any finite length impulse response can be made into a longer response by simply appending zeros to the *end*. To show that shifts obtained by adding zeros to the *front* of causal impulse responses corresponding to stationary points are also stationary points requires more careful examination of the gradient

of the particular cost function under study. Assume the length N_c impulse response $\boldsymbol{c}^*$ is a stationary point, and that $c^*[n] = 0$ for $n < 0$ or $n \geq N_c$. If it can be shown, for some cost function $J(\boldsymbol{c})$, that a delayed version of the impulse response results in a simple shift of the elements of the gradient vector, i.e. for some N_z,

$$\left.\frac{\partial J(\boldsymbol{c})}{\partial c[n]}\right|_{c[n]=c^*[n]} = \left.\frac{\partial J(\boldsymbol{c})}{\partial c[n+N_z]}\right|_{c[n]=c^*[n-N_z]} \tag{4.9}$$

then indeed shifted versions of stationary points will persist in higher dimensions.

The examination of finite-length channel/equalizer combined responses may not directly lead to a statement about global convergence behavior. However, in lieu of a global convergence proof, the technique can be used to build some confidence that the algorithm exhibits good behavior. If, in the search for stationary points, we observe the appearance of false local minima, we can possibly use their character to propose a fix to the algorithm.

If false local minima are observed, we would like have some idea about their regions of attraction in comparison to other candidate algorithms. One technique for comparing algorithms' regions of attraction is to initialize the algorithms to the ZF solution, and then gradually expand the initializations in a sphere around the ZF solution. The superior algorithm will be the one that succeeds in converging to the ZF solution when the sphere of possible initializations is largest.

After assessing the location and character of algorithm stationary points, the next stage of algorithm assessment is simulation in a practical scenario — on practical channels with AWGN. Further assessment of the candidate algorithm would include the effects of different levels AWGN, the end effects caused by using a finite-length equalizer, and studies of the regions of attraction of false minima.

4.6 Cost Function Selection and Property Restoral

Historically, most gradient descent-based blind equalization algorithms have been designed to restore some property of the original signal that was destroyed by the channel. For example, the CMA was originally developed to restore the constant modulus of such signals [42]. Similarly, the SWA was designed to restore the kurtosis of the source signal. Yet another example is MERRY, which attempts to restore the redundancy of the cyclic prefix in the multicarrier context [27]. Since the notion of property restoral has been used frequently in the development of blind algorithms in other applications, it is worthwhile to consider what features we observe in the energy efficient modulations considered in this dissertation.

In the following list, we use $\mathbf{b}, \mathbf{o}, \mathbf{t}$ to denote properties belonging to biorthogonal, orthogonal, and transorthogonal modulations, respectively:

- $\boldsymbol{x}[n]$ is zero mean (**b,t**)
- $\boldsymbol{U}\boldsymbol{a}[n]$ is zero mean (**o,t**)
- All symbols have equal power (**b,o,t**)*
- Chips are decorrelated when $K = N$ (**b**)
- Chips within a symbol are *not* correlated, but chips from different symbols *are* correlated (**o**)
- Ideal correlator outputs are (possibly negated) canonical unit vectors (**b,o,t**)*

This is certainly not an exhaustive list, and perhaps some properties are more suitable than others to use in a candidate property-restoral algorithm. While most of the properties in this list describe features of the first- and second-order statistics, properties of higher-order statistics could be used in a candidate algorithm, as

well. In fact, most stochastic gradient descent-based blind algorithms (including CMA and SWA) are based on higher order statistics. Consequently, it is likely to be the case that blind equalization algorithms for energy efficient modulations would also involve higher-order statistics. In the next chapter, we will consider two algorithms that make use of the properties indicated by a * above, and due to the construction of the cost function these algorithms will involve higher order statistics.

Chapter 5

Two Blind Equalization Algorithms for Biorthogonal Modulation

In applying the property restoral-based algorithm development methodology from the previous chapter, we had limited success in developing blind stochastic gradient decent algorithms for orthogonal and transorthogonal modulation[1]. Fortunately, we had more success in developing blind equalization algorithms for biorthogonal modulation. In this chapter, we consider the development and analysis of two algorithms for biorthogonal modulation. The first algorithm, called LTBOMB, is CMA-like in spirit, and we show that the zero-forcing solutions are locally stable under ideal conditions. The second algorithm, called TROMBONE, was designed with a SWA-like philosophy in mind, and thus relies on a spectral prewhitener before equalization. We show that the ZF solutions are stationary points of TROMBONE.

5.1 Preliminaries

We continue using the system model from the previous chapter, shown in Fig. 4.1 with corresponding equations (4.1)-(4.3). Throughout this chapter, we assume the modulation is biorthogonal, and in addition we make the simplifying assumption

[1]Several such attempts are provided in Appendix E.

that $K = N$ so that $\boldsymbol{S}$ is square. When $\boldsymbol{S}$ is square and orthogonal, we note that $\boldsymbol{S}^\top \boldsymbol{S} = \boldsymbol{S}\boldsymbol{S}^\top = \boldsymbol{I}$. From the second-order moments in (2.13), we see that by picking $\boldsymbol{S}$ to be square, the chips effectively become decorrelated so that

$$E[\boldsymbol{X}\boldsymbol{X}^\top] \;=\; \boldsymbol{I}. \tag{5.1}$$

As discussed in Section 3.1, the chip-level random process for biorthogonal modulation is in general a cyclostationary process, which results in the relation $E\left[x[n]x[m]\right] = E\left[x[n+Kp]x[m+Kp]\right]$ for all p. In this special situation where the chips are decorrelated, however, the process becomes wide-sense stationary since now $E\left[x[n]x[m]\right] = E\left[x[n+p]x[m+p]\right] = \delta[n-m]$. Consequently, with decorrelated chip statistics and no feedback equalizer, the block (polyphase) equalizer of Chapter 3 provides no advantage over the scalar equalizer of Chapter 2 for biorthogonal modulation since the second-order statistics are the same for each polyphase. In addition, we note that with $K = N$, perfect linear equalization is not possible without resorting to an arbitrarily long equalizer.

Throughout this chapter, we use the abbreviation "BOM" for the special case of biorthogonal modulation when $K = N$.

5.2 The LTBOMB Algorithm

5.2.1 Algorithm Description

Here, we propose the first of two gradient descent-based blind algorithms[2]. Most blind algorithms inherently depend on higher order statistics, and this will be the case for our algorithms. As shown in (5.1), the second order statistics and hence

[2]Portions of this work appeared in [20]

the MMSE equalizer for a BOM signal are independent of $\boldsymbol{S}$. However, the fourth-order statistics of $x[Kn-i]$ will *not* be independent of $\boldsymbol{S}$, and thus we expect the shape of the cost surface of any candidate algorithm to depend on $\boldsymbol{S}$. For now, we will consider the case of general $\boldsymbol{S}$, but will later consider the specific choice $\boldsymbol{S} = \boldsymbol{I}$. This choice of $\boldsymbol{S}$ is of interest because it was also the choice considered in the recent UWB proposal [9].

While the samples of the chip process $x[Kn-i]$ could assume a range of values that are disperse (depending on the choice of $\boldsymbol{S}$), the power of the BOM symbols is a constant — a property that was mentioned in the list in Section 4.6. Thus, as the cost function for the first blind algorithm, termed "LTBOMB" (for **L**inear **T**ransveral equalizer adaptation for **B**i**O**rthogonal **M**odulation, **B**lindly), we choose to penalize the dispersion of the symbol power at the equalizer output,

$$J_{LTB}(\boldsymbol{f}) = E\left[(||\boldsymbol{z}[n]||_2^2 - 1)^2\right]. \tag{5.2}$$

Due to the invariance of the ℓ_2 norm to orthogonal transforms, we could equivalently penalize the dispersion of the correlator output power (i.e. since $||\boldsymbol{S}^\top \boldsymbol{z}[n]||_2 = ||\boldsymbol{z}[n]||_2$). Taking the instantaneous gradient of (5.2) gives the update equation

$$\boldsymbol{f}_{LTB}[n+1] = \boldsymbol{f}_{LTB}[n] - \mu \boldsymbol{Y}[n](||\boldsymbol{z}[n]||_2^2 - 1)\boldsymbol{z}[n].$$

While at first glance this simple cost function seems to ignore a lot (and possible too much) of the structure which is present in the BOM signal, we show that this is not the case and we draw connections to several other blind algorithms. The form of (5.2) looks much like the CMA, and not surprisingly reduces to the CMA when $K = 1$ since the vectors become scalars. However, we note that in general the algorithm is structurally different from CMA, due to the appearance of cross terms upon expansion of the ℓ_2 norm which we will see in (5.3) below.

The LTBOMB cost function shares even more similarity with the Vector CMA [47], though it is distinct in that our algorithm is driven by data that is not i.i.d., and it operates only once every K chips. Because of these two facts, the cost surface and algorithm performance will be quite different from the Vector CMA. Borrowing an idea from [41], and noting that $\boldsymbol{z}[n] = [z[Kn] \dots z[Kn-K+1]]^\top$, we see that the cost function can be expanded as

$$\begin{aligned} J_{LTB}(\boldsymbol{f}) &= (1-K) + \sum_{i=0}^{K-1} E\left[(z^2[Kn-i]-1)^2\right] \\ &\quad + \sum_{i=0}^{K-1} \sum_{j=0, j\neq i}^{K-1} E[z^2[Kn-i]z^2[Kn-j]]. \end{aligned} \tag{5.3}$$

This gives an interesting interpretation since the second term is exactly the CMA cost (4.7) when operating chip-by-chip, while the third term represents a penalty of the cross-correlation of the squared equalizer output. Again, due to the invariance of the ℓ_2 norm to orthogonal transforms, we can equivalently replace $z[Kn-i]$ with the ith correlator output at time n, yielding the interpretation that the third term effectively penalizes the lack of biorthogonality in the signal.

5.2.2 Fourth-Order Cumulant Tensor of Received Signal

As mentioned in Section 4.3, much of the unsuitability in applying classical blind algorithms to BOM stems from the fact that the chip-level random process in a BOM system is not i.i.d. The symbols are i.i.d. however, which motivates an analysis comprised of symbol vectors. Cumulants can be described for a vector random process in an analogous way to those for scalar random processes [5] (see Appendix B for more details). For a vector $\boldsymbol{x}$, the fourth-order cumulant is a super-symmetric fourth-order tensor. From Appendix B, we can express the fourth-order

cumulant tensor for the BOM symbol $\boldsymbol{x}[n]$ in terms of its corresponding chips as

$$\begin{aligned}[\mathcal{C}_4(\boldsymbol{x}[n])]_{i_1,i_2,i_3,i_4} \triangleq\ & E[x[Kn-i_1]x[Kn-i_2]x[Kn-i_3]x[Kn-i_4]] \\ & -E[x[Kn-i_1]x[Kn-i_2]]E[x[Kn-i_3]x[Kn-i_4]] \\ & -E[x[Kn-i_1]x[Kn-i_3]]E[x[Kn-i_2]x[Kn-i_4]] \\ & -E[x[Kn-i_1]x[Kn-i_4]]E[x[Kn-i_3]x[Kn-i_2]].\end{aligned} \tag{5.4}$$

Note that we can drop the dependence on n since the vectors are i.i.d. As with cumulants for scalar random processes, cumulants for vector random processes obey a linearity property [5]. For an i.i.d vector process $\boldsymbol{x}[n]$ with $\boldsymbol{y}[n] = \sum_m \boldsymbol{H}[m]\boldsymbol{x}[n-m]$, we have

$$\begin{aligned}\mathcal{C}_4(\boldsymbol{y}) &= \mathcal{C}_4\left(\sum_m \boldsymbol{H}[m]\boldsymbol{x}[n-m]\right) \\ &= \sum_m \left[\mathcal{C}_4(\boldsymbol{x}) \times_1 \boldsymbol{H}[m] \times_2 \boldsymbol{H}[m] \times_3 \boldsymbol{H}[m] \times_4 \boldsymbol{H}[m]\right]\end{aligned}$$

where the symbol $\times_k$ denotes the k-mode tensor product [5]. Expanding the tensor product and substituting the channel impulse response gives the individual tensor elements

$$\begin{aligned}[\mathcal{C}_4(\boldsymbol{y})]_{i_1,i_2,i_3,i_4} = \sum_{j_1,j_2,j_3,j_4} [\mathcal{C}_4(\boldsymbol{x})]_{j_1,j_2,j_3,j_4} \sum_m & h[Km-i_1+j_1]h[Km-i_2+j_2] \\ & \cdot h[Km-i_3+j_3]h[Km-i_4+j_4].\end{aligned}$$

In Appendix C, we express the fourth-order cumulant tensor of a BOM source sequence explicitly in terms of $\boldsymbol{S}$. These formulas will be used in the behavioral analysis of the following section.

5.2.3 Stability of Zero-Forcing Solutions

To investigate the ZF solutions, we first assume that there is no AWGN, so $\sigma_w^2 = 0$. Recalling that $\boldsymbol{c} \triangleq \boldsymbol{\mathcal{H}}^\top \boldsymbol{f}$ and $E[\boldsymbol{X}\boldsymbol{X}^\top] = \boldsymbol{I}$, we can expand the cost function (5.2)

in terms of cumulants giving

$$\begin{aligned} J_{LTB}(\boldsymbol{f}) &= \sum_{i,j}[\mathcal{C}_4(\boldsymbol{z})]_{i,i,j,j} + 2\sum_{i,j}[\mathcal{C}_2(\boldsymbol{z})]_{i,j}^2 + \left[\left(\sum_i [\mathcal{C}_2(\boldsymbol{z})]_{i,i}\right) - 1\right]^2 \\ &= \sum_{i_1,i_2,i_3,i_4} [\mathcal{C}_4(\boldsymbol{x})]_{i_1,i_2,i_3,i_4} \sum_{j_1,j_2}\sum_p c[Kp - j_1 + i_1] \\ &\qquad \cdot c[Kp - j_1 + i_2]c[Kp - j_2 + i_3]c[Kp - j_2 + i_4] \\ &\quad + \frac{2}{K^2}\sum_{j_1,j_2}\left(\sum_p c[p - j_1]c[p - j_2]\right)^2 + \left[\left(\sum_p c^2[p]\right) - 1\right]^2 \end{aligned} \tag{5.5}$$

where $i_1, i_2, i_3, i_4, j_1, j_2 \in \{0, \ldots, K-1\}$. Taking the derivative of (5.5) gives

$$\frac{1}{4}\frac{\partial J_{LTB}(\boldsymbol{f})}{\partial f[n]} = \sum_m h[m-n]\Lambda[m] \tag{5.6}$$

where

$$\begin{aligned} \Lambda[m] &\triangleq \sum_{i_1,i_2,i_3,i_4} [\mathcal{C}_4(\boldsymbol{x})]_{i_1,i_2,i_3,i_4} \sum_{j_1,j_2}\sum_p \delta[m - Kp + j_1 - i_1]c[Kp - j_1 + i_2] \\ &\qquad \cdot c[Kp - j_2 + i_3]c[Kp - j_2 + i_4] \\ &\quad + \frac{2}{K^2}\sum_{j_1,j_2} c[m + j_1 - j_2]\left(\sum_p c[p - j_1]c[p - j_2]\right) \\ &\quad + c[m]\left[\left(\sum_p c^2[p]\right) - 1\right] \end{aligned} \tag{5.7}$$

and we have used the super-symmetry of the cumulant in the simplification. We can then write the gradient compactly from (5.6) and (5.7) as $\nabla J_{LTB}(\boldsymbol{f}) = 4\boldsymbol{\mathcal{H}}\boldsymbol{\Lambda}$ where $\boldsymbol{\Lambda} = [\Lambda[0], \ldots, \Lambda[N_c - 1]]^\top$. Continuing with the second derivative, we have

$$\frac{1}{4}\frac{\partial^2 J_{LTB}(\boldsymbol{f})}{\partial f[n_1]\partial f[n_2]} = \sum_{m_1,m_2} h[m_1 - n_1]h[m_2 - n_2][\boldsymbol{\Psi}]_{m_1,m_2} \tag{5.8}$$

where

$$
\begin{aligned}
[\boldsymbol{\Psi}]_{m_1,m_2} \triangleq & \sum_{i_1,i_2,i_3,i_4} \left[\mathcal{C}_4\left(\boldsymbol{x}\right)\right]_{i_1,i_2,i_3,i_4} \sum_{j_1,j_2} \sum_{p} \Big[\delta[Kp-j_1+i_1-m_1]c[Kp-j_2+i_4] \\
& \cdot \left(\delta[Kp-j_1+i_2-m_2]c[Kp-j_2+i_3]\right. \\
& \left. +2\delta[Kp-j_2+i_2-m_2]c[Kp-j_1+i_3]\right)\Big] \\
& +\frac{2}{K^2}\sum_{j_1,j_2}\delta[j_1-j_2+m_1-m_2]\left(\sum_{p} c[p-j_1]c[p-j_2]\right) \\
& +\frac{2}{K^2}\sum_{j_1,j_2} c[m_2+j_1-j_2]\left(c[m_1+j_1-j_2]+c[m_1-j_1+j_2]\right) \\
& +2c[m_1]c[m_2]+\delta[m_1-m_2]\left[\left(\sum_{p} c^2[p]\right)-1\right] \qquad (5.9)
\end{aligned}
$$

which allows us to write the Hessian matrix as $4\boldsymbol{\mathcal{H}}\boldsymbol{\Psi}\boldsymbol{\mathcal{H}}^{\top}$.

Before demonstrating that the ZF solutions are minima from these formulas for the first and second derivatives (5.6)-(5.9), we first prove two Lemmas.

Lemma 5.1 (Property of Cumulants of Biorthogonal Signals). *For a random vector process $\boldsymbol{x} \in \mathbb{R}^K$ where the vectors are drawn i.i.d. from a complete biorthogonal set, and some $i_1, i_2 \in \{0,\ldots,K-1\}$,*

$$
\sum_{j=0}^{K-1}\left[\mathcal{C}_4\left(\boldsymbol{x}\right)\right]_{i_1,i_2,j,j} = \begin{cases} -\frac{2}{K^2} & \textit{for } i_1 = i_2 \\ 0 & \textit{otherwise} \end{cases}
$$

Proof. Let the underlying orthogonal basis be described by the columns of the square matrix $\boldsymbol{S}$. From the cumulant definition (5.4) and the decorrelatedness of

the chip statistics we have

$$\begin{aligned}\sum_{j=0}^{K-1}\left[\mathcal{C}_4\left(\boldsymbol{x}\right)\right]_{i_1,i_2,j,j} &= \sum_{j=0}^{K-1}\big(E[x[-i_1]x[-i_2]x^2[-j]] - E[x[-i_1]x[-i_2]]E[x^2[-j]] \\ &\quad -2E[x[-i_1]x[-j]]E[x[-i_2]x[-j]]\big) \\ &= -\left(\frac{2}{K^2}+\frac{1}{K}\right)\delta[i_1-i_2] + \frac{1}{K}\sum_{j,k=0}^{K-1}[\boldsymbol{S}]_{i_1,k}[\boldsymbol{S}]_{i_2,k}[\boldsymbol{S}]_{j,k}^2 \\ &= -\frac{2}{K^2}\delta[i_1-i_2]\end{aligned}$$

where the last line uses the orthonormality of columns of $\boldsymbol{S}$. ∎

Lemma 5.2 (Positive definiteness of block diagonal matrix). *The block diagonal matrix*

$$\boldsymbol{\Psi} = \begin{bmatrix}\boldsymbol{\Psi}_1 & \mathbf{0} & \mathbf{0} \\ \mathbf{0} & \boldsymbol{\Psi}_2 & \mathbf{0} \\ \mathbf{0} & \mathbf{0} & \boldsymbol{\Psi}_3\end{bmatrix}$$

is positive definite if and only if $\boldsymbol{\Psi}_1$, $\boldsymbol{\Psi}_2$, *and* $\boldsymbol{\Psi}_3$ *are positive definite.*

Proof. If $\boldsymbol{\Psi}_1$, $\boldsymbol{\Psi}_2$, and $\boldsymbol{\Psi}_3$ are positive definite, then $\boldsymbol{x}_1^\top\boldsymbol{\Psi}_1\boldsymbol{x}_1 > 0$, $\boldsymbol{x}_2^\top\boldsymbol{\Psi}_2\boldsymbol{x}_2 > 0$, and $\boldsymbol{x}_3^\top\boldsymbol{\Psi}_3\boldsymbol{x}_3 > 0$ for all $\boldsymbol{x}_1, \boldsymbol{x}_2, \boldsymbol{x}_3$. Letting $\boldsymbol{x} \triangleq [\boldsymbol{x}_1^\top\boldsymbol{x}_2^\top\boldsymbol{x}_3^\top]$, we have

$$\begin{aligned}\boldsymbol{x}^\top\boldsymbol{\Psi}\boldsymbol{x} &= \boldsymbol{x}_1^\top\boldsymbol{\Psi}_1\boldsymbol{x}_1 + \boldsymbol{x}_2^\top\boldsymbol{\Psi}_2\boldsymbol{x}_2 + \boldsymbol{x}_3^\top\boldsymbol{\Psi}_3\boldsymbol{x}_3 \qquad (5.10) \\ &> 0\end{aligned}$$

for all $\boldsymbol{x}$, and hence $\boldsymbol{\Psi}$ is positive definite.

To prove the only if, we simply set $\boldsymbol{x}_2$ and $\boldsymbol{x}_3$ to zero in (5.10) to show that positive definiteness of $\boldsymbol{\Psi}$ implies positive definiteness of $\boldsymbol{\Psi}_1$. Similarly, $\boldsymbol{\Psi}_2$ and $\boldsymbol{\Psi}_3$ can each shown to be positive definite. ∎

We define the ZF solutions as those where the combined channel/equalizer response $\boldsymbol{c} = \pm\boldsymbol{e}_{K\Delta}$, though we only consider positive choices due to symmetry arguments. Note that, unlike more traditional equalization problems, our definition of the ZF solutions only includes responses with delays that are a multiple of K. In situations where the delay is not a multiple of K, the decision device will not be operating on the symbol boundary, and these points are not generally stable points of the algorithm. As we will discuss later in Section 5.2.6, the issues of equalization and symbol timing are tightly intertwined.

Theorem 5.1. *The ZF solutions $\boldsymbol{c} = \boldsymbol{e}_{K\Delta}$ are stationary points of the LTBOMB cost function (5.2).*

Proof. Substituting $\boldsymbol{c} = \boldsymbol{e}_{K\Delta}$ into (5.6) gives the gradient at the ZF solutions as

$$\begin{aligned}\frac{1}{4}\frac{\partial J_{LTB}(\boldsymbol{f})}{\partial f[n]}\bigg|_{\boldsymbol{c}=\boldsymbol{e}_{K\Delta}} &= \frac{2}{K}h[K\Delta - n] + \sum_{i_1,i_2,i_3} \left[\mathcal{C}_4\left(\boldsymbol{x}\right)\right]_{i_1,i_2,i_3,i_3} h[K\Delta - i_2 + i_1 - n] \\ &= 0\end{aligned}$$

where the last line follows from Lemma 5.1. ∎

Theorem 5.2. *For any choice of $\boldsymbol{S}$ satisfying positive definiteness of the symmetric matrix $\boldsymbol{\Psi}_2$ defined for $m_1, m_2 \in \{0, \ldots, 2K-2\}$ as*

$$\begin{aligned}[\boldsymbol{\Psi}_2]_{m_1,m_2} &= \frac{2}{K}\sum_{i_1,i_2,i_3,i_4}\sum_{\ell}\Big[\left[\boldsymbol{S}\right]_{i_1,\ell}\left[\boldsymbol{S}\right]_{i_2,\ell}\left[\boldsymbol{S}\right]_{i_3,\ell}\left[\boldsymbol{S}\right]_{i_4,\ell} \\ &\qquad \cdot \delta[K-1+i_1-i_2-m_1]\delta[K-1+i_3-i_4-m_2]\Big] \\ &\quad + \frac{2}{K}\delta[m_1-m_2]\left[1 - \frac{1}{K}\sum_{i_1,i_2}\delta[K-1+i_1-i_2-m_1]\right], \qquad (5.11)\end{aligned}$$

the ZF solutions are minima.

Proof. To show that the ZF solutions are minima, we need to consider the definiteness of the Hessian matrix $4\boldsymbol{\mathcal{H}}\boldsymbol{\Psi}\boldsymbol{\mathcal{H}}^{\top}$. Since $\boldsymbol{\mathcal{H}}$ is full rank, we only need to consider the positive definiteness of $\boldsymbol{\Psi}$. Substituting $\boldsymbol{c} = \boldsymbol{e}_{K\Delta}$ into (5.9) gives

$$\begin{aligned}
[\boldsymbol{\Psi}]_{m_1,m_2}\big|_{\boldsymbol{c}=\boldsymbol{e}_{K\Delta}} &= 2\sum_{i_1,i_2,i_3,i_4}\Big[[\mathcal{C}_4(\boldsymbol{x})]_{i_1,i_2,i_3,i_4} \\
&\qquad\qquad \cdot \delta[K\Delta + i_1 - i_2 - m_1]\delta[K\Delta + i_3 - i_4 - m_2]\Big] \\
&\quad + \frac{2}{K^2}\sum_{j_1,j_2}\delta[K\Delta + j_1 - j_2 - m_1]\delta[K\Delta - j_1 + j_2 - m_2] \\
&\quad + 2\delta[m_1 - m_2]\left[\frac{1}{K} + \delta[K\Delta - m_1]\right] \qquad (5.12)
\end{aligned}$$

Note that $\boldsymbol{\Psi}$ is a symmetric matrix. For either of

$$m_1, m_2 \notin \{K\Delta - K + 1, \ldots, K\Delta, \ldots, K\Delta + K - 1\},$$

the Kronecker delta functions in (5.12) with arguments containing $K\Delta$ go to zero yielding

$$[\boldsymbol{\Psi}]_{m_1,m_2}\big|_{\boldsymbol{c}=\boldsymbol{e}_{K\Delta}} = \frac{2}{K}\delta[m_1 - m_2]. \qquad (5.13)$$

Thus, $\boldsymbol{\Psi}$ has the form used in Lemma 5.2, where $\boldsymbol{\Psi}_1$ is the extraction of $\boldsymbol{\Psi}$ for $m_1, m_2 \in \{0, \ldots, K\Delta - K\}$, $\boldsymbol{\Psi}_2$ is the extraction for $m_1, m_2 \in \{K\Delta - K + 1, \ldots, K\Delta + K - 1\}$, and $\boldsymbol{\Psi}_3$ is the extraction for $m_1, m_2 \in \{K\Delta + K, \ldots, N_c\}$. From (5.13), we see that $\boldsymbol{\Psi}_1$ and $\boldsymbol{\Psi}_3$ are diagonal matrices with positive entries along the diagonal, and hence they are positive definite. From the assumption in the theorem statement (5.12), which was obtained by expanding the cumulant in (5.12) via (C.2), $\boldsymbol{\Psi}_2$ is positive definite. Finally, from Lemma 5.2 $\boldsymbol{\Psi}$ is positive definite, so the Hessian is positive definite and the ZF solutions are minima. ∎

Note that positive definiteness of (5.11) depends exclusively on the underlying signal bases $\boldsymbol{S}$, and can thus be readily tested. For the case $\boldsymbol{S} = \boldsymbol{I}$, we are

guaranteed positive definiteness, which can be seen by substituting (C.1) from Appendix C into (5.11) to give

$$[\boldsymbol{\Psi}_2]_{m_1,m_2} = 2\delta[m_1 - m_2]\left[\delta[K-1-m_1] + \frac{|m_1 - K + 1|}{K^2}\right]$$

which is a diagonal matrix with positive entries, and therefore positive definite. We conjecture that the condition holds for all choices of orthogonal set $\boldsymbol{S}$, as literally millions of numerical tests have not turned up a counterexample.

5.2.4 Example 5.2a: Case of Global Convergence

While we have demonstrated local convergence, we cannot make any claims about the global performance of the algorithm in general. Similar insurmountable difficulties were encountered in the global convergence analysis of the Vector CMA, due to the presence of the cross terms. It is precisely these cross terms, i.e. the last term in (5.3), which complicate analysis of our algorithm.

In light of this difficulty, we resort to considering a low-dimensional numerical example, as part of the strategy outlined in Section 4.5. Again, since this is purely an illustrative example, we operate exclusively in the combined channel/equalizer domain $\boldsymbol{c}$, thereby avoiding end effects that are known to plague finite-length chip-rate blind equalizers. We note that any stationary points that appear in this low-dimensional example will persist into higher dimensions. Furthermore, any of these stationary points delayed by a multiple of K will also be stationary points. This is true since condition (4.9) holds for any shift of K, and can be seen by substituting into (5.7) which is precisely the LTBOMB gradient in the combined channel/equalizer domain.

Letting $\boldsymbol{S} = \boldsymbol{I}_2$ and $N_c = 3$, the stationary points can be found by setting the non-trivial elements of the resulting gradient to zero, resulting in the system of

Table 5.1: LTBOMB Stationary Points for Example 5.2a

$\boldsymbol{c}^\top$	type
$[0, 0, 0]$	maximum
$\pm[1, 0, 0], \pm[0, 0, 1]$	minima
$\pm[0, \sqrt{2/3}, 0]$	saddle points
$\pm[\sqrt{1/3}, 0, -\sqrt{1/3}]$	degenerate saddle points

equations

$$\begin{aligned} c^3[0] + \frac{3}{2}c^2[1]c[0] + \frac{1}{2}c^2[1]c[2] + 2c^2[2]c[0] - c[0] &= 0 \\ c[0]c[1]c[2] + \frac{3}{2}c^2[2]c[1] + \frac{3}{2}c^2[0]c[1] + \frac{3}{2}c^3[1] - c[1] &= 0 \\ c^3[2] + 2c^2[0]c[2] + \frac{1}{2}c^2[1]c[0] + \frac{3}{2}c^2[1]c[2] - c[2] &= 0 \\ c[0]c[2]c[1] &= 0 \end{aligned}$$

Using Gröbner bases, we can solve for the locations of all stationary points exactly, and they have been tabulated in Table 5.1. For this particular example, we see that we can expect global convergence to the desired solution, as minima occur only at the ZF solutions. There are not minima at $\boldsymbol{c} = \pm[0, 1, 0]^\top$, and this point was specifically excluded in our definition of ZF solutions since the delay is not a multiple of K. We also note the appearance of degenerate saddle points. A degenerate saddle point is one where the Hessian is singular, which implies the cost surface is very flat, and the adaptive algorithm will likely suffer convergence speed problems as it passes through this region. In contrast to the DD-LMS example in Section 4.2.1, we observe no undesirable local minima here, and for this low-dimensional example the only minima of LTBOMB cost surface are the

ZF solutions.

5.2.5 Example 5.2b: Case of False Local Minima

While Example 5.2a provides some hope of convergence to solutions with globally optimal performance, we now investigate stationary points that arise in impulse responses with larger lengths of contiguous non-zero taps. Thus, we conducted a (non-exhaustive) numerical search for stationary points with larger channel/equalizer lengths, while maintaining $\boldsymbol{S} = \boldsymbol{I}_2$. The ZF solutions are of course minima in this situation, but we do observe the presence of additional local minima once the number of non-zero taps grows to $N_c \geq 6$.

A six-parameter system of equations was too complex for the use of Gröbner bases in calculating all of the stationary points, but through experimentation we found a class of stationary points with impulse response of the form $\boldsymbol{c} = \pm[0,\ \alpha,\ \beta,\ \gamma,\ -\beta\ , \alpha]^\top$. The symmetry enabled us to reduce the 6-parameter problem to a 3-parameter problem so that we could solve for the exact locations of this class of stationary points using Gröbner bases. The exact expressions for α, β, γ are unwieldy[3] , but their approximate values are $\alpha \approx 0.1741, \beta \approx 0.4718, \gamma \approx 0.5859$. The Hessian was found to have strictly positive eigenvalues $\{0.3968, 1.5300, 2.2798, 2.5430, 2.8521, 8.0000\}$ (which was confirmed through simulation), and hence this impulse response is indeed a false minimum of the algorithm. Again, we note that as N_c is increased beyond 6, this minima persists in higher dimensions. And, any $K = 2$ tap shift of this impulse response is also a local minimum (i.e. any response obtained by adding an even number of zeros to the front). The existence of this false local minimum has larger consequences since

[3]The exact expressions are included in Appendix D.

it suggests that the fractionally-spaced implementations of this algorithm would also have similar local minima.

5.2.6 On the Interaction of Symbol Timing and Equalization

The problems of symbol timing (i.e. finding the symbol boundary within a chip stream) and equalization are tightly related. Equalization algorithms with training data, like LMS, are effectively given the symbol timing information via the training data. Blind algorithms, however, do not have such information at their disposal.

As mentioned in Section 5.2.3, the ZF solutions are those responses that amount to a delay that is a multiple of K. When such a response is attained by the equalizer, symbol timing has effectively been acquired. If these ZF solutions were the only minima of the algorithm, we could rely on the blind algorithm to acquire the symbol timing and perform equalization simultaneously. However, we know this is not the case, as was shown by the false local minima of Example 5.2b.

We conjecture that the false local minima of the algorithm are caused in part by the symbol timing ambiguity. Thus, we suggest a scheme that attempts to simultaneously acquire the symbol timing and avoid the local minima. The rationale for the scheme is based on the fact that, in the combined channel/equalizer domain, any impulse response that is a (desired or undesired) minimum of the algorithm — shifted by K taps — is also a local minimum. Conversely, tap shifts that are *not* a multiple of K are typically *not* stable points of the algorithm.

Thus, we could operate K equalizers in parallel, each being updated once per symbol but operating on a different one of the K polyphases. After each of the equalizers has converged (i.e. once the update term is sufficiently small), we could

select the equalizer with lowest cost by computing a sample average of (5.2). Alternatively, if computational complexity were at a premium but convergence speed was less of a concern, the operation could be done serially with a single equalizer, testing each of the K hypotheses in series. We cannot verify the validity of this scheme, however, without investigating the regions of attraction of the algorithm, which is far beyond the scope of this dissertation. We will, however, show simulations of this scheme in Section 5.4.

5.3 The TROMBONE Algorithm

5.3.1 Algorithm Description

As we have discussed, the two most popular classical blind equalization algorithms are the CMA and the SWA. Since the LTBOMB algorithm draws largely from the spirit of the CMA, a sensible next step is to consider how we might apply the SWA philosophy to equalization of BOM signals.

When the channel has been appropriately equalized, the correlator output $\boldsymbol{S}^\top \boldsymbol{z}[n]$ should be a canonical unit vector (modulo sign). While the previous algorithm dealt exclusively with the ℓ_2 norm of the correlator output, we now consider other norms of the correlator output. In particular, we observe that for any ℓ_p norm, we desire $||\boldsymbol{S}^\top \boldsymbol{z}[n]||_p = 1$. As shown in [15], for any $p < q$ and any vector $\boldsymbol{x}$, we have

$$||\boldsymbol{x}||_p^m \geq ||\boldsymbol{x}||_q^m$$

with equality when $\boldsymbol{x}$ is a canonical unit vector. This fact is the motivation for our next algorithm, termed "TROMBONE" (for **T**he **R**ecovery **O**f $\boldsymbol{M}$-ary

Binary **O**rthogonal signals via p-**N**orm **E**quivalence) and having cost function

$$J_{TRO}(\boldsymbol{f}) \;=\; E\left[||\boldsymbol{S}^{\top}\boldsymbol{z}[n]||_p^m - ||\boldsymbol{S}^{\top}\boldsymbol{z}[n]||_q^m\right] \tag{5.14}$$

First, we note that when the equalizer is operating correctly so that the correlator outputs are "perfect", the cost will be zero as hoped. We also note that the trivial solution has zero cost, so to avoid this solution we need to impose a constraint on the algorithm. Here, we choose to constrain the equalizer output power to be $E[||\boldsymbol{z}[n]||_2^2] = E[||\boldsymbol{x}[n]||_2^2]$, which amounts to $\boldsymbol{c}^{\top}\boldsymbol{c} = 1$ in the absence of noise. While in general we could consider any m, p, q so long as $p < q$, we focus on the case $p = 2$, $m = q = 4$ due to its similarity with the LTBOMB algorithm, and its relative ease of implementation. Expanding the cost in terms of cumulants, the cost becomes

$$\begin{aligned} J_{TRO}(\boldsymbol{f}) \;&=\; E\left[||\boldsymbol{S}^{\top}\boldsymbol{z}[n]||_2^4 - ||\boldsymbol{S}^{\top}\boldsymbol{z}[n]||_4^4\right] \qquad (5.15)\\ &=\; \sum_{\substack{i,j\\ i\neq j}} [\mathcal{C}_4(\boldsymbol{S}^{\top}\boldsymbol{z})]_{i,i,j,j} + 2\sum_{i,j}\left[\mathcal{C}_2(\boldsymbol{S}^{\top}\boldsymbol{z})\right]_{i,j}^2 + \left(\sum_i \left[\mathcal{C}_2(\boldsymbol{S}^{\top}\boldsymbol{z})\right]_{i,i}\right)^2 \\ &\quad -3\sum_i \left[\mathcal{C}_2(\boldsymbol{S}^{\top}\boldsymbol{z})\right]_{i,i}^2 \end{aligned}$$

$$
\begin{aligned}
= & \sum_{i_1,i_2,i_3,i_4} \Bigg[[\mathcal{C}_4(\boldsymbol{x})]_{i_1,i_2,i_3,i_4} \\
& \cdot \sum_{j_1,j_2} \sum_{p} c[Kp+i_1-j_1]c[Kp+i_2-j_1]c[Kp+i_3-j_2]c[Kp+i_4-j_2] \Bigg] \\
& - \sum_{i_1,i_2,i_3,i_4} [\mathcal{C}_4(\boldsymbol{x})]_{i_1,i_2,i_3,i_4} \sum_{j_1,j_2,j_3,j_4} \sum_{k} \Bigg[[\boldsymbol{S}]_{j_1,k}[\boldsymbol{S}]_{j_2,k}[\boldsymbol{S}]_{j_3,k}[\boldsymbol{S}]_{j_4,k} \\
& \sum_{p} c[Kp+i_1-j_1]c[Kp+i_2-j_2]c[Kp+i_3-j_3]c[Kp+i_4-j_4] \Bigg] \\
& - \frac{3}{K^2} \sum_{j} \left[\sum_{p} \sum_{i_1,i_2} [\boldsymbol{S}]_{i_1,j}[\boldsymbol{S}]_{i_2,j} c[p-i_1]c[p-i_2] \right]^2 \\
& + \frac{2}{K^2} \sum_{i_1,i_2} \left[\sum_{p} c[p-i_1]c[p-i_2] \right]^2 + \left(\sum_{p} c^2[p] \right)^2
\end{aligned}
$$

The constraint that we have imposed, i.e. $\boldsymbol{c}^\top \boldsymbol{c} = 1$, is a function of the combined channel/equalizer response. In practice, we do not have knowledge of $\boldsymbol{c}$. However, if we assume spectral pre-whitening has been performed before equalization as in [33], thereby assuming the effective channel is white, the constraint becomes

$$
\boldsymbol{c}^\top \boldsymbol{c} = 1 \implies \boldsymbol{f}^\top \boldsymbol{\mathcal{H}} \boldsymbol{\mathcal{H}}^\top \boldsymbol{f} = \boldsymbol{f}^\top \boldsymbol{f} = 1
$$

so that normalization of the equalizer taps ensures that we will meet the constraint. The instantaneous gradient gives the algorithm update equation with a normalization step as

$$
\begin{aligned}
\boldsymbol{f}'_{TRO}[n+1] &= \boldsymbol{f}_{TRO}[n] - \mu \boldsymbol{Y}[n] \left(\boldsymbol{z}[n]^\top \boldsymbol{z}[n] \boldsymbol{I} - \boldsymbol{S} \mathrm{diag}(\boldsymbol{S}^\top \boldsymbol{z}[n])^2 \boldsymbol{S}^\top \right) \boldsymbol{z}[n] \\
\boldsymbol{f}_{TRO}[n+1] &= \boldsymbol{f}'_{TRO}[n+1] / \sqrt{\boldsymbol{f}'^\top_{TRO}[n+1] \boldsymbol{f}'_{TRO}[n+1]}
\end{aligned}
$$

where $\mathrm{diag}(\boldsymbol{x})$ is the square diagonal matrix having $\boldsymbol{x}$ along its diagonal.

We see this algorithm does appear to have some similarities with the SWA in that we have a constrained cost function, motivated by the fact that $||\boldsymbol{S}^\top \boldsymbol{z}[n]||_4^2 \geq ||\boldsymbol{S}^\top \boldsymbol{z}[n]||_4^4$ with equality when ISI has been eliminated. The algorithm also shares

some similarity with the Shtrom-Fan algorithms [34] in that it involves a difference of two ℓ_p-norms. Beyond this similarity, however, our algorithm is fundamentally different from the Shtrom-Fan algorithms. Our cost function is a function of the difference of two norms of the correlator output data. The Shtrom-Fan cost function, on the other hand, involves the difference of two norms of the combined channel/equalizer response, and relies on properties of scalar cumulants to map the cost function from the combined channel/equalizer space to the equalizer space. Thus, the Shtrom-Fan class of algorithms implicitly requires the data to be i.i.d. at the chip level, which is not the case for BOM.

We will now show that the ZF solutions are stationary points. Taking the derivative of the unconstrained TROMBONE cost function gives

$$\frac{1}{4}\frac{\partial J_{TRO}(\boldsymbol{f})}{\partial f[n]} = \sum_m h[p-n]\Lambda[m]$$

where

$$\begin{aligned}
\Lambda[m] = & \sum_{i_1,i_2,i_3,i_4} [\mathcal{C}_4(\boldsymbol{x})]_{i_1,i_2,i_3,i_4} \sum_{k_1,k_2} \sum_p [\delta[Kp+i_1-k_1-m] \\
& \cdot c[Kp+i_2-k_1]c[Kp+i_3-k_2]c[Kp+i_4-k_2]] \\
& - \sum_{i_1,i_2,i_3,i_4} [\mathcal{C}_4(\boldsymbol{x})]_{i_1,i_2,i_3,i_4} \sum_{k_1,k_2,k_3,k_4} \sum_j \Bigg[[\boldsymbol{S}]_{k_1,j}[\boldsymbol{S}]_{k_2,j}[\boldsymbol{S}]_{k_3,j}[\boldsymbol{S}]_{k_4,j} \\
& \cdot \sum_p \delta[Kp+i_1-k_1-m]c[Kp+i_2-k_2]c[Kp+i_3-k_3]c[Kp+i_4-k_4] \Bigg] \\
& - \frac{3}{K^2} \sum_{i_1,i_2,i_3,i_4} \sum_j [\boldsymbol{S}]_{i_1,j}[\boldsymbol{S}]_{i_2,j}[\boldsymbol{S}]_{i_3,j}[\boldsymbol{S}]_{i_4,j} \sum_p c[m+i_1-i_2]c[p-i_3]c[p-i_4] \\
& + \frac{2}{K^2} \sum_p \sum_{k_1,k_2} c[m+k_1-k_2]c[p-k_1]c[p-k_2] + c[m] \left(\sum_p c^2[p] \right)
\end{aligned}$$

Theorem 5.3. *The ZF solutions $\boldsymbol{c} = \boldsymbol{e}_{K\Delta}$ are stationary points of the TROMBONE cost function (5.15).*

Proof. First, note that $\boldsymbol{c} = \boldsymbol{e}_{K\Delta}$ satisfies the unit-norm constraint. We have

$$\begin{aligned}\Lambda[p] &= -\sum_{i_1,i_2,i_3,i_4} \left[\mathcal{C}_4\left(\boldsymbol{x}\right)\right]_{i_1,i_2,i_3,i_4} \sum_{j,k} [\boldsymbol{S}]_{k,j}[\boldsymbol{S}]_{i_2,j}[\boldsymbol{S}]_{i_3,j}[\boldsymbol{S}]_{i_4,j}\delta[K\Delta + i_1 - k - p] \\ &\quad + \left(1 - \frac{3}{K}\right)\delta[K\Delta - p] \\ &= 0\end{aligned}$$

where we substituted (C.2) in Appendix C for the cumulant tensor. ∎

We could have equivalently used the method of Lagrange multipliers, but since the ZF solutions are stationary points and simultaneously satisfy the unit-norm constraint, the Lagrange multiplier is zero. From our observations through simulation, we believe the stationary points at the ZF solutions are locally stable, as we have tested this claim on thousands of pre-whitened channels. Simple examination of the Hessian eigenvalues of constrained algorithms does not allow us to generically classify these stationary points as minima; we would need to resort to perturbation analysis or re-parameterization of the cost function as we will now show in a low dimensional example.

5.3.2 Example 5.3a: Stationary Points in Low Dimensions

As we did in Example 5.2a for LTBOMB, we now classify all the stationary points for the same numerical example. Again working in the combined channel/equalizer domain $\boldsymbol{c}$, we let $\boldsymbol{S} = \boldsymbol{I}_2$ and $N_c = 3$. Because the unit norm tap constraint is difficult to apply in the $\boldsymbol{c}$ domain, we need a transform to re-parameterize the cost function in a coordinate system that permits us to easily apply the constraint. We can re-parameterize the function of $\boldsymbol{c}$ in polar coordinates, having $N_c - 1$ rotation angles $\{\theta_0, \ldots, \theta_{N_c-2}\}$ and one radius r. One possibility [30] for parameterizing $\boldsymbol{c}$

Table 5.2: TROMBONE Stationary Points for Example 5.3a

$\boldsymbol{c}^\top$	type
$\pm[1,0,0], \pm[0,0,1]$	minima
$\pm[\sqrt{1/2},\ 0,\ -\sqrt{1/2}], \pm[\sqrt{1/2},\ 0,\ \sqrt{1/2}]$	saddle points
$\pm[0,\ 1,\ 0]$	degenerate saddle pts

in polar form is to choose

$$c[n] \ = \ \begin{cases} r\sin(\theta_n)\prod_{j=0}^{n-1}\cos(\theta_j) & \text{for } 0 \le n \le N_c-2 \\ r\cos(\theta_{N_c-1})\prod_{j=0}^{N_c-2}\cos(\theta_j) & \text{for } n = N_c-1 \end{cases} \tag{5.16}$$

so that by fixing $r = 1$, any arbitrary unit-norm $\boldsymbol{c}$ may be reached by appropriate choice of rotation angles[4].

Substituting (5.16) into the TROMBONE cost function with $\boldsymbol{S} = \boldsymbol{I}_2$, setting the gradient to zero, and zeroing all but $N_c = 3$ taps results in a system of equations in two parameters, θ_0 and θ_1. As before, we can solve for the locations of all stationary points exactly, and they have been tabulated in Table 5.2. The results here for the TROMBONE algorithm are very similar to those for the LTBOMB algorithm. We again see that we can expect global convergence to the desired solution, as minima occur only at the ZF solutions. Furthermore, we again note the appearance of degenerate saddle points, though they are in a slightly different location.

[4]For any $\boldsymbol{c}$, the "essential uniqueness" of the rotation angles for this transformation (5.16) is claimed in [30]. Presumably, the term "essential uniqueness" is used to exclude a few special non-unique cases such as $\boldsymbol{c} = [1,0,\ldots,0]^\top$, which can be reached for $\theta_0 = \pi/2$ and *any* θ_n for $n \ge 1$.

5.3.3 Example 5.3b: False Minima of TROMBONE

As was done for the LTBOMB in Section 5.2.5, we conducted a (non-exhaustive) numerical search for stationary points of the TROMBONE algorithm. Again, choosing $\boldsymbol{S} = \boldsymbol{I}_2$, we found that indeed, at least for this example, the ZF solutions are minima of the algorithm. In addition, we found false local minima with impulse response $\boldsymbol{c} = \pm[0,\ 0.2973,\ 0.5425,\ 0.4844,\ -0.5425,\ 0.2973]^\top$ which again have the form $\boldsymbol{c} = \pm[0,\ \alpha,\ \beta,\ \gamma,\ -\beta\ ,\alpha]^\top$ and also appear every 2-tap shift. This impulse response is very similar to the false minimum for LTBOMB, and so we see that both of these blind algorithms have an inherent problem. This is peculiar since, at least on the surface, the two cost functions attempt to restore different properties of the BOM signal. The fact that two blind algorithms, both designed with different criteria in mind, suffer from very similar spurious local minima raises questions about the existence of an algorithm exhibiting global convergence. Again, we conjecture that these false minima arise in part due to the symbol timing ambiguity. Use of the parallel equalizer scheme described in Section 5.2.6 may help circumvent this issue.

5.4 Numerical Examples

5.4.1 Visualizing the LTBOMB Cost Surface

We once again we consider the noiseless case with $\boldsymbol{S} = \boldsymbol{I}_2$ and $N_c = 2$, and we plot a 2-D slice[5] of the cost surface contours. The cost surface is shown in Fig. 5.1, where we observe the presence of a maximum at the origin and only 2 minima,

[5]While in general, stationary points of low-dimensional slices may change their character in higher dimensions, those shown here do not.

those at the ZF solution $\boldsymbol{c} = \pm[1, 0]^\top$. As expected minima do not also occur at $\boldsymbol{c} = \pm[0, 1]^\top$, but instead there are saddle points in that region. The fact that these are not minima implies that the proposed algorithm can acquire the symbol timing since, as hoped, minima only occur for delays that are a multiple of K. We refer the reader back to Fig. 4.3, where the cost surface for DD-LMS with the same system parameters exhibited false local minima.

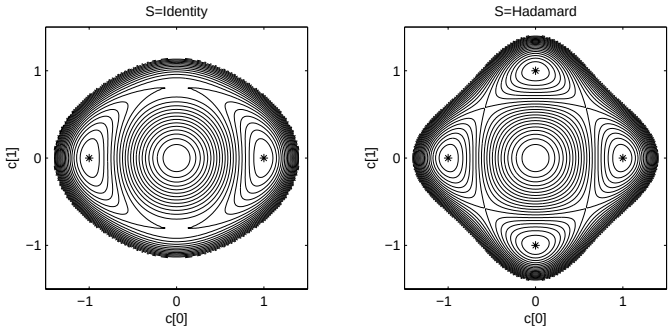

Figure 5.1: LTBOMB Cost Surface for Different Choices of $\boldsymbol{S}$

Since the cost function depends on the cumulants of the underlying signal basis $\boldsymbol{S}$, we expect the cost surface to look different for different choices of $\boldsymbol{S}$. If we change the underlying orthogonal basis so that $\boldsymbol{S}$ is the 2×2 Hadamard matrix, we arrive at the cost surface also shown in Fig. 5.1. In addition to the maximum at the origin and the minima at the ZF solutions, we observe that minima appear at $\boldsymbol{c} = \pm[0, 1]^\top$, which corresponds to a delay that is not a multiple of K. Note that for this choice of $\boldsymbol{S}$, the chip statistics are identical to BPSK since the symbols become $\pm[1, 1]/\sqrt{2}, \pm[1, -1]/\sqrt{2}$. Thus, when $\boldsymbol{S}$ is chosen to be the Hadamard matrix, the algorithm has no hope of recovering the symbol timing. Regardless, we emphasize that all choices of $\boldsymbol{S}$ that cause $\boldsymbol{\Psi}_2$ in (5.11) to be positive definite will exhibit local convergence to ZF solutions as proven in Section 5.2.3.

5.4.2 Visualizing the TROMBONE Cost Surface

Again considering the noiseless case with $\boldsymbol{S} = \boldsymbol{I}_2$ and $N_c = 2$, we have plotted the unconstrained TROMBONE cost surface in Fig. 5.2. The unit norm constraint will force the algorithm to stay on contour indicated by the dotted circle. For the case of $\boldsymbol{S} = \boldsymbol{I}$, the cost surface is a single trough with a bulb at the origin, and the cost is zero along the $c[0]$ axis. For the case of the Hadamard matrix there are two troughs, with zero cost along both axes.

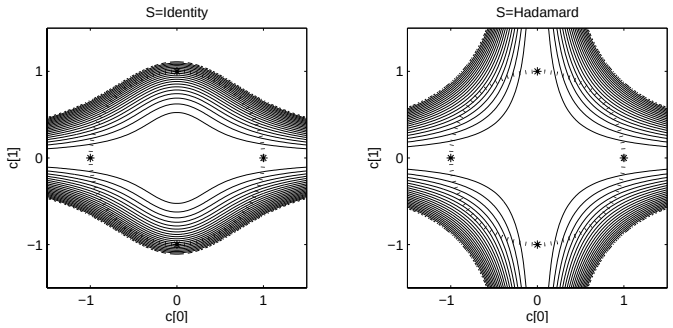

Figure 5.2: Unconstrained TROMBONE Cost Surface for Different Choices of $\boldsymbol{S}$

Identifying the stationary points from the unconstrained cost, however, is not easy. Thus, similar to what was done in Section 5.3.2, we transform the 2-parameter cost plot into polar coordinates with a single rotation angle. Looking at the cost function in polar coordinates, where the angle $\theta = \tan^{-1}(c[1]/c[0])$, we can more easily see the stationary points as shown in Fig. 5.3. We see that both examples result in minima at the ZF solutions, as well as minima at $\boldsymbol{c} = \pm[0, 1]^\top$, though this latter minimum is quite shallow for the case of $\boldsymbol{S} = \boldsymbol{I}$.

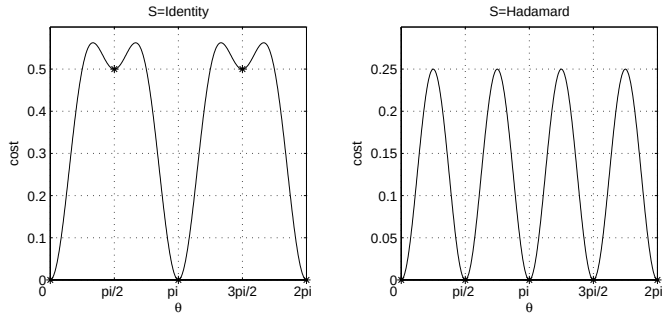

Figure 5.3: Polar Representation of TROMBONE Cost Surface

5.4.3 Simulation Near Zero-Forcing Solutions

To provide verification that our analysis of the local behavior of these algorithms is valid, we consider a simulation where we initialize the algorithms in a ball around a ZF solution. We operate in a noiseless scenario, a channel with impulse response $\boldsymbol{h} = [-0.4, 0.84, 0.336, 0.1344, 0.0538, 0.0215]^\top$, and we have chosen $N_f = 30$ equalizer taps. As before, we choose the signal bases $\boldsymbol{S} = \boldsymbol{I}_2$. The equalizer corresponding to the ZF solution at the chosen delay of $\Delta = 3$ has approximate impulse response

$$\begin{aligned}\boldsymbol{f}_{ZF} \;\approx\; & [0.009, 0.022, 0.054, 0.134, 0.336, 0.840, \\ & -0.399, 0.002, 0.003, 0.005, 0.006, -0.003, 0, \ldots, 0]^\top.\end{aligned}$$

Note that the channel response is approximately white (i.e. $\boldsymbol{\mathcal{H}}\boldsymbol{\mathcal{H}}^\top \approx \boldsymbol{I}$), and the corresponding ZF equalizer satisfies $\boldsymbol{f}_{ZF}^\top \boldsymbol{f}_{ZF} = 1$.

As an initialization, we chose 1,000 points uniformly distributed in a ball around the ZF solution, and we observed the ability of the algorithms to converge to a ZF solution as the radius of the ball is increased. We ran the algorithms for 10,000 symbols at each of the 1,000 initializations, and declared the algorithm to have converged if the mean-squared error was less than 10^{-3}. As shown in Fig. 5.4,

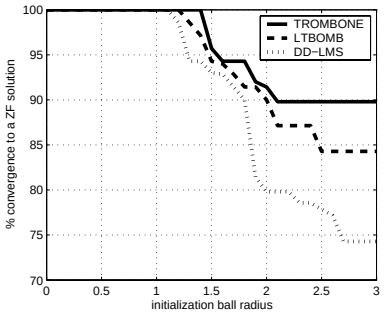

Figure 5.4: Convergence percentage vs. initialization distance from ZF solution

all of the algorithms converge to the ZF solution when the size of the ball of initializations around the ZF solution is less than 1, thus verifying our analysis of local convergence. For larger radii beyond 1, which we can hardly consider to be "local" to the ZF solutions, we see that all algorithms still converge with a fairly high percentage, though possibly to a ZF solution corresponding to some other delay. Furthermore, the blind algorithms both outperform DD-LMS. The curves are all monotone non-increasing, albeit with some sudden drops due to the nonlinear nature of the cost surfaces, and for very large radii we note that the convergence percentages eventually reach a constant value. This is because, beyond a sufficiently large initialization ball radius, there is no notion of locality; the ball grows to encompass the entire space, and so increasing the ball radius further has no effect on convergence percentage.

We note that the lack of a good adaptive algorithm for pre-whitening and the added complexity of pre-whitening suggests the practical superiority of LTBOMB over TROMBONE.

5.4.4 Simulation of a Practical Situation

Continuing with the strategy for algorithm assessment outlined in Section 4.5, we now consider the use of LTBOMB in a practical channel, which serves to justify our claims of local convergence, as well as the superior performance of our algorithm over decision-directed LMS. We focus on LTBOMB here because, as mentioned previously, TROMBONE requires a pre-whitening filter and may not be as useful in practice. It should be noted that the analysis up to now has ignored the effects of noise and has largely considered the cost surface in the combined channel/equalizer space, so these simulations will also provide some faith that our algorithm performs well in the presence of real channels with AWGN. As a channel model, we choose one based on the Saleh-Valenzuela [31] model of an indoor channel. The IEEE 802.153a committee has constructed a set of such channels [10] based on this model, and we have selected to use their channel model CM3 which models a non-line of sight indoor environment over distances of 4-10 meters. To convert the channels to a baseband equivalent tapped-delay line channel, we chose a carrier frequency of 3 GHz and a symbol period of 10 ns, and performed low-pass filtering using a raised-cosine filter with a rolloff factor of 0.5. We then zeroed any leading or trailing taps with energy less than 20 dB below the peak, which resulted in a set of baseband equivalent channels with lengths ranging from $4 \leq N_h \leq 13$, with the average channel length being 7.8 taps. Note that a large number of these channels were non-minimum phase, and often had roots near the unit circle. Furthermore, these channels were most definitely not white.

For the BOM source signal, we chose $\boldsymbol{S} = \boldsymbol{I}_2$. Furthermore, the SNR was set at 8 dB, the equalizer had length $N_f = 30$, and we used a centered double spike initialization. While an analysis of initialization strategies and regions of

Table 5.3: Simulation Results

Algorithm	percent converged to MMSE (single eq.)	percent converged to MMSE (dual eq.)
DD-LMS	64.3%	94.3%
LTBOMB	88.4%	99.2%

convergence is beyond the scope of this dissertation, we observed that for a BOM system with K chips per symbol and $\boldsymbol{S} = \boldsymbol{I}$, a K-spike initialization seemed to improve convergence over a single-spike initialization.

After generating 1,000 channel realizations, we ran LTBOMB on each channel, as well as DD-LMS. An equalizer was declared to have converged near the MMSE solution if its MSE was within 1 dB of the MSE of the nearest MMSE solution.

In addition, we considered 2 equalizer setups: one with just a single equalizer, and another setup with two equalizers operating in parallel as described in Section 5.2.6. In the setup with parallel equalizers, the equalizer with lower sample average cost was selected upon convergence, and compared with the nearest MMSE solution. The simulation results are shown in Table 5.3. We see that the LTBOMB algorithm does quite well, consistently beating the decision-directed algorithm. In addition, we note that the use of 2 parallel equalizers does buy us some improvement in convergence, with the LTBOMB converging nearly always. The decision-directed algorithm, too, sees a benefit from the use of 2 parallel equalizers. As a test, we also ran the TROMBONE algorithm without the required pre-whitening filter; unsurprisingly, it only converged 24.3% of the time with a single equalizer, and 36.7% in the dual equalizer setup. With a perfect pre-whitener in place, the

TROMBONE algorithm performance was on par with LTBOMB, converging 90.2% of the time with a single equalizer, and 99.1% with the dual equalizer. Again, we stress that LTBOMB may be more useful in practice due to the lack of need for a blind pre-whitener.

It is well known [29], at least for the AWGN channel, that increasing the constellation size in BOM lowers the bit-error rate at the expense of the data rate. Intuition would suggest a similar effect in ISI channels, which we have observed to be the case. Thus, for larger values of K, we can expect the decision device to make fewer errors, thereby improving the performance of decision-directed LMS. The performance of the blind algorithms will not benefit from an increase in K since they do not rely on correct decisions.

Chapter 6

Conclusion

In this chapter, we present a summary of results and a listing of some immediate open issues relating to equalization of energy efficient modulations.

6.1 Summary of Results

While energy efficient modulations have existed for decades, they have only recently been considered for use in ISI channels. In this dissertation, we have conducted the first comprehensive exploration of equalization for such modulations. We began by considering the use of a traditional DFE, and derived the MMSE equalizer setting for orthogonal, biorthogonal, and transorthogonal modulations. By exploiting properties of orthogonal signals, we were able redefine the MSE in such a way that perfect linear equalization is possible in some situations with a critically-sampled finite-length equalizer.

Next, we considered an improvement upon the scalar DFE, by extending the equalizer to be a multirate filterbank. This block structure brought about several benefits by exploiting properties unique to the multipulse energy efficient modulations under study. In particular, the use of a block equalizer further enlarged the class of signals for which perfect feedforward equalization is possible, it resulted in a reduction in computational complexity, and it reduced the effective delay through the feedback equalizer. We derived the MMSE equalizer setting for the

block structure, and presented the equations for adaptation of the equalizer taps via LMS and decision-directed LMS.

The second half of the thesis focused on blind adaptation of the equalizer. We demonstrated the shortcomings of decision-directed LMS as an algorithm for cold startup of the equalizer, thus pointing to the need for blind algorithms beyond decision-direction. As a first step, we considered the use of the two most popular blind algorithms — the Constant Modulus Algorithm and the Shalvi-Weinstein Algorithm — and showed that they were unsuitable for use with these modulations, largely due to their reliance on i.i.d. source statistics. With the lack of a suitable blind algorithm, we proceeded with a general discussion of blind algorithm development, including the desired properties of blind algorithm cost functions, a methodology for algorithm assessment, and guidelines for selecting cost functions.

Next, we presented the first two blind algorithms for biorthogonal modulation, including a discussion of their characteristics and convergence. The first algorithm, called LTBOMB, was CMA-like in spirit, and we showed that the zero-forcing solutions are locally stable under ideal conditions. The second algorithm, called TROMBONE, was designed with a SWA-like philosophy in mind, and thus relied on a spectral prewhitener before equalization. We showed that the ZF solutions are stationary points of TROMBONE, and included simulations demonstrating the performance of the two blind algorithms. Both algorithms performed quite well, handily outperforming DD-LMS in their ability, for arbitrary initialization, to converge near an MMSE solution. However, we did note the appearance of false local minima for both algorithms. Under the belief that the false minima were a result of the symbol timing ambiguity, we suggested a technique to minimize the likelihood of encountering these false minima, which resulted in an improvement

in our simulated results.

6.2 Open Issues

We now consider a list of open issues and possible future directions.

- **Feedback of Tentative Decisions:** As described in Section 2.1, the decision device needs to wait until all K chips of a symbol have been received before making a decision, thus introducing a $N-1$ chip delay in the feedback path. It may be possible to feed tentative chip decisions back through the filter, replacing them with more reliable values once the entire symbol has been received and estimated. The motivation for this is a reduced feedback delay; however, it is not clear how much this technique would help, in light of the fact that such chip decisions could be very unreliable. In addition, it is not clear what form such a tentative chip decision device should take.

- **Blind Algorithms for Orthogonal and Transorthogonal Modulations:** Though we provided several blind algorithms for equalization of orthogonal and transorthogonal modulations in Appendix E, preliminary simulations have not shown these algorithms to have desirable convergence behavior, particularly when compared with DD-LMS. Thus, there is still the lack of a blind algorithm that outperforms decision-direction for these modulations.

- **Globally Convergent Blind Algorithm for Biorthogonal Modulation:** The two blind algorithms that we proposed for biorthogonal modulation in Chapter 5 both performed quite well, but did show the presence of false local minima (which persist in infinite length equalizers). Ideally, we seek a blind algorithm that shares similar convergence behavior to that of the

CMA for M-PAM, i.e. global convergence in the absence of noise (with either a fractionally-spaced or infinite length equalizer) as described in Section 4.4.

- **Incorporation of Symbol Timing Knowledge into Blind Equalization Algorithm:** We believe that a successful blind algorithm for these energy efficient modulations will need to address the issue of symbol timing. Alas, in the presence of ISI, the location of the symbol boundary is not clear, which presents a bit of a chicken-and-egg problem. While ideally a potential blind algorithm would acquire symbol timing blindly and estimate the equalizer taps, this may be unreasonable. Thus, future directions may consider the incorporation of symbol timing knowledge into the equalization algorithm.

- **An Adaptive Prewhitener:** The TROMBONE algorithm relies on having a prewhitened signal at the input to the equalizer. However, an adaptive prewhitener has not been proposed for use with these algorithms. While prewhitening could be accomplished via eigen-decomposition of estimated received autocorrelation matrices, such a technique is less attractive than a completely adaptive solution. Thus, future work could investigate the development of an adaptive prewhitener, and could also examine the sensitivity of the TROMBONE algorithm to an imperfectly whitened input signal.

- **Proof that condition (5.11) is met for all $\boldsymbol{S}$:** We conjectured that (5.11) is satisfied for all $\boldsymbol{S}$. However, we have not yet found a proof of this. While millions of numerical examples have not turned up a counterexample, a proof of this conjecture is desired.

- **Investigation of Regions of Attraction of LTBOMB and TROMBONE:** Realizing that both the LTBOMB and TROMBONE algorithms exhibit false local minima, it would be quite useful to have some ideal of the regions of attraction of these algorithms.

Appendix A

Correlation Matrices for Scalar MMSE DFE

Here, we address calculation of the correlation matrices $\boldsymbol{R}_{xx}$, $\boldsymbol{R}_{x\hat{a}}$, $\boldsymbol{R}_{\hat{a}\hat{a}}$, and $\boldsymbol{R}_{ww}$ used in the scalar MMSE DFE design equations. Note that these expressions only apply to the scalar equalizer.

A.1 Biorthogonal Modulation

To calculate $\boldsymbol{R}_{xx}$, we note that symbols in $\boldsymbol{X}[n]$ appear in bands along skew diagonals, and we partition this matrix into square blocks $\tilde{\boldsymbol{X}}[n] \in \mathbb{R}^{K\times K}$ where $[\tilde{\boldsymbol{X}}[n]]_{i,j} = x[Kn - i - j]$ and

$$\boldsymbol{X}[n] = \begin{bmatrix} \\ \tilde{\boldsymbol{X}}[n] \\ \\ \\ \tilde{\boldsymbol{X}}[n-1] \\ \\ \\ \cdots \\ \\ \\ \end{bmatrix}$$

where the enclosed dotted regions indicate chips from the same symbol. Note that each block $\tilde{\boldsymbol{X}}[n]$ contains chips from the nth and $(n-1)$th symbol, i.e. $\boldsymbol{x}[n]$ and $\boldsymbol{x}[n-1]$. Due to lack of a compact closed-form expression for $E[\boldsymbol{X}[n]\boldsymbol{S}\boldsymbol{S}^\top\boldsymbol{X}[n]^\top]$, we specify the constituent blocks of the matrix

$$E[\boldsymbol{X}[n]\boldsymbol{S}\boldsymbol{S}^\top\boldsymbol{X}[n]^\top] \;=\; \begin{bmatrix} E[\tilde{\boldsymbol{X}}[n]\boldsymbol{S}\boldsymbol{S}^\top\tilde{\boldsymbol{X}}[n]^\top] & E[\tilde{\boldsymbol{X}}[n]\boldsymbol{S}\boldsymbol{S}^\top\tilde{\boldsymbol{X}}[n-1]^\top] & \cdots \\ E[\tilde{\boldsymbol{X}}[n-1]\boldsymbol{S}\boldsymbol{S}^\top\tilde{\boldsymbol{X}}[n]^\top] & E[\tilde{\boldsymbol{X}}[n-1]\boldsymbol{S}\boldsymbol{S}^\top\tilde{\boldsymbol{X}}[n-1]^\top] & \\ \vdots & & \ddots \end{bmatrix}$$

by calculating $E[\tilde{\boldsymbol{X}}[n]\boldsymbol{S}\boldsymbol{S}^\top\tilde{\boldsymbol{X}}[m]^\top]$. The i,jth entry of $E[\tilde{\boldsymbol{X}}[n]\boldsymbol{S}\boldsymbol{S}^\top\tilde{\boldsymbol{X}}[m]^\top]$ can be calculated by expanding the matrix products, resulting in

$$\begin{aligned}
&\left[E[\tilde{\boldsymbol{X}}[n]\boldsymbol{S}\boldsymbol{S}^\top\tilde{\boldsymbol{X}}[m]^\top]\right]_{i,j} \\
&\quad= \sum_{k_1,k_2=0}^{K-1} E\left[[\tilde{\boldsymbol{X}}[n]]_{i,k_1}[\tilde{\boldsymbol{X}}[m]]_{j,k_2}\right][\boldsymbol{S}\boldsymbol{S}^\top]_{k_1,k_2} \\
&\quad= \sum_{k_1=i}^{K-1}\sum_{k_2=j}^{K-1}\left[E[\boldsymbol{x}[n]\boldsymbol{x}^\top[m]]\right]_{k_1,k_2}[\boldsymbol{S}\boldsymbol{S}^\top]_{k_1-i,k_2-j} \\
&\qquad+ \sum_{k_1=i}^{K-1}\sum_{k_2=0}^{j-1}\left[E[\boldsymbol{x}[n]\boldsymbol{x}^\top[m-1]]\right]_{k_1,k_2}[\boldsymbol{S}\boldsymbol{S}^\top]_{k_1-i,K+k_2-j} \\
&\qquad+ \sum_{k_1=0}^{i-1}\sum_{k_2=j}^{K-1}\left[E[\boldsymbol{x}[n-1]\boldsymbol{x}^\top[m]]\right]_{k_1,k_2}[\boldsymbol{S}\boldsymbol{S}^\top]_{K+k_1-i,k_2-j} \\
&\qquad+ \sum_{k_1=0}^{i-1}\sum_{k_2=0}^{j-1}\left[E[\boldsymbol{x}[n-1]\boldsymbol{x}^\top[m-1]]\right]_{k_1,k_2}[\boldsymbol{S}\boldsymbol{S}^\top]_{K+k_1-i,K+k_2-j}. \qquad \text{(A.1)}
\end{aligned}$$

The second-order moments (2.13) can be substituted to give

$$\begin{aligned}
&\left[E[\tilde{\boldsymbol{X}}[n]\boldsymbol{S}\boldsymbol{S}^\top\tilde{\boldsymbol{X}}[m]^\top]\right]_{i,j} \\
&\quad= \frac{1}{M}\sum_{k_1=i}^{K-1}\sum_{k_2=j}^{K-1}\delta[n-m]\left[\boldsymbol{S}\boldsymbol{S}^\top\right]_{k_1,k_2}\left[\boldsymbol{S}\boldsymbol{S}^\top\right]_{k_1-i,k_2-j} \\
&\quad\quad+\frac{1}{M}\sum_{k_1=i}^{K-1}\sum_{k_2=0}^{j-1}\delta[n-m+1]\left[\boldsymbol{S}\boldsymbol{S}^\top\right]_{k_1,k_2}\left[\boldsymbol{S}\boldsymbol{S}^\top\right]_{k_1-i,K+k_2-j} \\
&\quad\quad+\frac{1}{M}\sum_{k_1=0}^{i-1}\sum_{k_2=j}^{K-1}\delta[n-m-1]\left[\boldsymbol{S}\boldsymbol{S}^\top\right]_{k_1,k_2}\left[\boldsymbol{S}\boldsymbol{S}^\top\right]_{K+k_1-i,k_2-j} \\
&\quad\quad+\frac{1}{M}\sum_{k_1=0}^{i-1}\sum_{k_2=0}^{j-1}\delta[n-m]\left[\boldsymbol{S}\boldsymbol{S}^\top\right]_{k_1,k_2}\left[\boldsymbol{S}\boldsymbol{S}^\top\right]_{K+k_1-i,K+k_2-j}. \qquad \text{(A.2)}
\end{aligned}$$

Finally, the elements of $\boldsymbol{R}_{xx} = E[\boldsymbol{X}[n]\boldsymbol{S}\boldsymbol{S}^\top\boldsymbol{X}[n]^\top]$ are given by

$$[\boldsymbol{R}_{xx}]_{i,j} = \left[E\left[\tilde{\boldsymbol{X}}\left[n-n'\right]\boldsymbol{S}\boldsymbol{S}^\top\tilde{\boldsymbol{X}}\left[n-n''\right]^\top\right]\right]_{i-Kn',j-Kn''} \qquad \text{(A.3)}$$

where

$$\begin{aligned}
n' &= \left\lfloor\frac{i}{K}\right\rfloor \\
n'' &= \left\lfloor\frac{j}{K}\right\rfloor
\end{aligned}$$

Calculation of $\boldsymbol{R}_{x\hat{a}}$ is also quite tedious. Under the assumption of feedback of correct decisions, $\hat{\boldsymbol{a}}[n] = \boldsymbol{a}[n-\Delta]$, so the ith column and jth row of $\boldsymbol{R}_{x\hat{a}}$ can be expanded as

$$\begin{aligned}
[\boldsymbol{R}_{x\hat{a}}]_{i,j} &= E\left[\boldsymbol{X}[n]\boldsymbol{S}\hat{\boldsymbol{A}}^\top[n-1]\right] \\
&= \sum_{k=0}^{K-1}\sum_{\ell=0}^{N-1}E\left[x[Kn-i+k]a[N(n-\Delta-1)-j+\ell]\right]\left[\boldsymbol{S}\right]_{k,\ell} \qquad \text{(A.4)}
\end{aligned}$$

where the expectation can be expanded using

$$\begin{aligned}
E\left[\boldsymbol{x}[n]\boldsymbol{a}^\top[m]\right] &= \boldsymbol{S}E\left[\boldsymbol{a}[n]\boldsymbol{a}^\top[m]\right] \\
&= \begin{cases} \frac{1}{M}\boldsymbol{S} & n = m \\ \boldsymbol{0}_{K\times K} & n \neq m \end{cases} \qquad \text{(A.5)}
\end{aligned}$$

Fortunately, calculation of $\boldsymbol{R}_{\hat{a}\hat{a}}$ is much more straightforward. Again using the assumption of feedback of correct decisions,

$$\begin{aligned} E\left[\hat{\boldsymbol{a}}[n]\hat{\boldsymbol{a}}^{\top}[m]\right] &= E\left[\boldsymbol{a}[n-\Delta]\boldsymbol{a}^{\top}[m-\Delta]\right] \\ &= E\left[\boldsymbol{a}[n]\boldsymbol{a}^{\top}[m]\right] \\ &= \begin{cases} \frac{1}{M}\boldsymbol{I}_N & n = m \\ \boldsymbol{0}_{K\times K} & n \neq m \end{cases} \\ \Longrightarrow \boldsymbol{R}_{\hat{a}\hat{a}} &= \frac{1}{M}\boldsymbol{I}_{N_g} \end{aligned} \tag{A.6}$$

which satisfies the invertibility required by the MMSE DFE design equations (2.21) and (2.22).

Finally, $[\boldsymbol{R}_{ww}]_{i,j}$ can be expanded as

$$[\boldsymbol{R}_{ww}]_{i,j} = \sum_{k_1,k_2=0}^{K-1} E\left[w[Kn-i+k_1]w[Kn-j+k_2]\right] \sum_{\ell=0}^{N-1} [\boldsymbol{S}]_{k_1,\ell}\,[\boldsymbol{S}]_{k_2,\ell}\,.$$

In the case when w is AWGN, this becomes

$$[\boldsymbol{R}_{ww}]_{i,j} = \sigma_w^2 \sum_{k_1,k_2=0}^{K-1} \delta[j-i+k_1-k_2] \sum_{\ell=0}^{N-1} [\boldsymbol{S}]_{k_1,\ell}\,[\boldsymbol{S}]_{k_2,\ell}\,.$$

A.2 Orthogonal and Transorthogonal Modulation

To calculate $\boldsymbol{R}_{xx} = E\left[\boldsymbol{X}[n]\boldsymbol{S}\boldsymbol{J}\boldsymbol{S}^\top\boldsymbol{X}^\top[n]\right]$, we start by substituting $\boldsymbol{S}\boldsymbol{J}\boldsymbol{S}^\top$ for $\boldsymbol{S}\boldsymbol{S}^\top$ in (A.1), giving

$$\begin{aligned}
&\left[E[\tilde{\boldsymbol{X}}[n]\boldsymbol{S}\boldsymbol{J}\boldsymbol{S}^\top\tilde{\boldsymbol{X}}[m]^\top]\right]_{i,j} \\
&\quad= \sum_{k_1=i}^{K-1}\sum_{k_2=j}^{K-1}\left[E[\boldsymbol{x}[n]\boldsymbol{x}^\top[m]]\right]_{k_1,k_2}[\boldsymbol{S}\boldsymbol{J}\boldsymbol{S}^\top]_{k_1-i,k_2-j} \\
&\qquad+\sum_{k_1=i}^{K-1}\sum_{k_2=0}^{j-1}\left[E[\boldsymbol{x}[n]\boldsymbol{x}^\top[m-1]]\right]_{k_1,k_2}[\boldsymbol{S}\boldsymbol{J}\boldsymbol{S}^\top]_{k_1-i,K+k_2-j} \\
&\qquad+\sum_{k_1=0}^{i-1}\sum_{k_2=j}^{K-1}\left[E[\boldsymbol{x}[n-1]\boldsymbol{x}^\top[m]]\right]_{k_1,k_2}[\boldsymbol{S}\boldsymbol{J}\boldsymbol{S}^\top]_{K+k_1-i,k_2-j} \\
&\qquad+\sum_{k_1=0}^{i-1}\sum_{k_2=0}^{j-1}\left[E[\boldsymbol{x}[n-1]\boldsymbol{x}^\top[m-1]]\right]_{k_1,k_2}[\boldsymbol{S}\boldsymbol{J}\boldsymbol{S}^\top]_{K+k_1-i,K+k_2-j}.
\end{aligned}$$

Then, the second-order moments (2.12) or (2.14) can be substituted, and then the elements of $\boldsymbol{R}_{xx} = E[\boldsymbol{X}[n]\boldsymbol{S}\boldsymbol{J}\boldsymbol{S}^\top\boldsymbol{X}[n]^\top]$ are given by

$$[\boldsymbol{R}_{xx}]_{i,j} = \left[E\left[\tilde{\boldsymbol{X}}\left[n-n'\right]\boldsymbol{S}\boldsymbol{J}\boldsymbol{S}^\top\tilde{\boldsymbol{X}}\left[n-n''\right]^\top\right]\right]_{i-Kn',j-Kn''} \tag{A.7}$$

where

$$\begin{aligned}
n' &= \left\lfloor\frac{i}{K}\right\rfloor \\
n'' &= \left\lfloor\frac{j}{K}\right\rfloor
\end{aligned}$$

For $\boldsymbol{R}_{x\hat{a}}$, the ith column and jth row of $\boldsymbol{R}_{x\hat{a}}$ can be expanded as above, giving

$$\begin{aligned}
[\boldsymbol{R}_{x\hat{a}}]_{i,j} &= E\left[\boldsymbol{X}[n]\boldsymbol{S}\boldsymbol{J}\hat{\boldsymbol{A}}^\top[n-1]\right] \\
&= \sum_{k=0}^{K-1}\sum_{\ell=0}^{N-1}E\left[x[Kn-i+k]a[N(n-\Delta-1)-j+\ell]\right][\boldsymbol{S}\boldsymbol{J}]_{k,\ell}
\end{aligned} \tag{A.8}$$

where the expectation can be expanded using

$$\begin{aligned} E\left[\boldsymbol{x}[n]\boldsymbol{a}^\top[m]\right] &= \boldsymbol{S}E\left[\boldsymbol{a}[n]\boldsymbol{a}^\top[m]\right] \\ &= \begin{cases} \frac{1}{N}\boldsymbol{S} & n = m \\ \frac{1}{N^2}\boldsymbol{S}\mathbf{1}_{N\times N} & n \neq m \end{cases} \end{aligned} \tag{A.9}$$

Now, for calculation of $\boldsymbol{R}_{\hat{a}\hat{a}}$, we again use the assumption of feedback of correct decisions, so

$$\begin{aligned} E\left[\hat{\boldsymbol{a}}[n]\hat{\boldsymbol{a}}^\top[m]\right] &= E\left[\boldsymbol{a}[n-\Delta]\boldsymbol{a}^\top[m-\Delta]\right] \\ &= E\left[\boldsymbol{a}[n]\boldsymbol{a}^\top[m]\right] \\ &= \begin{cases} \frac{1}{N}\boldsymbol{I}_N & n = m \\ \frac{1}{N^2}\mathbf{1}_{N\times N} & n \neq m \end{cases} \end{aligned}$$

Thus,

$$\begin{aligned} [\boldsymbol{R}_{\hat{a}\hat{a}}]_{i,j} &= \left[E\left[\hat{\boldsymbol{A}}[n-1]\boldsymbol{J}\hat{\boldsymbol{A}}^\top[n-1]\right]\right]_{i,j} \\ &= \sum_{k,\ell=0}^{N-1} E\left[\hat{a}[N(n-1)-k-i]\hat{a}[N(n-1)-\ell-j]\right][\boldsymbol{J}]_{k,\ell} \end{aligned} \tag{A.10}$$

Finally, $[\boldsymbol{R}_{ww}]_{i,j}$ can be expanded as

$$[\boldsymbol{R}_{ww}]_{i,j} = \sum_{k_1,k_2=0}^{K-1} E\left[w[Kn-i+k_1]w[Kn-j+k_2]\right] \sum_{\ell=0}^{N-1} [\boldsymbol{S}\boldsymbol{J}]_{k_1,\ell}\,[\boldsymbol{S}]_{k_2,\ell}\,.$$

In the case when w is AWGN, this becomes

$$[\boldsymbol{R}_{ww}]_{i,j} = \sigma_w^2 \sum_{k_1,k_2=0}^{K-1} \delta[j-i+k_1-k_2] \sum_{\ell=0}^{N-1} [\boldsymbol{S}\boldsymbol{J}]_{k_1,\ell}\,[\boldsymbol{S}]_{k_2,\ell}\,.$$

Appendix B

Cumulants of Vector Random Processes

The first, second, and fourth order cumulants of an i.i.d. vector random process $\boldsymbol{x} \in \mathbb{R}^K$ are defined as [5]

$$\begin{aligned}
[\mathcal{C}_1(\boldsymbol{x})]_{i_1} &\triangleq E[x_{i_1}] \\
[\mathcal{C}_2(\boldsymbol{x})]_{i_1,i_2} &\triangleq E[x_{i_1}x_{i_2}] - E[x_{i_1}]E[x_{i_2}] \\
[\mathcal{C}_4(\boldsymbol{x})]_{i_1,i_2,i_3,i_4} &\triangleq E\Big[(x_{i_1} - [\mathcal{C}_1(\boldsymbol{x})]_{i_1}) \cdot (x_{i_2} - [\mathcal{C}_1(\boldsymbol{x})]_{i_2}) \\
&\qquad\qquad \cdot (x_{i_3} - [\mathcal{C}_1(\boldsymbol{x})]_{i_3}) \cdot (x_{i_4} - [\mathcal{C}_1(\boldsymbol{x})]_{i_4})\Big] \\
&\quad - [\mathcal{C}_2(\boldsymbol{x})]_{i_1,i_2}\,[\mathcal{C}_2(\boldsymbol{x})]_{i_3,i_4} - [\mathcal{C}_2(\boldsymbol{x})]_{i_1,i_3}\,[\mathcal{C}_2(\boldsymbol{x})]_{i_2,i_4} \\
&\quad - [\mathcal{C}_2(\boldsymbol{x})]_{i_1,i_4}\,[\mathcal{C}_2(\boldsymbol{x})]_{i_2,i_3}
\end{aligned}$$

for $i_1, i_2, i_3, i_4 \in \{0, 1, \ldots, K-1\}$. The first order cumulant is the mean vector, the second order cumulant is the covariance matrix, and the fourth-order cumulant is a super-symmetric fourth-order tensor. Furthermore, we note that when $K = 1$ so that $\boldsymbol{x}$ is a scalar, the cumulant definitions reduce to the definition of cumulants of a scalar random process. Much like cumulants of scalar random processes, cumulants of vector random processes also obey a linearity property. When $\boldsymbol{x}$ is a linear function of a random vector process $\boldsymbol{a}$, related via $\boldsymbol{x} = \boldsymbol{S}\boldsymbol{a}$, the Nth order cumulant obeys

$$\begin{aligned}
\mathcal{C}_N(\boldsymbol{x}) &= \mathcal{C}_N(\boldsymbol{S}\boldsymbol{a}) \\
&= \mathcal{C}_N(\boldsymbol{a}) \times_1 \boldsymbol{S} \times_2 \boldsymbol{S} \ldots \times_N \boldsymbol{S}
\end{aligned}$$

where $\times_N$ denotes the n-mode product of a tensor and a matrix, which, for an Nth order tensor $\mathcal{C} \in \mathbb{R}^{M \times M \times \ldots \times M}$ and a matrix $\boldsymbol{S} \in \mathbb{R}^{K \times M}$ is defined as

$$[\mathcal{C} \times_n \boldsymbol{S}]_{i_1, i_2, \ldots, i_n, \ldots, i_N} \triangleq \sum_j [\mathcal{C}]_{i_1, i_2, \ldots, j, \ldots, i_N} [\boldsymbol{S}]_{i_n, j}$$

Appendix C

Fourth-Order Cumulant Tensor of BOM Source

Here, we provide an expression for the fourth-order cumulant tensor of a BOM source in terms of $\boldsymbol{S}$. First, we consider the choice $\boldsymbol{S} = \boldsymbol{I}$. Due to the super-symmetry of the cumulant tensor, we can consider an ordering $i_1 \geq i_2 \geq i_3 \geq i_4$ without loss of generality. From (5.4), averaging over all possible symbols gives the cumulant tensor for $\boldsymbol{S} = \boldsymbol{I}$ as

$$[\mathcal{C}_4(\boldsymbol{x})]_{i_1,i_2,i_3,i_4} = \begin{cases} \frac{1}{K} - \frac{3}{K^2} & \text{for } i_1 = i_2 = i_3 = i_4 \\ -\frac{1}{K^2} & \text{for } i_1 = i_2 > i_3 = i_4 \\ 0 & \text{otherwise} \end{cases} \tag{C.1}$$

Next, note that for any choice of $\boldsymbol{S}$, we can express the source symbol $\boldsymbol{x}[n] = \boldsymbol{S}\boldsymbol{x}'[n]$ where $\boldsymbol{x}'[n]$ is a BOM symbol for the particular choice $\boldsymbol{S} = \boldsymbol{I}$. Thus, exploiting the linearity property of cumulants and using (C.1), we have for all $i_1, i_2, i_3, i_4 \in \{0, \ldots, K-1\}$

$$\begin{aligned} [\mathcal{C}_4(\boldsymbol{x})]_{i_1,i_2,i_3,i_4} &= [\mathcal{C}_4(\boldsymbol{S}\boldsymbol{x}')]_{i_1,i_2,i_3,i_4} \\ &= \sum_{k_1,k_2,k_3,k_4} [\mathcal{C}_4(\boldsymbol{x}')]_{k_1,k_2,k_3,k_4} [\boldsymbol{S}]_{i_1,k_1} [\boldsymbol{S}]_{i_2,k_2} [\boldsymbol{S}]_{i_3,k_3} [\boldsymbol{S}]_{i_4,k_4} \\ &= \frac{1}{K} \sum_{\ell} [\boldsymbol{S}]_{i_1,\ell} [\boldsymbol{S}]_{i_2,\ell} [\boldsymbol{S}]_{i_3,\ell} [\boldsymbol{S}]_{i_4,\ell} - \frac{1}{K^2}\delta[i_1 - i_3]\delta[i_2 - i_4] \\ &\quad -\frac{1}{K^2}\delta[i_1 - i_2]\delta[i_3 - i_4] - \frac{1}{K^2}\delta[i_1 - i_4]\delta[i_2 - i_3] \end{aligned} \tag{C.2}$$

Appendix D

Impulse Response of False Local Minima for LTBOMB

As described in Section 5.2.5, false local minima in LTBOMB that occur when $\boldsymbol{S} = \boldsymbol{I}_2$ have the form $\boldsymbol{c}^* = \pm[0,\ \alpha,\ \beta,\ \gamma,\ -\beta\ ,\alpha]^\top$. Using the Gröbner basis technique, the exact values of α, β, γ were found to be

$$\begin{aligned}
\alpha &= \frac{1}{3064}\,\gamma\left(15896\gamma^2 - 5584 + 8815\gamma^4\right) \\
\beta &= \sqrt{b_2 + b_3 b_1^{1/3} + b_4 b_1^{2/3}} \\
\gamma &= \sqrt{\frac{2}{5289}}\sqrt{b_1^{1/3} + 12226 b_1^{-1/3} + 526}
\end{aligned}$$

where

$$\begin{aligned}
b_1 &= 20801089 + 5289\,\sqrt{15402345} \\
b_2 &= \frac{251}{5289} \\
b_3 &= \frac{2617563071280444348696367 8 - 4894846657232724650142\sqrt{15402345}}{151394859138606^2} \\
b_4 &= \frac{9749633283977658762238 32 - 2450225874551306630 04\sqrt{15402345}}{151394859138606^2}
\end{aligned}$$

Appendix E

Candidate Blind Algorithms for Orthogonal and Transorthogonal Modulation

The following candidate algorithms were tested for equalization of orthogonal and transorthogonal modulation. While we did not conduct a thorough study of these algorithms (as we did for blind algorithms for biorthogonal modulation in Chapter 5), simulations have suggested that these are not suitable choices. All of these algorithms were meant for adaptation of the scalar linear equalizer presented in Chapter 4. They all exhibited poor convergence and spurious local minima, and none appeared to outperform DD-LMS. We list them simply as documentation of failed algorithms, so that we can avoid these as pitfalls in subsequent algorithm development for orthogonal and transorthogonal modulations.

E.1 Candidate Algorithm #1

We attempted a CMA-like algorithm which is identical to LTBOMB but for orthogonal and transorthogonal modulation, and attempts to exploit the fact that, when the equalizer is operating correctly, the power of the correlator output $\tilde{\boldsymbol{a}}[n]$ is constant, so

$$J(\boldsymbol{f}) \;=\; E\left[(||\tilde{\boldsymbol{a}}[n]||_2^2 - 1)^2\right]$$

resulting in the algorithm update equation

$$\boldsymbol{f}[n+1] \;=\; \boldsymbol{f}[n] - \mu \boldsymbol{Y}[n]\boldsymbol{S}\tilde{\boldsymbol{a}}[n](||\tilde{\boldsymbol{a}}[n]||_2^2 - 1)$$

E.2 Candidate Algorithm #2

A slight modification of the previous algorithm, this algorithm forms the error in a space of reduced dimension, and does not penalize DC offsets:

$$\begin{aligned} J(\boldsymbol{f}) &= E\left[\left(||\boldsymbol{U}\tilde{\boldsymbol{a}}[n]||_2^2 - \frac{N-1}{N}\right)^2\right] \\ &= E\left[\left(\tilde{\boldsymbol{a}}[n]^\top \boldsymbol{J}\tilde{\boldsymbol{a}}[n] - \frac{N-1}{N}\right)^2\right] \end{aligned}$$

and corresponding algorithm update equation

$$\boldsymbol{f}[n+1] = \boldsymbol{f}[n] - \mu \boldsymbol{Y}[n]\boldsymbol{S}\boldsymbol{J}\tilde{\boldsymbol{a}}[n]\left(||\boldsymbol{U}\tilde{\boldsymbol{a}}[n]||_2^2 - \frac{N-1}{N}\right)$$

E.3 Candidate Algorithm #3

We also tried an algorithm (for orthogonal modulation only) that is identical to TROMBONE,

$$J(\boldsymbol{f}) = E\left[||\tilde{\boldsymbol{a}}[n]||_2^4 - ||\tilde{\boldsymbol{a}}[n]||_4^4\right]$$

and corresponding algorithm update equation

$$\boldsymbol{f}[n+1] = \boldsymbol{f}[n] - \mu \boldsymbol{Y}[n]\boldsymbol{S}\left(\tilde{\boldsymbol{a}}[n]^\top \tilde{\boldsymbol{a}}[n]\boldsymbol{I} - \mathrm{diag}(\tilde{\boldsymbol{a}}[n])^2\right)\tilde{\boldsymbol{a}}[n].$$

Like TROMBONE, this algorithm needs a constraint. We chose the constraint $E[\tilde{\boldsymbol{a}}[n]^\top \tilde{\boldsymbol{a}}[n]] = 1$.

Appendix F

Extension of LTBOMB to DFE with Complex Signals

First, we redevelop the model in Fig. 2.1 for the complex case. Now, instead of imposing conditions on $\boldsymbol{S}^\top \boldsymbol{S}$ as in Table 1.2, we make the same requirements on $\boldsymbol{S}^H \boldsymbol{S}$ where ^{H} denotes conjugate transpose. Thus, for example, with orthogonal and biorthogonal modulations $\boldsymbol{S}$ must be unitary. We continue to employ the minimum Euclidean distance detector, which in the complex case requires the insertion of a real operator $\Re(\cdot)$ at the input to the "choose max" detectors described in Section 1.4. The equations to describe the complex model are nearly identical to the real case, with the only change being the equation for $\tilde{\boldsymbol{a}}[n]$, giving

$$\boldsymbol{x}[n] = \boldsymbol{S}\boldsymbol{a}[n] \tag{F.1}$$

$$\boldsymbol{Y}[n] = \boldsymbol{\mathcal{H}}\boldsymbol{X}[n] + \boldsymbol{W}[n] \tag{F.2}$$

$$\boldsymbol{z}[n] = \boldsymbol{Y}^\top[n]\boldsymbol{f} \tag{F.3}$$

$$\tilde{\boldsymbol{a}}[n] = \Re\left\{\boldsymbol{S}^H \boldsymbol{z}[n]\right\} + \hat{\boldsymbol{A}}^\top[n-1]\boldsymbol{g}. \tag{F.4}$$

Note that $\boldsymbol{S}$, $\boldsymbol{x}[n]$, $\boldsymbol{Y}[n]$, $\boldsymbol{H}$, $\boldsymbol{W}[n]$, $\boldsymbol{z}[n]$, and $\boldsymbol{f}$ are all complex variables. On the other hand, $\boldsymbol{a}[n]$, $\tilde{\boldsymbol{a}}[n]$, $\hat{\boldsymbol{A}}[n-1]$, and $\boldsymbol{g}$ assume only real values.

While the complex extension to the system model in (F.1)-(F.4) applies to all of the modulations, we now consider the particular case of DFE adaptation via LTBOMB, which is was studied in Chapter 5 for use with biorthogonal modulation when $K = N$. For DFE adaptation with complex signals, the LTBOMB cost function is given by

$$J_{LTB}(\boldsymbol{f}, \boldsymbol{g}) = E\left[\left(\tilde{\boldsymbol{a}}^\top[n]\tilde{\boldsymbol{a}}[n] - 1\right)^2\right]. \tag{F.5}$$

Taking the instantaneous derivatives with respect to $\boldsymbol{f}$ and $\boldsymbol{g}$ gives the complex DFE LTBOMB update equations

$$\boldsymbol{\epsilon}_{LTB}[n] = \tilde{\boldsymbol{a}}[n]\left(\tilde{\boldsymbol{a}}^{\top}[n]\tilde{\boldsymbol{a}}[n] - 1\right) \tag{F.6}$$

$$\boldsymbol{f}_{LTB}[n+1] = \boldsymbol{f}_{LTB}[n] - \mu_1 \boldsymbol{Y}[n]\boldsymbol{S}^{*}\boldsymbol{\epsilon}_{LTB}[n] \tag{F.7}$$

$$\boldsymbol{g}_{LTB}[n+1] = \boldsymbol{g}_{LTB}[n] - \mu_2 \hat{\boldsymbol{A}}[n-1]\boldsymbol{\epsilon}_{LTB}[n] \tag{F.8}$$

where $\boldsymbol{S}^{*}$ is the complex conjugate of $\boldsymbol{S}$.

BIBLIOGRAPHY

[1] J. R. Barry, E. A. Lee, and D. G. Messerschmitt, *Digital Communication*, 4th ed. Upper Saddle River, N.J.: Kluwer Academic Publishers, 2004.

[2] J. Barry, "Sequence Detection and Equalization for Pulse-Position Modulation," in *Proc. IEEE International Conference on Communications (ICC'94)*, May 1994, pp. 1561–1565.

[3] M. Castella, J.-C. Pesquet, and A. P. Petropulu, "New contrasts for blind separation of non iid sources in the convolutive case," in *Proc. European Signal Processing Conf. (EUSIPCO'02)*, vol. 2, Sept. 2002, pp. 107–110.

[4] D. Cox, J. Little, and D. O'Shea, *Ideals, Varieties, and Algorithms.* Berlin: Springer Verlag, 1992.

[5] L. De Lathauwer, "Signal processing based on multilinear algebra," Ph.D. dissertation, Katholieke Universiteit Leuven, Leuven, Belgium, Sept. 1997.

[6] Z. Ding and C. R. Johnson, Jr., "On the nonvanishing stability of undesirable equilibria for FIR godard blind equalizers," *IEEE Trans. Signal Processing*, vol. 41, pp. 1940–1944, May 1993.

[7] T. J. Endres, B. D. O. Anderson, C. R. Johnson, Jr., and L. Tong, "On the robustness of FIR channel identification from fractionally-spaced received signal second-order-statistics," *IEEE Signal Processing Letters*, vol. 3, pp. 153–155, May 1996.

[8] I. Fijalkow, A. Touzni, and J. R. Treichler, "Fractionally spaced equalization using CMA: Robustness to channel noise and lack of disparity," *IEEE Trans. Signal Processing*, vol. 45, pp. 56–66, Jan. 1997.

[9] R. Fisher *et al.*, "DS-UWB physical layer submission to 802.15 task group 3a," IEEE P802.15-04/01373r3, July 2004.

[10] J. Foerster, Ed., "Channel modeling sub-committee report final," IEEE P802.15-02/490, Feb. 2003.

[11] G. J. Foschini, "Equalizing without altering or detecting data," *Bell System Technical Journal*, vol. 64, pp. 1885–1911, Oct. 1985.

[12] M. Ghosh, "Analysis of the MMSE DFE with error propagation," in *Proc. IEEE GLOBECOM Commun. Theory Mini-Conf.*, vol. 4, Nov. 1997, pp. 85–89.

[13] D. N. Godard, "Self-recovering equalization and carrier tracking in two-dimensional data communication systems," *IEEE Trans. Commun.*, vol. 28, pp. 1867–1875, Nov. 1980.

[14] G. H. Golub and C. F. V. Loan, *Matrix Computations*, 3rd ed. Baltimore, MD: The Johns Hopkins University Press, 1996.

[15] G. H. Hardy, J. E. Littlewood, and G. Polya, *Inequalities*. London: Cambrige Univ. Press, 1934.

[16] S. Haykin, *Adaptive Filter Theory*, 4th ed. Upper Saddle River, N.J.: Prentice Hall, 2001.

[17] R. A. Horn and C. R. Johnson, *Matrix Analysis*. Cambridge, UK: Cambridge University Press, 1985.

[18] C. R. Johnson, Jr. *et al.*, "Blind equalization using the constant modulus criterion: A review," *Proc. IEEE*, vol. 86, pp. 1927–1950, Oct. 1998.

[19] R. Kennedy, B. Anderson, and R. Bitmead, "Tight bounds on the error probabilities of decision feedback equalizers," *IEEE Trans. Commun.*, vol. 35, pp. 1022–1028, Oct. 1987.

[20] A. G. Klein, C. R. Johnson, Jr., and P. Duhamel, "On blind equalization of M-ary bi-orthogonal signaling," in *Proc. IEEE Intl. Conf. on Acoustics, Speech, and Signal Processing (ICASSP'05)*, Mar. 2005.

[21] A. G. Klein, D. R. Brown III, and C. R. Johnson, Jr., "MMSE decision feedback equalization of orthogonal multipulse modulated signals," in *Proc. Conf. on Information Sciences and Systems (CISS'04)*, Mar. 2004.

[22] A. G. Klein and C. R. Johnson, Jr., "MMSE decision feedback equalization of pulse position modulated signals," in *Proc. IEEE Intl. Conf. on Communications (ICC'04)*, June 2004.

[23] J. P. LeBlanc, I. Fijalkow, and C. R. Johnson, Jr., "CMA fractionally spaced equalizers: Stationary points and stability under IID and temporally correlated sources," *Intl. Journal of Adaptive Control and Signal Processing*, vol. 12, pp. 135–155, Mar. 1998.

[24] Y. Li and Z. Ding, "Global convergence of fractionally spaced godard (CMA) adaptive equalizers," *IEEE Trans. Signal Processing*, vol. 44, pp. 818–826, Apr. 1996.

[25] R. W. Lucky, "Automatic equalization for digital communications," *Bell Systems Technical Journal*, vol. 44, pp. 547–588, Apr. 1965.

[26] O. Macchi and E. Eweda, "Convergence analysis of self-adaptive equalizers," *IEEE Trans. Inform. Theory*, vol. 30, pp. 161–176, Mar. 1984.

[27] R. K. Martin, J. Balakrishnan, W. A. Sethares, and C. R. Johnson, Jr., "A blind adaptive TEQ for multicarrier systems," *IEEE Signal Processing Lett.*, vol. 9, pp. 341–343, Nov. 2002.

[28] R. K. Martin, "Blind, adaptive equalization for multicarrier receivers," Ph.D. dissertation, Cornell University, Ithaca, NY, May 2004.

[29] J. G. Proakis, *Digital Communications*, 4th ed. New York: McGraw-Hill, 2000.

[30] P. A. Regalia, "On the equivalence between the godard and shalvi-weinstein schemes of blind equalization," *Signal Processing (Elsevier)*, vol. 73, pp. 185–190, Feb. 1999.

[31] A. Saleh and R. Valenzuela, "A statistical model for indoor multipath propagation," *IEEE J. Select. Areas Commun.*, vol. SAC-5, pp. 128–137, Feb. 1987.

[32] A. Shah, S. Biracree, R. A. Casas, T. J. Endres, *et al.*, "Global convergence of a single-axis constant modulus algorithm," in *Proc. IEEE Workshop on Statistical Signal and Array Processing (SSAP'00)*, vol. 9, Aug. 2000, pp. 645–649.

[33] O. Shalvi and E. Weinstein, "New criteria for blind deconvolution of nonminimum phase systems (channels)," *IEEE Trans. Inform. Theory*, vol. 36, pp. 312–321, Mar. 1990.

[34] V. Shtrom and H. H. Fan, "New class of zero-forcing cost functions in blind equalization," *IEEE Trans. Signal Processing*, vol. 46, pp. 2674–2683, Oct. 1998.

[35] C. Simon, P. Loubaton, C. Vignat, C. Jutten, and G. d'Urso, "Blind source separation of convolutive mixtures by maximization of fourth-order cumulants : the non i.i.d. case," in *Proc. Asilomar Conf. on Signals, Systems, and Computers*, vol. 2, Nov. 1998, pp. 1584–1588.

[36] M. K. Simon, S. M. Hinedi, and W. C. Lindsey, *Digital Communication Techniques*. Englewood Cliffs, NJ: Prentice Hall, 1995.

[37] M. Steiner, "The strong simplex conjecture is false," *IEEE Trans. Inform. Theory*, vol. 40, pp. 721–731, May 1994.

[38] M. S. Stone and C. L. Weber, "On the globally optimum M-ary noncoherent digital communication system," *Proc. IEEE*, vol. 57, pp. 1203–1204, June 1969.

[39] K. Takizawa and R. Kohno, "Low-complexity RAKE reception and equalization for MBOK DS-UWB systems," in *Proc. IEEE Global Telecommunications Conf. (GLOBECOM'04)*, vol. 2, Nov. 2004, pp. 1249–1253.

[40] *Mobile Station/Base Station Compatibility Standard for Dual-Mode Wideband Spread Spectrum Cellular Systems*, Telecommunications Industry Association Std. IS-95a, 1995.

[41] A. Touzni, L. Tong, R. A. Casas, and C. R. Johnson, Jr., "Vector-CM stable equilibrium analysis," *IEEE Signal Processing Lett.*, vol. 7, pp. 31–33, Feb. 2000.

[42] J. R. Treichler and B. G. Agee, "A new approach to multipath correction of constant modulus signals," *IEEE Trans. Acoust., Speech, Signal Processing*, vol. ASSP-31, pp. 459–472, Apr. 1983.

[43] J. R. Treichler, C. R. Johnson, Jr., and M. G. Larimore, *Theory and Design of Adaptive Filters*. Upper Saddle River, NJ: Prentice Hall, 2001.

[44] M. K. Varanasi, "Equalization for multipulse modulation," in *Proc. IEEE Intl. Conf. on Personal Wireless Communications (ICPWC'97)*, Dec. 1997, pp. 48–51.

[45] A. J. Viterbi, *Principle of Coherent Communication*. McGraw-Hill, 1966.

[46] M. Webster *et al.*, "Proposal for a high speed PHY for the 2.4 GHz band," IEEE P802.11-98/47, Jan. 1998.

[47] V. Y. Yang and D. L. Jones, "A vector constant modulus algorithm for shaped constellation equalization," *IEEE Signal Processing Lett.*, vol. 5, pp. 89–91, Apr. 1998.

[48] H. H. Zeng, L. Tong, and C. R. Johnson, Jr., "Relationships between the constant modulus and wiener receivers," *IEEE Trans. Inform. Theory*, vol. 44, pp. 1523–1538, July 1998.